The Pennsylvania State University

The Graduate School

Department of Geography

SYNOPTIC AND MESOSCALE CLIMATE FORCING ON ANTARCTIC ICE SHELF SURFACE MELT DYNAMICS

A Dissertation in

Geography

by

Christopher Karmosky

Submitted in Partial Fulfillment
of the Requirements
for the Degree of

Doctor of Philosophy

May 2013

The dissertation of Christopher Karmosky was reviewed and approved* by the following:

Derrick J. Lampkin
Assistant Professor of Geography, Assistant Professor of Geosciences
Dissertation Advisor
Chair of Committee

Andrew M. Carleton
Professor of Geography

Richard B. Alley
Evan Pugh Professor of Geosciences

Michael E. Mann
Professor of Meteorology

Karl S. Zimmerer
Professor of Geography
Head of the Department

*Signatures are on file in the Graduate School

ABSTRACT

Given that the polar regions, especially the Antarctic Peninsula, have experienced one of the largest temperature increases on Earth over the last few decades, an understanding of Antarctic climate has become more urgent. Ice shelves themselves are located at the intersection of the atmosphere, hydrosphere and the cryosphere—the air-ice-ocean boundary, and are sensitive to changes in any of these media. In addition to being particularly sensitive to changes in climate, ice shelves play an important role in controlling the flow of glaciers into the ocean, which has important implications for sea level changes. In a warming world, an increased understanding of how climate change is affecting Antarctic ice shelves is valuable for assessing vulnerable regions of the Antarctic that may be prone to further instability. This work focuses on determining the underlying climatic processes controlling energy and mass balance responsible for driving melting over ice shelves. A novel melt-magnitude retrieval method is presented that uses Moderate Resolution Imaging Spectroradiometer (MODIS)-derived near-IR reflectance coupled with ice surface temperature as a proxy for surface melt magnitude. This method has a higher spatial resolution than passive microwave melt detection, has the added benefit of retrieving melt magnitude rather than a binary melt occurrence or non-occurrence, but has a lower temporal resolution than either passive-microwave or microwave-scatterometry melt detection. This limitation is a result of the opacity of cloud cover to both visible and IR radiation, requiring more satellite overpasses to obtain spatially contiguous imagery. This work also examines several weather variables associated with a large-extent, long-duration surface melt event on the Ross Ice Shelf. It is shown that cloudy conditions coupled with increased sensible and latent heat flux to the surface were present during the event, and these conditions are consistent with those that induce surface melting. Finally, an analysis of co-occurring climate conditions and surface melting over a recent 15-year time period (1987-2002) is presented. This analysis examines

surface melt extent in three regions: Ross Ice Shelf, Larsen Ice Shelf and the Amundsen-Bellingshausen Region. Self-Organizing Maps (SOMs) are used to categorize weather patterns for each December and January day during the study period, and the average surface melt extent for each SOM pattern is computed. These values are compared to average December and January surface melt extents for each region to determine the SOM patterns associated with significantly greater or significantly less melt than the 15-year average. Over the Ross region, increases in sensible and latent heat fluxes are associated with greater surface melt extent, as is the presence of cyclonic circulation in the Ross Sea that drives mild maritime air poleward. In the Larsen and Amundsen-Bellingshausen regions, radiation fluxes appear to be more closely associated with surface melt extent, although the relationship for the geographically heterogeneous Amundsen-Bellingshausen region is less clear. These results can guide future mesoscale modeling studies that will be able to more precisely determine the causative role of each atmospheric variable in generating surface melting on West Antarctic ice shelves.

TABLE OF CONTENTS

LIST OF FIGURES

LIST OF TABLES

ACKNOWLEDGEMENTS

While a dissertation represents the culmination of work by person in finishing an academic program, it is not a work conducted in a vacuum, devoid of assistance of many sorts. Therefore, it is fitting to recognize those who have graciously provided such assistance to me in a myriad of ways in the past several years. Most especially, this includes my family and friends, who have been a pillar of support for me my entire life. I would also like to thank my adviser and my dissertation committee members. My work would not have been possible without their assistance, insight, resources, and certainly not least: their signatures! I would also like to thank the Penn State Ice and Climate research group (PSICE) for their assistance and support over the years and for providing an incubator for ice-related scientific ideas on the Penn State campus.

With regard to the MODIS melt magnitude retrieval project, I would like to thank Dr. Doug MacAyeal and Dr. Konrad Steffen for supplying information used to construct the initialization stratigraphy for SNTHERM. Many thanks also to Dr. Steve Daly and Dr. Sally Shoop from CRREL for providing information regarding the NSF radiation data for McMurdo station. This work was funded through NASA Grant Numbers: NNX06AE50G and NNX09AO49H, and I would be remiss to not thank NASA for their generous funding. Many thanks!

I owe an incredible amount of gratitude to Dr. Dave Reusch for his assistance with the Self-Organizing maps portion of this work. I will never know as much about SOMs as he, and I am thankful for the many hours of tutoring and feedback he has provided.

This work is dedicated to the memory of Stephen W. and Emilie Cernik, Charles Sr. and Betty Karmosky, Wayne Karmosky, and Charles Karmosky, Jr.

AMDG

Chapter 1

Introduction

Temperatures in West Antarctica are increasing (King et al., 2002; Turner et al., 2005; Steig et al., 2009), and it is thought that anthropogenic greenhouse warming may threaten the stability of the West Antarctic Ice Sheet (Oppenheimer, 1998). It is known that surface melting can contribute to the collapse of ice shelves, as in the case of the Larsen B (Sergienko and MacAyeal, 2005), and that land glacier speeds can increase when ice shelf buttressing is reduced or eliminated (Scambos et al., 2004), contributing to global sea level rise. Despite the link between ice-shelf surface melt, removal of glacier buttressing and eventual global sea level rise, specific climatic mechanisms that drive surface melting remain relatively unexplored. This work 1) develops a new method for the detection and quantification of surface melt on Antarctic Ice Shelves; 2) uses Self-Organizing Maps with a passive microwave melt detection algorithm to determine the weather patterns associated with ice shelf surface melting in several regions of West Antarctica over a 15-year period (1987-2002), and 3) examines a series of weather patterns associated with two large-scale surface melt event on Ross Ice Shelf to determine the meteorological forcing mechanisms responsible for the melt event.

The detection of surface melt through the use of satellite remote sensing platforms is critical in Antarctica. Satellite imagery remains the only source of information for broad areas of the continent that remain largely inaccessible, many of which are long distances from any ground-based weather stations. This work examines a new method for the detection and quantification of surface melt using relatively high-resolution imagery from the Moderate Resolution Imaging Spectroradiometer (MODIS). Current melt detection algorithms using the microwave portion of the electromagnetic spectrum rely on an abrupt change in the dielectric constant of the firn as it changes from dry to wet. This allows for a binary assessment of surface

melt occurrence/non-occurrence, but does not permit detection of the amount of liquid water in the firn. However, melt detection in the near-infrared relies on a more gradual change in effective grain size as the firn melts, making the detection of liquid water fraction possible (Chapter 2). A three-dimensional feature space is calibrated using four weather stations across the Ross Ice Shelf to determine the relationship between modeled surface liquid water fraction at the reference stations, MODIS near-IR reflectance, and MODIS skin temperature (Thermal IR emission). Once this relationship is determined, it allows for the retrieval of surface melt magnitude at locations across the Ross Ice Shelf where MODIS imagery is available, but are geographically distant from weather stations.

Because the Ross Ice Shelf is one of the coldest ice shelves on Antarctica, and surface melting in this area is relatively infrequent, it is important compare several other ice shelf regions when examining the weather and climate forcing of surface melt in a holistic fashion. Surface melt extent in each of three regions--Ross, Larsen, and Amundsen-Bellingshausen Sea (ABS)--is obtained by a passive microwave melt retrieval algorithm, and is compared with SOM-derived spatial patterns in each of seven different weather variables determined to be important in generating surface melt. SOM patterns that occur on days when surface melt extent is significantly above or below monthly mean melt extent in each region are examined to determine their potential for causing or inhibiting surface melting—e.g. the advection of warm air, changes in boundary-layer turbulence, or an increase in radiation flux to the surface. This work can provide a context for mesoscale modeling of physical processes to determine the causative factors for surface melting across West Antarctica, and provide an important context to potential changes as a result of anthropogenic climate change (Chapter 3).

As mentioned earlier, the Ross Ice Shelf is the largest ice shelf in Antarctica, but its more poleward location typically precludes large-scale surface melt events. During the 1991-92 summer season, however, a large-extent (~200,000 km^2), long duration (~6 week) surface melt

event occurred on the eastern portion of Ross Ice Shelf. Self-Organizing Maps (SOMs) are used to isolate particular spatial patterns in several weather variables that were anomalously frequent (relative to a 1987-2002 baseline period) during and immediately prior to the 1991-92 surface melt event. These patterns are then examined to determine the potential for each pattern to contribute to surface melting on Ross Ice Shelf. This anomalous event provides some important clues as to the physical processes responsible for creating large-scale surface melt events on a cold ice shelf, such as Ross. A second case study is also examined, specifically a melt event that occurred in 2005. This event was characterized by a relatively small spatial extent adjacent to the Transantarctic range near the western edge of the Ross Ice Shelf. This melt event, however, extended to the most poleward portion of the Ross Ice Shelf, at a latitude of 85^{o}S. This melt event is thought to be related to weather processes similar to Foehn winds, and is a result of adiabatic warming of air as it descends 2km off of the Antarctic Plateau (Chapter 4).

References

King, J.C.; Turner, J.; Marshall, G.J.; Connolley, W.M.; and Lachlan-Cope, T.A. (2002). Antarctic Peninsula Climate Variability and its Causes as Revealed by Analysis of Instrumental Records. *British Antarctic Survey*, *Natural Environment Research Council*

Oppenheimer, M. (1998). Global Warming and the Stability of the West Antarctic Ice Sheet. *Nature*. **393**, pp. 325-332.

Scambos, T.A; Bohlander, J.A.; Shuman, C.A.; and Skvarca, P. (2004). Glacier Acceleration and Thinning after Ice Shelf Collapse in the Larsen B Embayment, Antarctica. *Geophysical Research Letters*. **31**, L18402.

Sergienko, O.; and MacAyeal, D. R. (2005). Surface Melting on the Larsen Ice Shelf, Antarctica. *Annals of Glaciology*. **40,** pp. 215-218.

Steig, E.J., Schneider, D.P., Rutherford, S.D., Mann, M.E., Comiso, J.C., and Shindell, D.T.: Warming of the Antarctic Ice Sheet Surface since the 1957 International Geophysical Year. Nature, 457, 459-462, 2009.

Turner, J.; Colwell, S.R.; Marshall, G.J.; Lachlan-Cope, T.A.; Carleton, A.M.; Jones, P.D.; Lagun, V.; Reid, P.A.; and Iagovkina, S. (2005). Antarctic Climate Change During the Last 50 Years. *International Journal of Climatology*. **25**: pp. 279-294.

Chapter 2

Estimation of Surface Melt Magnitude Over Ross Ice Shelf, Antarctica, Using Satellite-Derived Estimates of Liquid Water Fraction

Satellite based assessments of melt from passive microwave systems are typically used to detect the presence of surface melt on Antarctic Ice Shelves, although they are limited in that they only provide an indication of melt occurrence and have coarse spatial resolution. What follows is an algorithm developed to retrieve surface melt magnitude using coupled near-IR and thermal surface measurements from MODIS, calibrated by estimates of liquid water fraction (LWF) in the upper 1cm of the firn derived from a one-dimensional thermal snowmelt model (SNTHERM). SNTHERM was forced by hourly meteorological data from automatic weather station (AWS) data at four reference sites spanning a range of melt conditions across the Ross Ice Shelf during the most extensive melt season in the MODIS satellite record, 2002-03. Effective melt magnitude or $LWF_{<eff>}$ was derived for 8-day composite periods covering the Austral summer months of December and January at a 4km resolution over the entire Ross Ice Shelf, and ranges from 0-0.5% $LWF_{<eff>}$ in early December to as much as 1% $LWF_{<eff>}$ during the time of peak surface melt in late January in areas along the coast. This work represents a step forward in characterizing not only melt occurrence and duration but also melt magnitude, and at a higher spatial resolution than current passive microwave melt detection methods.

Introduction

The dramatic response of an ice shelf to recent atmospheric warming is exemplified along the Antarctic Peninsula (AP), which has experienced significant warming of up to 0.56^{o}C per decade in the latter half of the 20th century (King et al. 2002; Turner et al. 2005). The recent disintegration of the Larsen A (1600 km^2) and B (3200 km^2) Ice Shelf complex in 1995 and 2002

prompted interest in understanding the role of regional climate warming in the stability of Antarctic ice shelves. In particular, surface melt on Larsen B has been shown to not only have been substantial during the 2001-2002 melt season (Sergienko and MacAyeal 2005) but also one of the primary causes of its collapse through surface ponding and melt-enhanced fracture propagation (Scambos et al., 2004; van den Broeke 2005). More recently, Steig et al. (2009) documented increasing temperatures (0.17^{o}C +/- 0.06^{o}C increase per decade) over West Antarctica, especially during the spring and winter months. These temperature increases would support a likely greater frequency of ice shelf collapse in the future if surface melting were to become more frequent as well.

Although surface melt is not the only driver for mass loss--basal melting due to ocean heat flux may also be significant (e.g. Rignot and Jacobs, 2002)--it remains an important component. Currently, surface melt is assessed as a binary melt state of occurrence or non-occurrence, primarily through the use of passive microwave approaches (e.g. Ridley 1993; Abdalati and Steffen 1995; Tedesco 2007) or microwave scatterometry (e.g. Nghiem et al. 2001; Steffen et al. 2004). A broader evaluation of the spatio-temporal variability of surface melt over all Antarctic ice shelves would improve our ability to assess how changes in climate affect ice shelf stability. This study develops a method for the determination of surface liquid water fraction; a quantitative measure of surface melt magnitude that is not measured with existing microwave melt algorithms. This increased level of melt detection has important implications for the detection of total surface melt, and could be used operationally in the future to detect the early stages of melt lake formation—beyond the initial melting but prior to the formation of melt ponds that could be detected through the use of visible satellite imagery.

Background

Previous studies addressing the issue of surface melt have focused on the use of microwave radiometry and scatterometry melt detection algorithms applied to both Antarctica and Greenland, which take advantage of rapid increases in microwave emissivity when surface scattering begins to dominate emissions of the ice surface over volume scattering (Mätzler and Hüppi 1989; Jezek et al. 1994; Ridley 1993; Zwally and Fiegles 1994; Abdalati and Steffen 1995; Mote and Anderson 1995; Nghiem et al. 2001; Mote, 2007 and several others). A sharp change in brightness temperature, measured from microwave radiometers, quickly saturates at approximately 1% liquid water fraction, and prevents the quantitative assessment of surface melt fraction using microwave frequencies. Surface melt derived from scatterometry cannot resolve the absolute wetness of the snowpack, as radar backscatter amounts depend not only on snow wetness but also on grain size. The effect of grain size on backscatter is minimized by focusing on diurnal backscatter differences and assuming that the grain size does not change over the course of the day, and that diurnal backscatter changes are the result of a change in snow wetness (Nghiem et al., 2001). This is a reasonable assumption, as the solid/liquid state of the snowpack near the surface is more ephemeral than changes in effective grain size.

Other parts of the electromagnetic spectrum (EMS) offer potential advantages for the retrieval of surface melt magnitude. Snow is a selective absorber in the near-IR portion (wavelength 1.2-1.4 μm) of the EMS, with albedo ranging from near-complete reflectance to near-complete absorbance over the solar (wavelength 0.3-3.0 μm) spectrum (Nolin and Dozier 2000). While the bulk optical properties of ice and water are similar, reflectance and transmittance are largely dependent on variations in the complex refractive index of the ice, where specifically absorption is due to variations in the imaginary part of the complex refractive index of ice (Dozier 1989). The absorption coefficient varies substantially in the wavelengths

from 0.4 to 2.4 μm (Dozier 1989). Several studies have examined the strong relationship between snow spectral reflectance and grain-size, and modeled snow reflectance from the optical properties of snow and ice (Bohren and Barkstrom 1974; Wiscombe and Warren 1981; Nolin and Dozier 2000; Painter et al. 2003). Changes in snow reflectance in the near-infrared (NIR) band are strongly dependent on changes in optical grain size (Warren and Wiscombe 1980), with an inverse relationship between albedo and grain size. This relationship is strongest at 1.03μm and 1.26μm where the difference in reflectance between small and large grains is most substantial (Hyvärinen and Lammasniemi 1987; Nolin and Dozier 2000). As grain size increases, optical depth in the near-IR decreases from 3cm to about 0.5cm, assuming constant snowpack density (Nolin and Dozier 2000). In wet snow with high liquid water content, heat flow from large grains causes smaller particles, which are at lower temperature, to melt and merge into larger clusters (Colbeck 1982; Colbeck 1989). As bulk grain cluster radius increases, an incident photon will have a high probability of being scattered when it traverses the air-ice interface, but a greater chance of absorption while passing through the ice grain (Warren 1982). Grain clusters optically behave as single grains, increasing the mean photon path length, subsequently increasing the opportunity for absorption and reduction in reflectance. Larger grains increase the degree of absorption, particularly in the near-IR region, causing a substantial reduction in reflectance. The maximum sensitivity of reflectance to changes in grain size is in the near-IR region of the EMS at approximately 1.1 μm (Nolin and Dozier 2000). Because near-IR reflectance is proportional to grain size, which in turn is partially dependent on the degree of melting that has occurred, it can be used as a proxy for quantifying the amount of surface melt present in the snowpack (Lampkin and Yool 2004; Peng 2007; Lampkin and Peng 2008). However, the use of snow surface reflectance alone to track surface melt is not sufficient, because substantial decreases in reflectance are not due solely to grain enlargement associated with entrained liquid water. For example, small amounts of absorbing impurities can also reduce snow reflectance in the visible

wavelengths (Warren and Wiscombe 1981; Grenfell et al. 1981; Bohren 1986). In this case, surface temperature can be used as a plausible mechanism in isolating the component in reduced reflectance that is due to the melt process—this is described below.

Snow thermal emission (8-14 μm wavelengths) is a function of snow surface skin temperature and emissivity (Marks and Dozier 1992). Snow surface temperature information coupled with near-IR reflectance information can assist in refining the assessment of melt magnitude acquired from near-IR reflectance alone. Surface melt is physically driven by increases in skin temperature above freezing, and higher temperatures can therefore be correlated to areas where more surface melt is occurring. Lampkin and Yool (2004) employed visible, near-IR, and thermal-IR information from satellite imagery to create a near-surface moisture index (NSMI), which provided a categorical determination of snow wetness in alpine areas, but not quantitative estimates for liquid water fraction. This index relied on the decreased visible and near-IR albedo of snow as melting and grain size increased.

Lampkin and Peng (2008) demonstrated the feasibility of retrieval of effective surface liquid water fraction ($LWF_{<eff>}$) through calibrating satellite-derived near-IR and thermal signatures from MODIS with a physical snowmelt model (SNTHERM89) forced by meteorological data collected from Greenland Climate Network (GC-Net) stations on the western portion of the Greenland Ice Sheet. This empirical retrieval has been designated as effective melt magnitude (E-melt) primarily because it represents a measure of temporally-integrated liquid water fraction over an 8-day period at $1km^2$ within the upper 5cm of the glacial firn at a relative accuracy of ~ ±2%, rather than an instantaneous measurement of surface liquid water faction at a point. This methodology is limited to an 8-day temporal resolution due to the opacity of clouds to near-IR and thermal-IR radiation, requiring multiple satellite overpasses to obtain a spatially contiguous image. I propose using a similar method for detecting and quantifying surface melt on Antarctic ice shelves. Due to the lack of significant numbers of meteorological instruments on

most West Antarctic ice shelves, I focus the development of the retrieval algorithm over the Ross Ice Shelf. The Ross Ice Shelf contains the largest density of surface AWS locations of any area of Antarctica. Therefore, this study will focus on the better-instrumented Ross Ice Shelf for the development of an empirical method to quantify $LWF_{<eff>}$ in the upper layers of firn. This method relies on changes in the bulk crystal size of the firn as melt is occurring, which is detected via: 1) the relationship between optical grain size and near-IR albedo, and 2) the relationship between thermal emission and melt conditions.

Study Region

The Ross Ice Shelf (Figure 1) spans a region along the Antarctic coast from 165^{o}W across the 180th meridian to 165^{o}E. Although the grounding line of Ross extends poleward to approximately 86^{o}S, most surface melt is typically confined to the warmest areas along the coastal ice shelf margin as well as at the base of the Transantarctic Range (Liu et al. 2006). Sea ice abuts the ice shelf front, which extends northward to 77^{o}S at the westernmost corner, and 78^{o}S on the eastern side. The Transantarctic Mountains border the western flank of the Ross Ice Shelf, and the Siple Coast is located along the eastern Side. Several large ice streams feed the ice shelf from the Siple Coast side, while smaller but still significant outlet glaciers through the Transantarctic range provide paths for both ice and katabatic winds to flow onto the shelf from the East Antarctic Plateau. These winds are seen to be important controls on the climate of the Ross Ice Shelf as is discussed in Chapter 4.

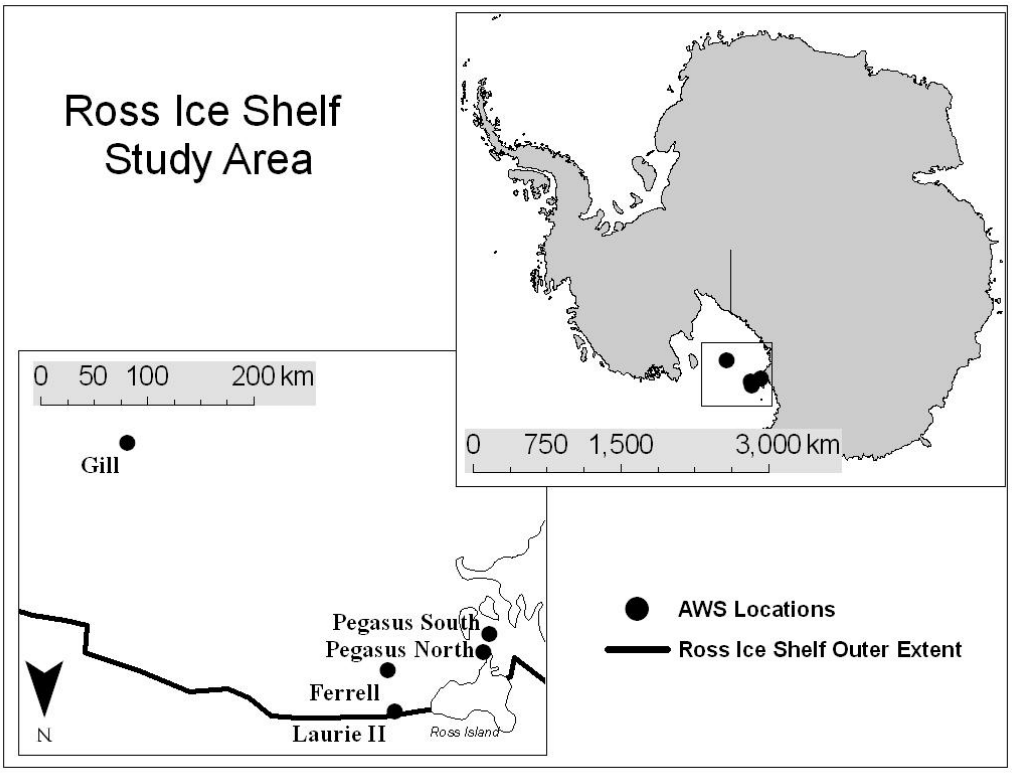

Figure 2-1: Ross Ice Shelf Study Area

Data

Output from a one-dimensional snow energy balance model (SNTHERM89, Jordan, 1991) is used to calibrate MODIS satellite data in both the near-IR band 5 (wavelength 1.23-1.25μm) as well as surface skin temperature. SNTHERM89 requires several input variables that are not all currently recorded by any AWS network. Consequently, several other sources of data were necessary to acquire and use as SNTHERM89 input. Data used in this study included AWS-recorded wind speed, temperature, and relative humidity; National Centers for Environmental Prediction(NCEP)/National Center for Atmospheric Research (NCAR) Reanalysis-derived radiation fluxes and precipitation, measured shortwave radiation from the National Science Foundation (NSF) UV-Vis Monitoring Network, and MODIS near-IR and surface skin

temperature imagery for the Dec 2002-Jan 2003 time period. While wind direction is included with the AWS data, SNTHERM89 is purely a physical model and does not allow for the input of wind direction as a variable. Even though the Antarctic Peninsula (AP) has experienced the largest changes in surface temperatures, and has experienced some of the most significant effects of ice shelf surface melting, readily available AWS data for the AP is limited to only one location (the Larsen AWS) for our study time period. Additionally, the AP is unlikely to be representative of other areas of Antarctica, given its northerly latitude. Therefore, to create a robust empirical model for surface melt, data must be used from another location that has a denser network of weather stations. The Ross Ice Shelf serves as a location where some surface melt occurs during the peak of the summer season, but with an overall lower ambient temperature than Larsen, and contains several AWSs with a continuous meteorological record over a summer season (2002-03) when some surface melting is known to have occurred from Cross-Polarized Gradient Ratio (XPGR; Abdalati and Steffen, 1995 and 1997) passive microwave measurements (Liu et al. 2006).

AWS Network

The National Science Foundation Office of Polar Programs AWS project (Stearns, et al. 2009) comprises a variably dense network across Antarctica used to support field forecasting as well as a range of climate studies. It is supported by the University of Wisconsin Antarctic Meteorological Research Center, with data available online. Several Ross Ice Shelf stations have data for the 2002-03 study season, allowing for a wide sampling of climate conditions. Five stations are used for the model calibration, including: Pegasus North, Pegasus South, Gill, Ferrell, and Laurie II. These sites record temperature, wind speed, and relative humidity as well as other weather variables. Data were obtained for each of the listed variables at 10-minute intervals for

all five stations. They were then manually quality-controlled and averaged to 6-hourly time-steps to correspond with the 6-hourly output from NCEP/NCAR reanalysis.

NCEP/NCAR Reanalysis

The NCEP/NCAR reanalysis (Kalnay et al. 1996) output is available online at a 2.5^{o}x2.5^{o}, 6-hourly resolution. Several meteorological variables not available from the AWS network were obtained for the reanalysis gridpoint closest to each reference AWS site. From 6-hourly averaged precipitation rate estimates, 6-hourly precipitation totals were calculated. Downwelling shortwave, reflected shortwave, and downwelling longwave radiation fluxes were also obtained from the reanalysis dataset. Bromwich and Fogt (2004) mention that ERA40 reanalysis is more accurate than NCEP/NCAR reanalysis output for the middle and high latitudes of the southern hemisphere; however, ERA40 reanalysis has been compiled only through Aug, 2002. There is no ERA40 reanalysis information currently available for any melt season with a spatially and/or temporally substantial (as determined by XPGR) amount of surface melting on the Ross Ice Shelf that falls within the MODIS archive time period. The quality of the NCEP/NCAR output has been shown, however, to be better for the summer months and toward the latter part of the data record, when more satellite information was fed into the reanalysis algorithms. Despite the coarse spatial resolution of the NCEP/NCAR reanalysis dataset, generally low precipitation amounts, and the insensitivity of our calibration procedure to precipitation forcing render the reanalysis output sufficient for our analysis.

NSF UV/VIS (UltraViolet/VISible) Monitoring Network

Although downwelling solar radiation data is available from the NCEP/NCAR reanalysis project, a sensitivity study described later in this chapter showed that these radiation values create unrealistically high liquid water fractions at the reference stations, and reanalysis values were substantially larger than radiation fluxes measured at the ground in other locations. For this reason, it was determined that the radiation output from the NCEP/NCAR reanalysis was unsuitable for this study. Measured radiation data from a ground source were therefore necessary for SNTHERM forcing. Radiation data from McMurdo station were provided by the NSF UV Monitoring Network, operated by Biospherical Instruments Inc., under a contract from the United States National Science Foundation's Office of Polar Programs via Raytheon Polar Services Company. Mean incoming shortwave measurements over the 0.29 to 0.6μm wavelengths were averaged over 6-hourly time periods for the 2002-03 ablation season, then the values were doubled to provide an "upper-bound" estimate for insolation over the UV and visible wavelengths. This "doubling" is intended to account for the fact that this data does not include the entire solar spectrum, but only a portion. We found that shortwave radiation fluxes were substantially lower than those estimated in the NCEP/NCAR reanalysis dataset, often by as much as 50% for some time periods. Reflected shortwave radiation was estimated by calculating the surface albedo from NCEP/NCAR reanalysis and applying that factor to the measured radiation from the NSF UV monitoring network. It is thought that the surface albedo from the NCEP/NCAR reanalysis is more reliable than the radiation data itself. Because measured downwelling longwave measurements were not available, it was necessary to use estimates from NCEP/NCAR reanalysis for this SNTHERM input.

Satellite Data

MODIS reflectance in the near-IR (1.23-1.25 μm) and thermal-IR derived surface skin temperatures were obtained from the NASA Warehouse Inventory Search Tool (WIST). MODIS/Aqua Surface Reflectance 8-Day L3 Global 500m SIN Grid V004 and MODIS/Aqua Sea Ice Extent and Ice Surface Temperature Daily L3 Global 4km Ease-Grid Day V005 imagery (Hall et al. 2007), products MYD09A1and MYD29E1, respectively, were used in this study. The Near-IR reflectance was obtained via MODIS band 5, a region of the EMS where reflectance is known to be highly dependent on snow grain size, and therefore carries a signature of surface melt history. Because cloud cover is opaque to infrared radiation, it is impossible for the satellite to detect near-IR reflection and surface skin temperature values at the Earth's surface unless a clear sky is present. Therefore, a cloud mask is applied to the MODIS imagery product, significantly reducing the temporal frequency of the available clear-sky imagery. To reduce the number of data gaps caused by this effect, composite imagery over a number of consecutive days was necessary, increasing the geographic coverage but decreasing the temporal resolution. Version 4 8-day composite imagery is available for surface reflectance; however Version 5 data is currently unavailable for near-IR reflectance for this time period and study area, as MODIS imagery is no longer processed south of 70^{o}S. Because 8-day composite imagery is unavailable for ice shelf surface temperature it was necessary to manually composite the thermal imagery to the same 8-day periods as the reflectance imagery. The MYD29E1 product was used to composite 8-day imagery from the daily 4km Land (skin) Surface Temperature (LST) product and stored on a 4km grid as the average values of clear-sky LST during an 8-day period. Although 1km resolution ice surface temperature is available from the NSIDC, these data have significant gaps across the 180^{o} meridian, which crosses through the middle of the study area, so the more spatially contiguous 4km resolution imagery was used.

Passive microwave brightness temperatures (Armstrong and Brodzik, 1995, updates through 2011) were obtained for XPGR validation. Ascending and Descending horizontal and vertical polarizations at 19GHz (19H) and 37GHz (37V) were used to obtain a daily averaged XPGR for the Ross Ice Shelf and vicinity (Abdalati and Steffen 1995; Abdalati and Steffen 1997). These data are available online from the National Snow and Ice Data Center (NSIDC).

Methods

The calibration phase of this study involves using SNTHERM89 to produce estimates of snow pack near surface bulk liquid water content. SNTHERM89 is a one-dimensional mass and energy balance model for estimating mass and energy fluxes through strata of snow and soil. It is comprehensive in scope, capable of simulating dynamic processes (Jordan 1991). The version used in this project was adapted to estimate model snow melt conditions over glacier ice, which involved adding ice material properties to the SNTHERM89 material library (modifications courtesy of S. Frankenstein, CRREL). SNTHERM89 was forced (Figure 2-2, boxes 1, 2, 3) using 2m air temperature, relative humidity, and wind speed (all from the AWS); downwelling shortwave (NSF UV/Vis); reflected shortwave (NSF UV/Vis) multiplied by albedo (calculated from NCEP/NCAR reanalysis); downwelling longwave radiation and precipitation amount (both from NCEP/NCAR Reanalysis). In addition to the meteorological forcing data, SNTHERM89 also requires precipitation type and effective diameter of precipitation as input. It was assumed for purposes of this study that precipitation remained frozen; with an effective diameter of 0.5mm (Sensitivity studies described later in this chapter show that SNTHERM89 is not sensitive to initial grain size). SNTHERM89 initialization snowpack stratigraphy was supplied by Dr. Konrad Steffen (personal communication, 2008) from a snow pit dug on the Greenland ice sheet. While not necessarily representative of initial conditions on the Ross Ice Shelf, our sensitivity tests show

that SNTHERM89 responds quickly to atmospheric forcing such that melt conditions in the upper layers are not dependent on initial conditions after about 72 hours of simulation.

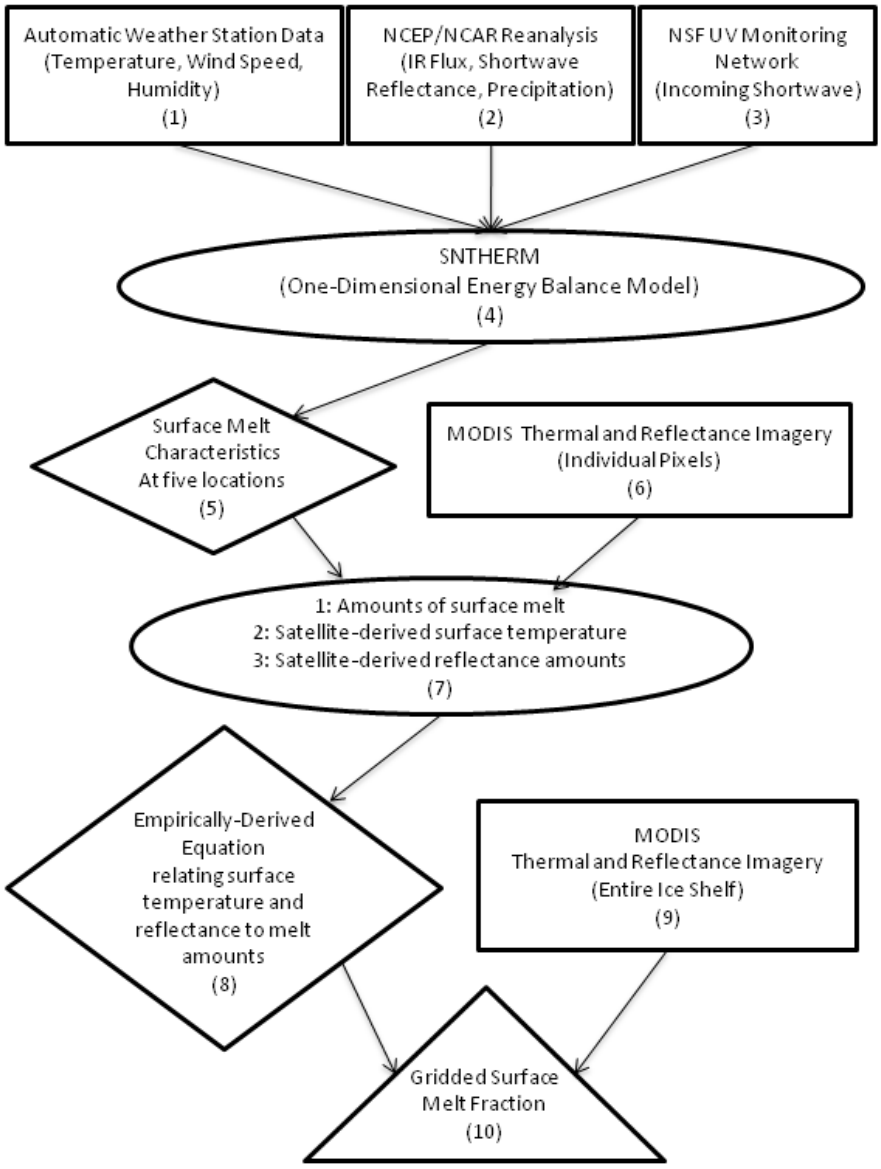

Figure 2-2: Process Flowchart (Rectangle = Primary Data Source, Oval= Processes, Diamond = Intermediate Output, Triangle = Primary Output)

SNTHERM89 output was retrieved at 6-hourly time steps over the two month study period (Figure 2-2, box 4). Liquid Water Fraction (LWF) in the upper 1cm of the snowpack

(Figure 2-2, box 5) was used as representative of the effective optical retrieval depth through which the MODIS satellite can collect reflectance and thermal information. Simulated daily LWF was recorded at 12z, which is closest to the MODIS overpass time, and averaged over each 8-day composite period for each of the four AWS reference sites. A 3-dimensional planar regression was obtained between LWF (dependent variable) and MODIS band 5 reflectance and MODIS-derived skin temperature (independent variables, Figure 2-2, box 6) for each composite period and each study site on the Ross Ice Shelf (Figure 2-2, box 7). From this regression, a relationship for LWF as a function of reflectance and thermal signature was developed (Figure 2-2, box 8). This function was applied to the entire Ross Ice Shelf (Figure 2-2, box 9) where MODIS band 5 reflectance and MODIS skin temperature are known, but melt fraction is unknown—the empirical retrieval of $LWF_{<eff>}$ (Figure 2-2, box 10). Table 1 compares the spatial, temporal, and melt resolutions of three methods for assessing surface melt. XPGR has a coarser spatial resolution than the coupled near-IR and thermal method, and neither QuikSCAT nor XPGR are able to resolve effective liquid water fraction to obtain a magnitude of surface melt.

Table 2-1: Comparison of Various Methods for Assessing Surface Melt

	XPGR (Passive Microwave)	QuikSCAT Backscatter (Microwave Scatterometer)	Coupled near-IR and Thermal IR
Spatial Resolution	12.5-25km	2.225km	1-4km
Temporal Resolution	Daily	Daily	8-day
Melt Resolution	Binary	Binary	Magnitude

MODIS LST was processed at a 4km scale over Antarctic ice shelves, giving the coupled near-IR and thermal retrieval model an effective 4km resolution over the Ross Ice Shelf. MODIS

LST and atmospherically corrected shortwave Infrared (SWIR) surface reflectance grids were acquired over an analysis period spanning from December through January, during the 2002-03 Antarctic ablation season in 8-day composite periods. Although this retrieval scheme has a lower temporal resolution than standard passive microwave techniques, our method has higher spatial resolution and will allow for the determination of melt water fraction in the firn, whereas active and passive microwave methodologies only detect the presence or absence of melt above some fixed threshold. Additionally, the coupled near-IR and thermal method is particularly useful for detecting local-scale melt events that are unresolved by coarser-resolution passive microwave techniques. The finer spatial resolution provides important information about melt events despite the necessarily lower temporal resolution.

Results

Melt Magnitude Retrieval Model Results

The coupled near-IR and thermal retrieval model shows little to no melt for five of the seven composite periods and spatially-constrained areas of low liquid water fraction (0.5-1%) for the other two composite periods. Throughout most of December, most of the Ross Ice Shelf experiences no surface melting at all. An increase in surface melt fractions is seen during the January 2-9 composite period over the western half of the ice shelf (Figure 2-3). This is followed by a refreeze during the Jan 10-17 period (Figure 2-4) and a spatially expansive surface melt event on the coastal eastern portion of the ice shelf from Jan 18-25 (Figure 2-5). Although the two detected melt events (Jan 2-9 and Jan 18-25) were spatially coherent, the magnitude of the surface melting was low (1% or less) in both cases.

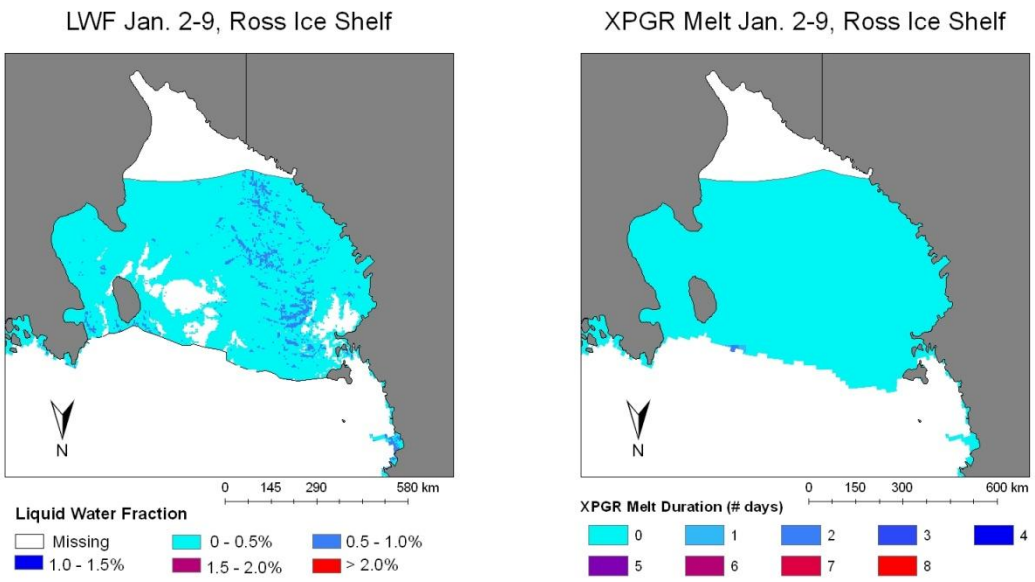

Figure 2-3 : Effective Surface Melt Magnitude (left) and XPGR melt occurrence (right) for Composite Period Jan. 2-9, 2003

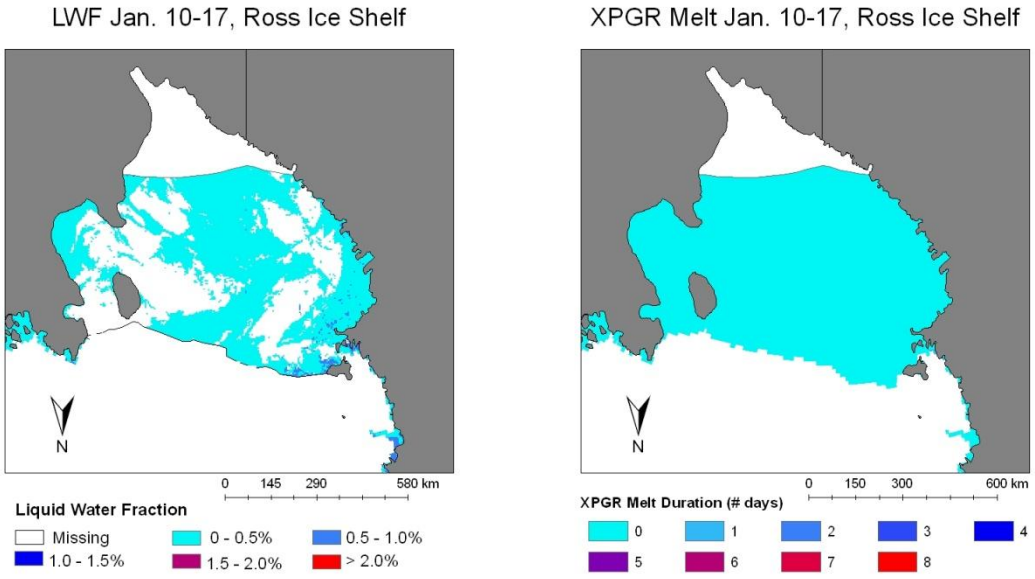

Figure 2-4: Effective Surface Melt Magnitude (left) and XPGR melt occurrence (right) for Composite Period Jan. 10-17, 2003

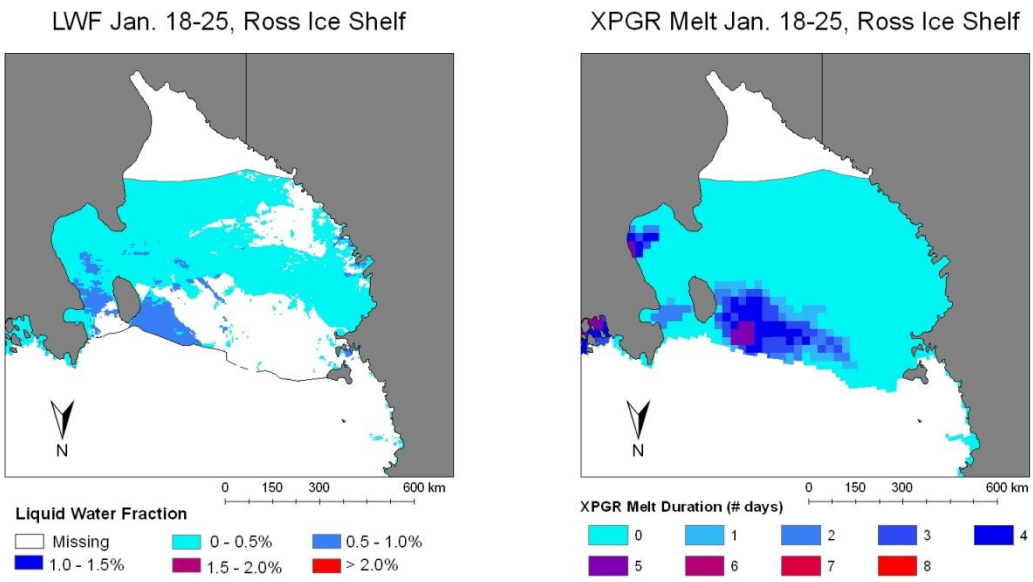

Figure 2-5: Effective Surface Melt Magnitude (left) and XPGR melt occurrence (right) for Composite Period Jan. 18-25, 2003

During the January 2-9 melt event there is both a signature in reflection and surface skin temperature that is consistent with a low $LWF_{<eff>}$ melting event. Temperatures in the > 0.5% melt are slightly above 269K (-4°C). A transect of $LWF_{<eff>}$, reflectance and surface temperature through the area experiencing melt (Figure 2-6) shows a strong signal in the ice surface temperature associated with higher $LWF_{<eff>}$ values, and ambient temperatures that are close enough to freezing for some melt to occur. While temperatures remain ~4K below freezing, it is possible that surface melt is occurring if there is some temperature heterogeneity over the 8-day composite period and over the spatial extent of the 4km grid size. As the surface skin temperature is providing only the average temperature value integrated over an 8-day period and a 4km pixel size, some temperatures are necessarily higher than reported, and some may therefore be above freezing. This melt event was marginal, with very low $LWF_{<eff>}$, and with a spatial distribution that would be difficult to detect in passive microwave analyses due to their coarse spatial resolution (Figure 2-3).

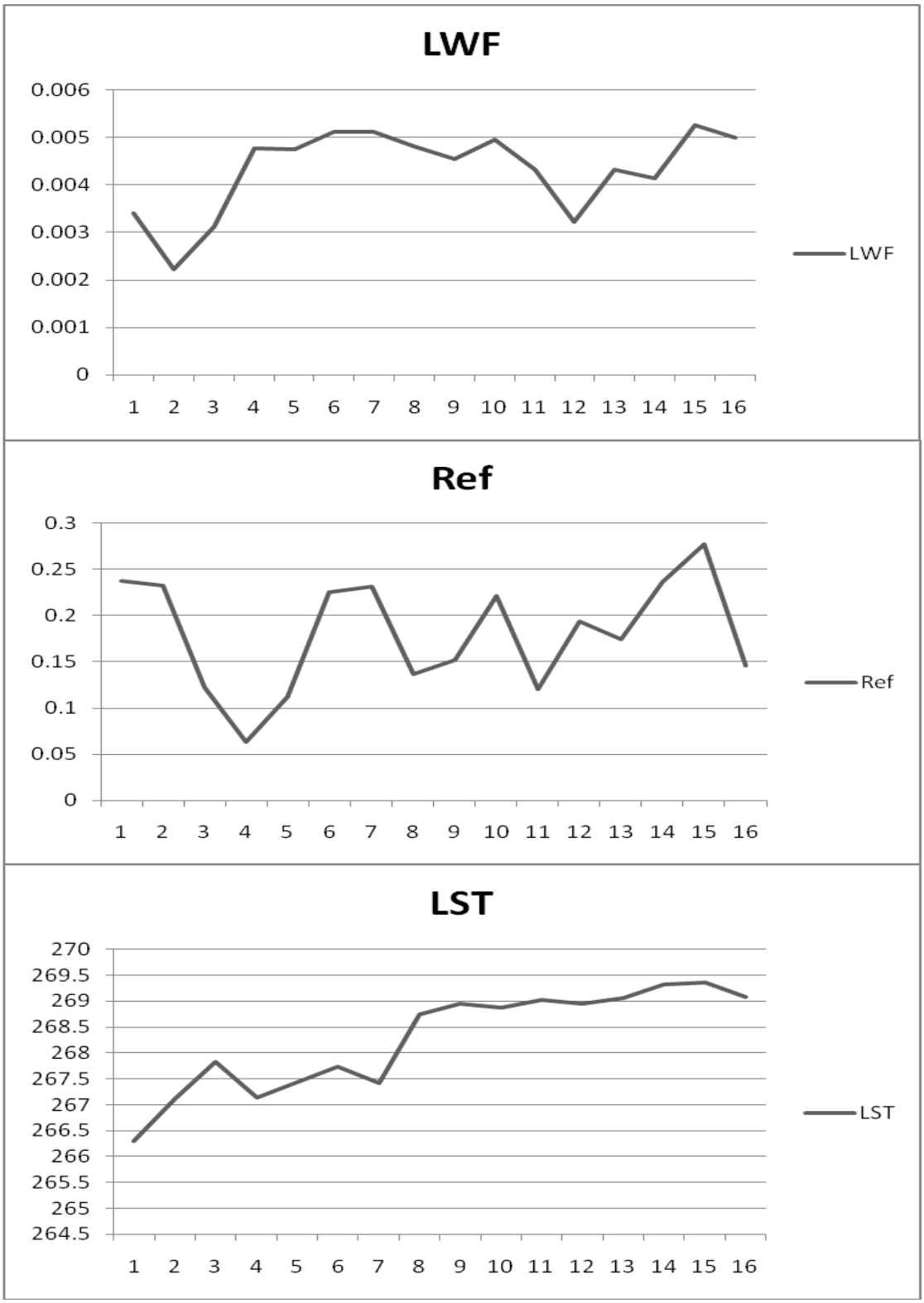

Figure 2-6: E-W Transect through low LWF melt area on Ross Ice Shelf

XPGR Comparison

The melt magnitude retrieval model comparison was accomplished using the XPGR (Abdalati and Steffen 1995; Abdalati and Steffen 1997) over the Ross Ice Shelf for coincident time periods. The XPGR provides a binary indication of melt occurrence, and is sensitive to changes in the dielectric constant of ice as surface liquid water fractions rise above 1%. Although daily XPGR were calculated, these were aggregated to the same 8-day composite periods as the MODIS archive for a more direct comparison of the two melt characterization methods. Therefore, the number of melt days for each pixel during each MODIS 8-day composite period is presented.

The coupled near-IR and thermal melt magnitude retrieval model shows generally good agreement with passive microwave XPGR melt occurrence, that is the presence of melt in the XPGR was generally recorded as a melt event in the coupled near-IR and thermal method. Of the seven composite periods in the December-January study period, five exhibited little to no surface melting anywhere on the ice shelf. One composite period showed melt in a coincident time and place between the two melt assessments (January 18-25). Finally, one (January 2-9) had some discrepancies between the two melt retrieval methods where XPGR showed no melting and the coupled near-IR/thermal method showed discontinuous areas on the western half of the ice shelf of 0.5 to 1% $LWF_{<eff>}$.

The largest spatially contiguous area of surface melting is found during the last (January 18-25) composite period (Figure 2-5), where large areas of the Ross Ice Shelf surrounding Roosevelt Island show as much as 1% surface melting. This melting is seen in both the XPGR surface melt determination as well as the near-IR and thermal effective melt retrieval, and both methods show the melt as being both spatially and temporally consistent with one another. Effective melt magnitudes range from 0.5% to 1% during this time period within the areas shown

by XPGR to be experiencing surface melting. XPGR detected surface melting during one to five of the eight days of the composite period (depending on exact location), so it is likely that surface melt magnitudes were in excess of 1% for part of the composite period, even though the average melt over the entire 8-day composite period was below the 1% threshold for XPGR detection. Most differences between the two melt detection methods are likely due to differences in spatial resolution. The MODIS methodology is able to detect small melt events that the XPGR is unable to detect. Each of the discontinuous areas of surface melt retrieved by the MODIS methodology was small enough such that it may not have been detected by the XPGR methodology.

Further evaluation of MODIS-derived melt magnitude was undertaken by examining how $LWF_{<eff>}$ varies with melt duration (the number days melt was detected) for certain locations on the ice sheet. This is accomplished by calculating a mean $LWF_{<eff>}$ of all pixels that correspond to particular melt duration (number of melt days), as determined from XPGR within each 8-day composite period (Figure 2-7). A comparison between $LWF_{<eff>}$ and XPGR melt duration for the January 18-25 composite period shows the lowest $LWF_{<eff>}$values (average of 0.29%) corresponding to XPGR melt duration of zero days. Slightly higher $LWF_{<eff>}$ (average of 0.43%) are seen for an XPGR melt duration of one day. At XPGR melt durations of two to five days, average $LWF_{<eff>}$ was between 0.53% and 0.54%, indicating only slightly higher $LWF_{<eff>}$ values for XPGR melt durations of 5 days than for XPGR melt durations of 2 days. During this melt event, XPGR did not detect any areas with melt durations longer than five days.

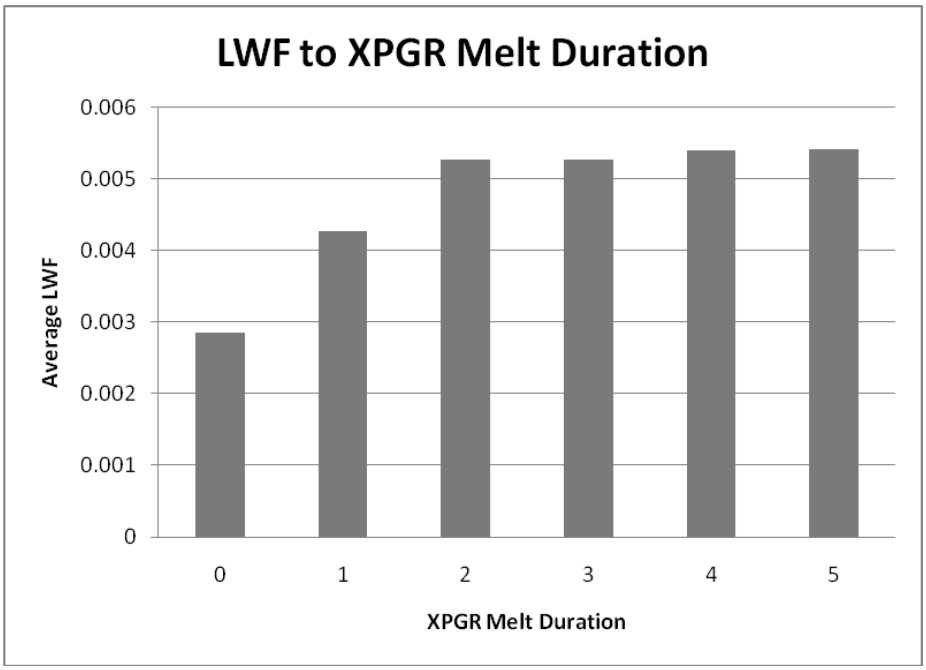

Figure 2-7: Comparison of LWF to XPGR Melt Duration

Model Validation and Uncertainty

Several sensitivity tests were performed to analyze the effects of downscaling uncertainty from the use of gridded NCEP/NCAR reanalysis output as SNTHERM input variables. Although NCEP/NCAR incoming shortwave radiation output was not used in the calibration of LWF in this study, it is useful in explaining how variation in radiation input to SNTHERM can affect liquid water fraction. Precipitation and radiation measurements were estimated from reanalysis output for each of the five AWS reference locations on the Ross Ice Shelf. To test how SNTHERM responded to changes in these variables, several melt simulations were calculated for Pegasus South using 2x, 4x and 0.5x precipitation (Figure 2-8), and incoming shortwave radiation plus 5% and minus 5% (Figure 2-9).

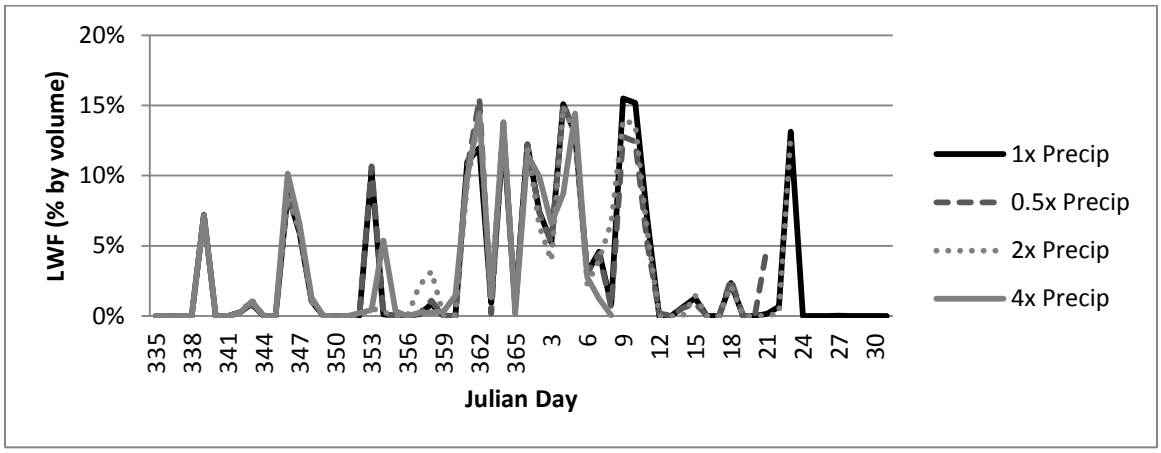

Figure 2-8: Precipitation Sensitivity Analysis at 8-day composite (top) and Daily (bottom) time intervals using NCEP/NCAR Reanalysis Radiation data and 0.5x, 1x, 2x and 4x precipitation for SNTHERM forcing at Pegasus South station.

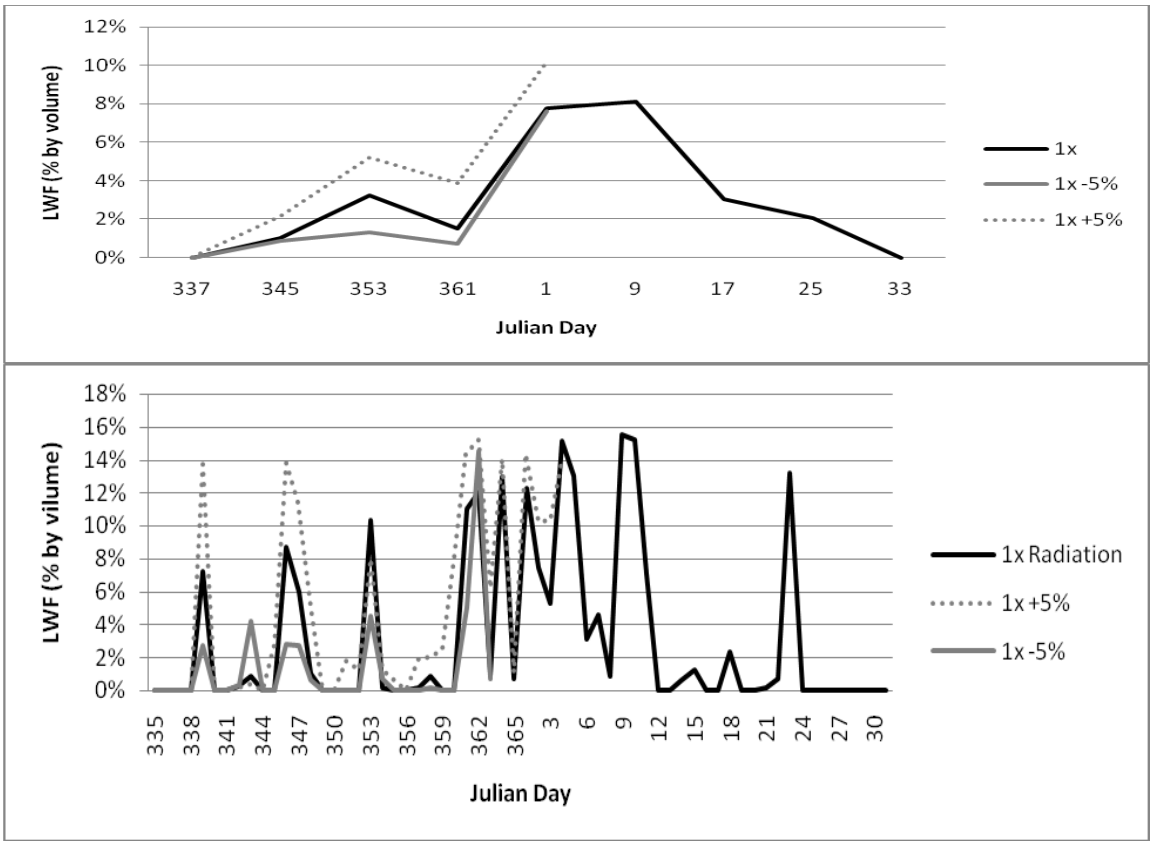

Figure 2-9: Radiation Sensitivity Analysis at 8-day composite (top) and Daily (bottom) time intervals using variations in NCEP/NCAR radiation data as forcing for SNTHERM at Pegasus South Station

The changes in incoming solar radiation represent a range of downscaling uncertainty in cloud cover over the reanalysis grid cell. From these runs, it was clear that precipitation has little effect (less than 1% LWF) on the melt characterization at Pegasus South. Although precipitation rates can vary within the area comprising a reanalysis grid cell, these variations would not induce large changes in surface LWF within the cell. Larger changes were seen in the radiation sensitivity test. Increasing the downward flux of shortwave radiation by 5% doubled the LWF at the test site, whereas decreasing the radiation flux by 5% halved the LWF. These sensitivity tests show that uncertainty in the downscaling of radiation flux can have a significant effect on SNTHERM output, which can therefore cause uncertainty in the retrieved surface LWF values. If accurate radiation measurements were obtainable at each AWS site, a more precise estimation of surface $LWF_{<eff>}$ could be obtained using the coupled near-IR/thermal method.

Another sensitivity test was used to determine the effects of the SNTHERM initialization snow stratigraphy on surface LWF (Figure 2-10). Observed temperatures at depth for December, 2007 at Nascent Iceberg, Ross Ice Shelf, supplied by Dr. Doug MacAyeal (Personal Communication, 2009) were substituted into the original SNTHERM stratigraphy. This caused a net change in surface LWF of less than 1% for each of the December composite periods. Little variation was seen even in the LWF values at the daily scale. As the SNTHERM model responds quickly to meteorological forcing conditions, differences in the initialization parameters have little effect on surface melt output. Consequently, as long as a reasonable initialization stratigraphy is used, there is little influence on surface LWF values from subtle differences in firn stratigraphy.

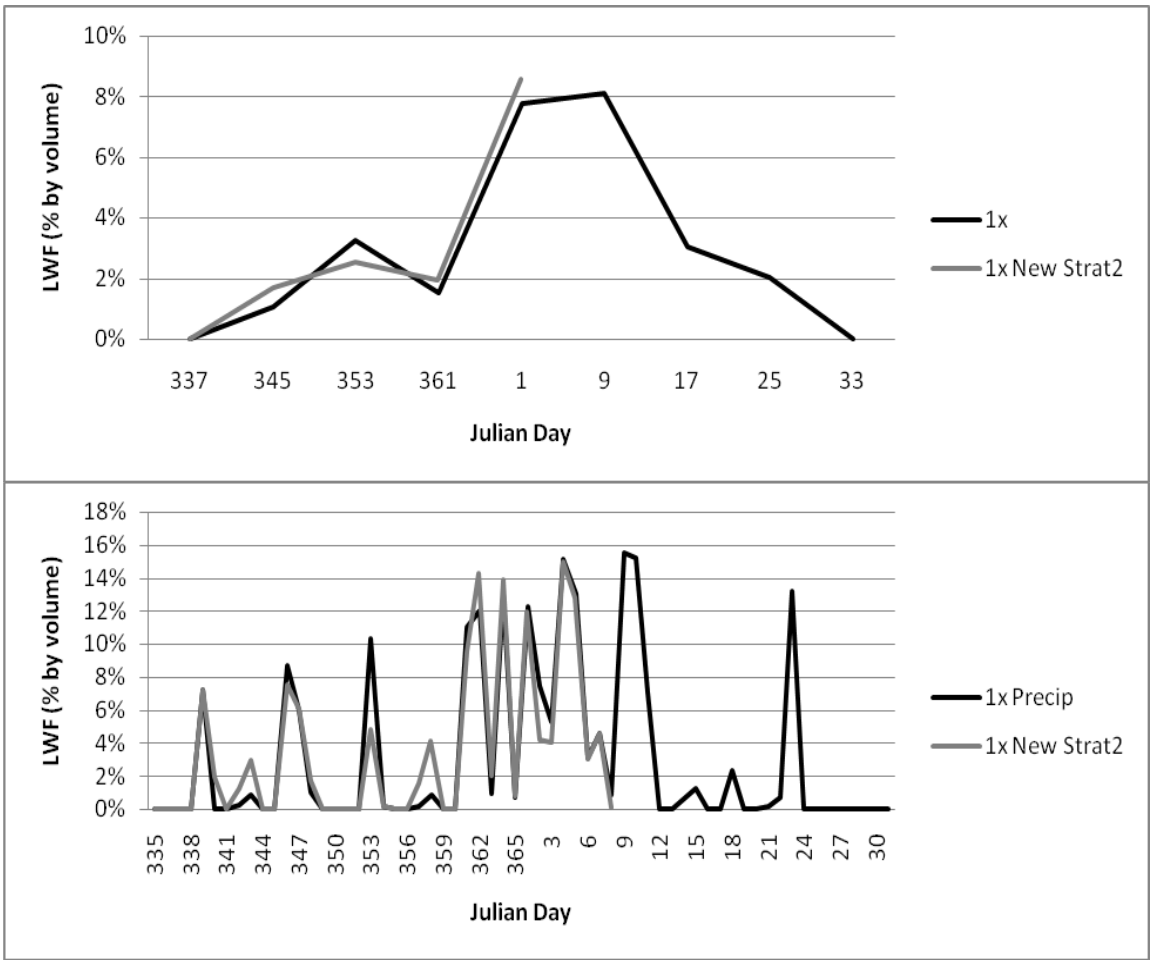

Figure 2-10: Stratigraphy Sensitivity Analysis at 8-day composite (top) and Daily (bottom) time intervals using NCEP/NCAR radiation forcing for SNTHERM at Pegasus South Station.

Additionally, a sensitivity test was conducted to examine the effects of running SNTHERM at time scales that are more conducive to capturing energy flux changes on the hourly scale. These short-term energy fluxes are thought to be responsible for the majority of surface melting on cold ice shelves. A power law relationship was derived between timescale and the standard deviation of insolation to determine the hourly variability of insolation (Figure 2-11). SNTHERM was then forced with hourly AWS measurements and pseudo-random hourly insolation values (insolation values varying with the same mean and standard deviation as those outputted in the reanalysis) with a mean interpolated from average insolation at each hour across

the two-month timescale, and an appropriate standard deviation of 60% of the mean as obtained from Figure 2-11. LWF values aggregated to 8-day composite periods using SNTHERM forced on an hourly timescale did not differ significantly from values obtained using the six-hourly forcing.

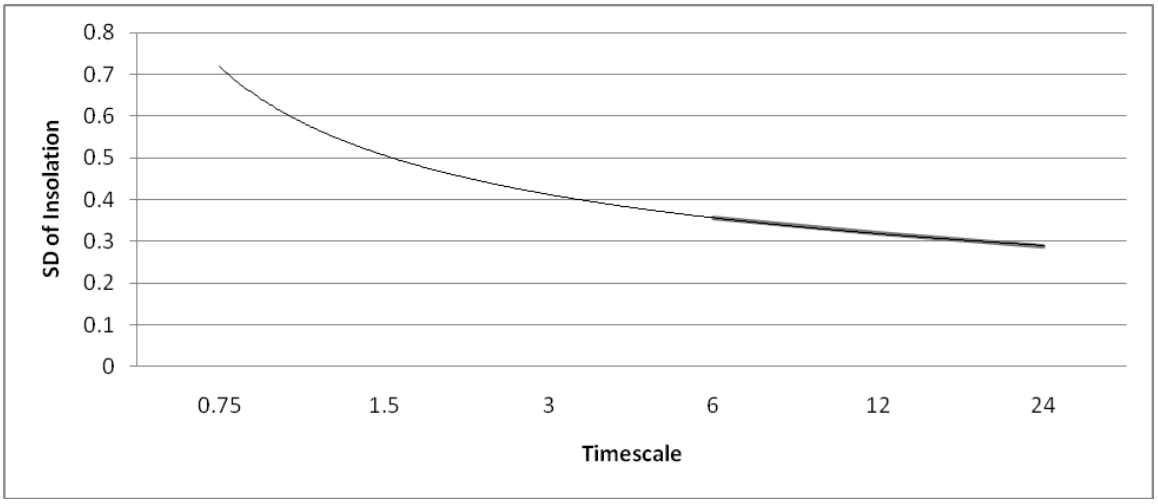

Figure 2-11: Variability in the Standard Deviation of incoming solar radiation as a power function of time scale in hours.

Further validation of the coupled near-IR and thermal methodology was accomplished by spot checks of $LWF_{<eff>}$ as a function of Positive Degree Days (PDD) at four reference locations for the 2004-05 and 2005-06 melt seasons (Figure 2-12). PDD was calculated as the average number of degrees Celsius above freezing ($0^{o}C$) each day for the 8-day composite period. These spot-checks showed generally low $LWF_{<eff>}$ for Gill AWS (<0.2%) coinciding with low PDD values (<0.1 PDD/day). Pegasus North AWS and Ferrell AWS demonstrate a positive relationship between $LWF_{<eff>}$ and PDD, while the relationship between $LWF_{<eff>}$ and PDD appears to saturate for Pegasus South AWS at approximately 1%, which is the upper limit of the effectiveness of the $LWF_{<eff>}$ calibration. The relationship was best described by a logarithmic curve with Pearson's R value of 0.61.

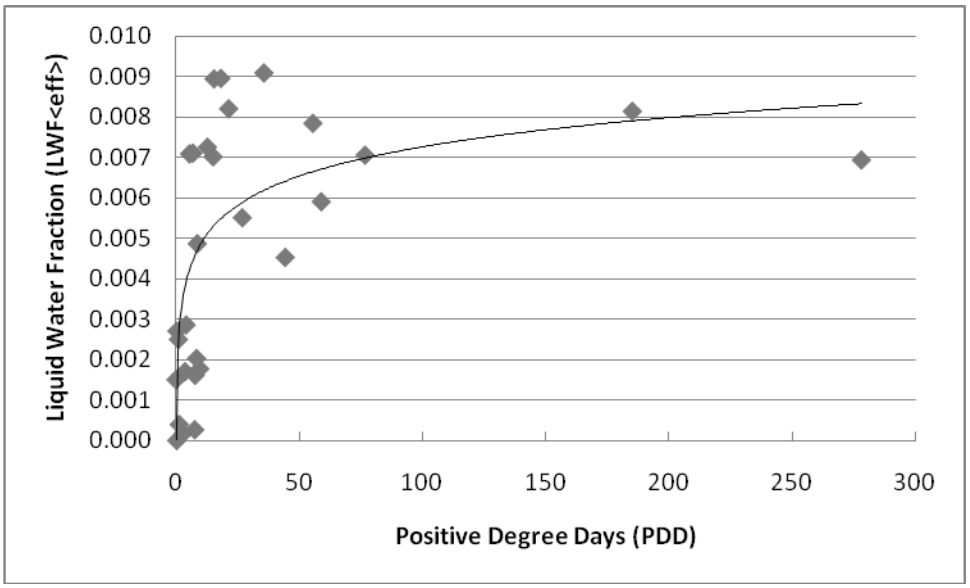

Figure 2-12: Liquid Water Fraction as a Function of Positive Degree Days (per day) at four Ross Ice Shelf locations for melt seasons 2004-05 and 2005-06. R2 = 0.43, R = 0.66.

As the MODIS calibration empirical model contains many data sources, there are several potential error sources that need to be accounted for (Table 2). The relative error contribution from MODIS data includes 0.38% from ice surface temperature (Wan et al. 2004; Hall et al. 2004) and 2% from reflectance (Liang et al. 2002). Resistances in AWS thermistors are known to within 1% and anemometers are calibrated to a 0.5% tolerance (Stearns et al. 1993). Sensitivity analyses show that a doubling of precipitation creates a 0.5% variation, and varying the radiation by +/- 5% can affect LWF values by 1.4%. The standard error of regression for the MODIS calibration was 0.5%. The total relative error in this study was 2.8%.

Table 2-2: Relative Error Estimates

Error Source	Error Amount	Citation
Ice Surface Temperature	+/- 0.38% (1^{o}C)	Wan et al., 2004; Hall et al, 2004
Reflectance	+/- 2%	Liang et al., 2002
Precipitation	+/- 0.5%	Sensitivity Testing
Radiation	+/- 1.4%	Sensitivity Testing
AWS Thermistor Error	+/- 1%	Stearns et al., 1993
AWS Anemometer Error	+/- 0.5%	Stearns et al., 1993
Regression Error	+/- 0.5%	Standard Error
Total Relative Error	+/- 2.8%	

Discussion

In general, the two methodologies for assessing surface melt conditions, XPGR and the coupled near-IR and thermal method for retrieving effective melt magnitude are consistent with one another. Effective melt magnitudes were low, mostly 0-0.5% when/where XPGR did not detect any surface melting, and slightly higher, mostly 0.5-1%, when/where XPGR detected melting. While this melt event would correspond to only the most marginal of events for an area such as the Antarctic Peninsula, it was a fairly substantial melt event for the much colder Ross Ice Shelf.

One melt event not detected by XPGR was identified in the coupled near-IR and thermal methodology during the January 2-9 composite period. Melt signatures associated with strong downsloping winds (as shown by NCEP/NCAR reanalysis composite maps) are especially evident in the center of the ice shelf at this time. Strong southerly winds were indicated by NCEP/NCAR reanalysis over the eastern half of the Ross Ice Shelf. Effective melt is shown to

increase at this time over the center of the ice shelf spatially coincident with the path of these katabatic-like winds. While katabatic winds are typically considered to be a result of cold air descending off the Antarctic Plateau, there are other instances (as described in Chapter 4) where winds with similar spatial patterns and intensity are not driven by the decent of dense cold air. Rather, in some instances, cyclonic circulation can develop over the Ross Sea and draw air downward from the plateau. This would have the net effect of adiabatically warming the air from the plateau, which can be detected as a temperature increase at the level of the ice shelf. The signature observed in the coupled near-IR and thermal methodology may be an increase in surface melt fraction that is not yet high enough (or at a spatial scale large enough) to cause changes in the bulk dielectric constant of the surface at the 25km resolution, and therefore cannot be detected through passive microwave imagery. Bromwich (1989) noted that katabatic wind strength can be identified in warm thermal IR signatures, which understandably are manifested in the surface melt magnitude derived using the thermal IR band. Alternatively, the increase in effective melt during the January 2-9 composite period not identified by XPGR could be explained as a coarsening of grains as a result of wind sorting. This would decrease the near-IR reflectance of the firn and would produce a signature in the coupled near-IR and thermal methodology similar to that of melt.

By the middle of January (Figure 2-4), large areas of the ice sheet begin to show little effective melt again, and the katabatic-like regime of the previous composite period weakens. Analysis of surface LWF during this period is complicated by the persistent cloud cover over most of the eastern half of the ice sheet, and large portions of the western half as well, although cloud-free pixels in this region show what appears to be re-freezing taking place. Southwesterly winds predominate over the ice sheet during this period, inhibiting any marine influence from offshore polynyas.

The January 18-25 composite period was the more substantial melt event and was detected by both XPGR and the coupled near-IR and thermal methods. The surface melting during this period corresponded to weak, onshore surface winds on the eastern half of the ice shelf advecting warm maritime air over the ice shelf. This suggests that the maritime influence of surface air blowing over a near-shore polynya may contribute to conditions that are conducive to surface melting. Near McMurdo, which was not identified as an area experiencing surface melt in XPGR, stronger offshore winds seemed to inhibit the generation of surface melt. This indicates the presence of at least two different synoptic-scale weather patterns that can contribute to surface melting with distinct signatures. Onshore winds can create large-scale areas of surface melting along the shoreline, whereas offshore winds generate surface melting at a smaller scale and confined to the areas where winds are strongest.

The comparison between average $LWF_{<eff>}$ at $4km^2$ resolution and XPGR (Figure 2-7) shows monotonic increase in $LWF_{<eff>}$ for XPGR melt duration of zero, one, and two days, with a saturation in $LWF_{<eff>}$ at an XPGR melt duration of 2 days or longer. This saturation effect is likely the result of low amounts of surface melting during this event, with no areas recording greater than 1% surface LWF during any composite period. The sample size for the XPGR melt durations of four and five days were each less than ten pixels, while the number of pixels with zero day melt duration was greater than 400. For XPGR, there is evidence that the category of no-melt, or zero days of occurrence, consistently exhibits effective melt fractions between 0-0.4% and can be slightly higher (0.3-0.5%) for a single occurrence throughout the composite period. Abdalati and Steffen (1997) specify that the XPGR threshold will register a pixel as melting when surface LWFs by volume are in excess of 1%. Although no pixels showed $LWF_{<eff>}$ values of greater than 1%, no pixels experienced melt every day during the composite period as determined by XPGR. A refreezing during part of the composite period—which was evidenced in the XPGR methodology—would effectively dilute a marginal melt event such that the $LWF_{<eff>}$ would be

less than 1% when aggregated over 8-days despite LWF values greater than 1% over some individual days.

Although the coupled near-IR and thermal methodology for effective melt fraction retrieval is an advancement on previous melt detection algorithms, further calibration is necessary for improving the accuracy of effective melt retrieval over warmer ice shelves such as Larsen. Current calibration is only useful for detection of surface melt magnitude of 2.5% or less. In addition, the relationship derived between LWF, near-IR reflectance and ice surface temperature that is created during the calibration process is not necessarily best represented by a planar correlation. Surface melting cannot occur with surface skin temperatures below freezing, but because of variations in surface temperature within a spatially heterogeneous pixel, a fixed 273K cutoff for surface melting is not realistic. To remedy this problem, an investigation using artificial neural networking to generate a calibration curve would be useful.

Conclusions

The coupled near-IR and thermal method for assessing surface melt offers several advantages over passive microwave and microwave scatterometry (Table 2-1). The spatial resolution is higher than passive microwave, and the coupled near-IR/thermal method can therefore detect melt events occurring on a smaller spatial scale. The ability to retrieve surface melt magnitude is another improvement over both passive microwave and microwave scatterometry. The most significant drawback of the coupled near-IR/thermal methodology is the decrease in temporal resolution from daily to 8-day although it is balanced by the increased information offered regarding melt magnitude as opposed to merely melt occurrence. The coupled near-IR/thermal methodology, while providing important information regarding the state of surface melt on Antarctic ice shelves, is not meant to replace traditional methods for detecting

surface melt presence, such as XPGR. Rather, when used in combination with these methods, the coupled near-IR/thermal method can provide a quantitative estimate of melt fraction which has not previously been available through other remote sensing methodologies. Ground-based validation of the surface liquid water retrieval method would be beneficial in further constraining the error in this analysis. At the current time, insufficient surface observation networks prevent such validation in the near-term.

Whereas this chapter focused on the detection and quantification of surface melt, the next chapter examines the climatology of surface melt events across other West Antarctic ice shelves. This brings about a better understanding of the meteorological conditions that generate surface melt, and provides an important context to understanding how surface melt conditions may change in a warming climate.

References

Abdalati, W. and Steffen, K.: Passive Microwave-Derived Snow Melt Regions on the Greenland Ice Sheet. Geophysical Research Letters, 22, 787-790, 1995.

Abdalati, W. and Steffen, K.: Snowmelt on the Greenland Ice Sheet as Derived from Passive Microwave Satellite Data. Journal of Climate, 10, 165-175, 1997.

Armstrong, R.L. and Brodzik, M.J.: An Earth-Gridded SSM/I Data Set for Cryospheric Studies and Global Change Monitoring. Advances in Space Research, 16, 155-163. 1995. Data available online: http://nsidc.org/data/docs/daac/nsidc0032_ssmi_ease_tbs.gd.html

Bohren, C.: Applicability of effective-medium theories to problems of scattering and absorption by nonhomogeneous atmospheric particles. Journal of Atmospheric Science, 43, 468-475, 1986.

Bohren, C. and Barkstrom, B.: Theory of the optical properties of snow. Journal of Geophysical Research, 79, 4527-4535, 1974.

Bromwich, D.H.: Satellite Analyses of Antarctic Katabatic Wind Behavior. Bulletin of the American Meteorological Society, 70, 738-749, 1989.

Bromwich, D.H. and Fogt, R.L.: Strong Trends in the Skill of the ERA-40 and NCEP-NCAR Reanalyses in the High and Midlatitudes of the Southern Hemisphere, 1958-2001. Journal of Climate, 17, 4603-4619, 2004.

Colbeck, S.C.: An Overview of Seasonal Snow Metamorphism. Reviews of Geophysics and Space Physics. 20, 45-61, 1982.

Colbeck, S.: Snow-crystal Growth with varying surface temperatures and radiation penetration. Journal of Glaciology, 35, 23-29, 1989.

Dozier, J.: Spectral Signature of Alpine Snow Cover from the Landsat Thematic Mapper. Remote Sensing of the Environment, 28, 9-22, 1989.

Grenfell, T., Perovich, D., and Ogren, J.: Spectral albedo of an alpine snowpack. Cold Regions Science and Technology, 4, 121-127, 1981.

Hall, D.K., Key, J.R., Casey, K.A., Riggs, G.A., and Cavalieri, D.J.: Sea Ice Surface Temperature Product from MODIS. IEEE Transactions on Geoscience and Remote Sensing. 42, 5, 1076-1087, 2004.

Hall, D.K., Riggs G.A., and Salomonson, V.V.: MODIS/Aqua Sea Ice Extent and IST Daily L3 Global 4km EASE-Grid Day V005, Dec. 1, 2002-Jan 25, 2003. Boulder, Colorado USA: National Snow and Ice Data Center. Digital media. 2007, updated daily.

Hyvärinen, T., and Lammasniemi, J.: Infrared Measurement of Free-Water Content and Grain Size of Snow. Optical Engineering, 26, 342-348, 1987.

Jezek, K., Gogineni, P., and Shanableh, M.: Radar Measurements of Melt Zones on the Greenland Ice Sheet. Geophysical Research Letters. 21, 33-36, 1994.

Jordan, R.: A One-Dimensional Temperature Model for a Snow Cover, Technical Documentation for SNTHERM89. 1991.

Kalnay, E., Kanamitsu, M., Kistler, R., Collins, W., Deaven, D., Gandin, L., Iredell, M., Saha, S., White, G., Woollen, J., Zhu, Y., Leetmaa, A., and Reynolds, B.: The NCEP/NCAR Reanalysis 40-year Project. Bulletin of the American Meteorological Society, 77, 437-471, 1996.

King, J.C., Turner, J., Marshall, G.J., Connolley, W.M., and Lachlan-Cope, T.A. Antarctic Peninsula Climate Variability and its Causes as Revealed by Analysis of Instrumental Records. British Antarctic Survey, Natural Environment Research Council. 2002.

Lampkin, D. and Peng, R.: Empirical Retrieval of Surface Melt Magnitude from Coupled MODIS Optical and Thermal Measurements over the Greenland Ice Sheet during the 2001 Ablation Season. Sensors, 8, 4915-4947, 2008.

Lampkin, D.J. and Yool, S. R.: Monitoring Mountain Snowpack Evolution Using Near-Surface Optical and Thermal Properties. Hydrological Processes. 18, 3527-3542, 2004.

Liang, S., Fang, H., Chen, M., Shuey, C.J., Walthall, C., Daughtry, C., Morisette, J., Schaaf, C., and Strahler, A.: Validating MODIS land surface reflectance and albedo products: methods and preliminary results. Remote Sensing of Environment, 83, 149-162, 2002.

Liu, H.; Wang, L.; and Jezek, K. C.: Spatiotemporal Variations of Snowmelt in Antarctica Derived from Satellite Scanning Multichannel Microwave Radiometer and Special Sensor Microwave Imager Data (1978-2004). Journal of Geophysical Research, 111, F01003, 2006.

Marks, D., and J. Dozier.: Climate and energy exchange at the snow surface in the alpine region of the Sierra Nevada, 2: Snow cover energy balance, Water Resources Research, 28, 3043-3054, 1992.

Mätzler, C. and Hüppi, R.: Review of Signature Studies for Microwave Remote Sensing of Snowpacks. Advances in Space Research, 9, (1)253-(1)265, 1989.

Mote, T.L.: Greenland surface melt trends 1973-2007: Evidence of a large increase in 2007, Geophysical Research Letters, 34, L22507, 2007.

Mote, T. and Anderson, M.: Variations in snowpack melt on the Greenland ice sheet based on passive microwave-measurements, Journal of Glaciology. 41, 51-60, 1995.

Nghiem, S.V., Steffen, K., Kwok, R., and Tsai, W.-Y.: Detection of Snowmelt Regions on the Greenland Ice Sheet using Diurnal Backscatter Change. Journal of Glaciology, 47, 539-547, 2001.

Nolin, A.W. and Dozier, J.: A Hyperspectral Method for Remotely Sensing the Grain Size of Snow. Remote Sensing of the Environment, 74, 207-216, 2000.

Painter, T., Dozier, J., Roberts, D., Davis, R., and Green, R.: Retrieval of subpixel snow-covered area and grain size from imaging spectrometer data. Remote Sensing of Environment, 85, 64-77, 2003.

Peng, R.: Estimation of surface melt intensity using optical and thermal measurements over the Greenland ice sheet, M.S. thesis, Department of Geography, Pennsylvania State University. 2007.

Ridley, J.: Surface Melting on Antarctic Peninsula Ice Shelves Detected by Passive Microwave Sensors. Geophysical Research Letters, 20, 2639-2642, 1993.

Rignot, E., and Jacobs, S.S.: Rapid Bottom Melting Widespread near Antarctic Ice Sheet Grounding Lines. Science, 296, 5575, 2020-2023, 2002.

Scambos, T.A, Bohlander, J.A., Shuman, C.A., and Skvarca, P.: Glacier Acceleration and Thinning after Ice Shelf Collapse in the Larsen B Embayment, Antarctica. Geophysical Research Letters, 31, L18402, 2004.

Sergienko, O. and MacAyeal, D. R.: Surface Melting on the Larsen Ice Shelf, Antarctica. Annals of Glaciology, 40, 215-218, 2005.

Steffen, K., Nghiem, S.V., Huff, R., and Neumann, G.: The Melt Anomaly of 2002 on the Greenland Ice Sheet from Active and Passive Microwave Satellite Observations. Geophysical Research Letters, 31, L20402, 2004.

Steig, E.J., Schneider, D.P., Rutherford, S.D., Mann, M.E., Comiso, J.C., and Shindell, D.T.: Warming of the Antarctic Ice Sheet Surface since the 1957 International Geophysical Year. Nature, 457, 459-462, 2009.

Stearns, C.R., Keller, L.M., Weidner, G.A., and Stevens, M.: Monthly Mean Climatic Data for Antarctic Automatic Weather Stations, in: Antarctic Meteorology and Climatology: Studies Based on Automatic Weather Stations, AGU Antarctic Research Series, American Geophysical Union, Washington, DC, 1-21, 1993.

Stearns, C.: Automatic Weather Station Project, University of Wisconsin-Madison, funded by the National Science Foundation of the United States of America. Ongoing.

Tedesco, M.: Snowmelt Detection over the Greenland Ice Sheet from SSM/I Brightness Temperature Daily Variations. Geophysical Research Letters, 34, L02504, 2007.

Turner, J., Colwell, S.R., Marshall, G.J., Lachlan-Cope, T.A., Carleton, A.M., Jones, P.D., Lagun, V., Reid, P.A., and Iagovkina, S.: Antarctic Climate Change during the Last 50 Years. International Journal of Climatology, 25, 279-294, 2005.

van den Broeke, M.: Strong Surface Melting Preceded the Collapse of Antarctic Peninsula Ice Shelf. Geophysical Research Letters, 32, L12815, 2005.

Wan, Z., Zhang, Y., Zhang, Q., and Li, Z.-L.: Quality assessment and validation of the MODIS global land surface temperature. International Journal of Remote Sensing, 25, 1, 261-274, 2004.

Warren, S.G.: Optical Properties of Snow. Reviews of Geophysics and Space Physics, 20, 67-89, 1982.

Warren, S.G. and Wiscombe, W.J.: A Model for the Spectral Albedo of Snow. II: Snow Containing Atmospheric Aerosols. Journal of the Atmospheric Sciences, 37, 2734-2745, 1980

Wiscombe, W. J. and Warren, S.G.: A Model for the Spectral Albedo of Snow. I: Pure Snow. Journal of the Atmospheric Sciences, 37, 2712-2733, 1981.

Zwally, H. and Fiegles, S.: Extent and duration of Antarctic surface melt, Journal of Glaciology, 40, 463-476, 1994.

Chapter 3

Synoptic-Scale Weather Forcing of Surface Melt on West Antarctic Ice Shelves from 1987-2002

Introduction

This chapter examines the extent to which several atmospheric variables force surface melt on several West Antarctic Ice Shelves. Although the previous chapter examined surface melting on the Ross Ice Shelf specifically, this area is not prone to surface melt events that are large in extent, magnitude or duration. The Larsen Ice Shelf and the series of ice shelves along the Amundsen Bellingshausen Sea coastline experience surface melt conditions much more frequently than Ross Ice Shelf, so when the three regions are considered together, a broad range of surface melt conditions can be examined.

Recent work (Steig et al., 2009) has reaffirmed that Antarctica has warmed over the last several decades, and the Antarctic Peninsula in particular has undergone a rapid regional warming of greater than 0.5^{o}C per decade in the latter half of the 20^{th} Century (Turner et al., 2005). In a warming climate, surface melting on polar ice shelves is of great concern because it can lead to ice shelf destabilization and collapse. The recent dramatic temperature increases along the Antarctic Peninsula coincided with the collapse of both the Larsen B Ice Shelf in 2002 and large portions of the Wilkins Ice Shelf in 2008. Prior to the collapse of the Larsen Ice Shelf, large ponds developed as a result of substantial surface melting (Sergienko and MacAyeal, 2005) and these ponds were discernible with MODIS visible satellite imagery. The melt ponds drained into crevasses, allowing cracks to propagate to the base of the ice sheet, leading to fragmentation and ultimately catastrophic collapse (van den Broeke, 2005). Basal melt is another important

consideration in the ice sheet mass balance system, especially at the grounding line and under fast-moving glaciers, and is highly correlated to changes in ocean temperature (Rignot and Jacobs, 2002). Although collapse of the ice shelves does not directly contribute to sea level rise, glaciers previously feeding collapsed ice shelves become unbuttressed and surge rapidly, by as much as a 600% velocity increase in the case of Larsen B (Scambos et al., 2004). This rapid increase of glacier velocity can contribute to sea level rise, which is of particular concern in coastal regions worldwide. Ice shelves, therefore, provide an important constraint on ice sheet stability, and are components of an ice sheet system that are both vulnerable to surface warming, and crucial to maintaining ice sheet equilibrium.

While anthropogenic greenhouse warming is thought to threaten stability of the West Antarctic Ice Sheet (Oppenheimer, 1998), the specific climatic mechanisms that drive surface melting remain unexplored in any comprehensive manner. I hypothesize that mesoscale and synoptic scale interactions in the coupled system of atmosphere, ocean, sea ice and ice shelf present important controls on heat exchange responsible for driving the duration and magnitude of ice-shelf surface melt dynamics. Antarctic sea ice plays an important role in the Antarctic climate system, through modifying radiative, energy, and mass exchange processes occurring via the ice-albedo feedback, its insulating effect on ocean-to-atmosphere moisture and heat exchanges, deep water formation and the fresh water budget (Curry et al., 1995; Rind et al., 1995). In particular, sea ice affects the surface energy balance by capping the upper layer of the ocean, thereby reducing the exchange of heat and moisture between the ocean and the atmosphere. The opening of off-shore leads and sustained coastal polynyas causes significant increases in temperature and humidity along the margins of the ice sheet (Kottmeier and Engelbart, 1992), with evidence of an increase in latent and sensible heat flux over open ocean water as compared to sea ice (Ledley, 1988). Changes in atmospheric circulation affecting the dominant wind direction have the potential to advect relatively warm, moist maritime air

(potentially modulated by sea ice conditions) onto an ice shelf. Or conversely, offshore winds may advect cold, dry air off the ice shelves, initially inhibiting melting, but opening up polynyas and leads. Solar heating and katabatic winds are also important processes that can influence ice shelf surface energy balance, and are thought to have positive and negative influences on surface melting (respectively). Providing an assessment of the climatic controls on surface melting would assist in determining which ice shelves would be at risk of high surface melt rates and potential collapse given certain climate conditions.

One way to assess the climate forcing of historical melt events is through the use of a synoptic classification technique. Yarnal et al. (2001) and Hewitson and Crane (2002) point to the use of Self-Organizing Maps (SOMs), a neural-network approach to climate downscaling, as one of the more promising methods of synoptic weather type classification following the GIS revolution of the late 1990s. This innovation is significant in that it allows for a non-liner relationship among different climate variables to be explained. Coupled with a 20-year record of melt occurrence from passive microwave (XPGR), SOMs can provide information about climate and physical conditions that prevail during melt events. Identification of the associated synoptic-scale weather patterns can provide insight to the physical processes responsible for the generation and persistence of surface melt conditions over Antarctic ice shelves.

Study Area

The areas considered in this analysis are separated into three regions (Figure 3-1). The first region is the Ross Ice Shelf (Ross Region), which is bisected by the 180^{o} meridian and extends from approximately 77^{o}S to 86^{o}S. The second region is the Larsen Ice Shelf (Larsen Region). This ice shelf is significantly farther north than the Ross Ice Shelf, and is located along the Antarctic Peninsula near 60^{o}W longitude at approximately 65^{o}S. The Larsen Ice Shelf

experiences greater than 50% surface melt extent at some point in nearly every summer season (Liu et al., 2006), and is the northernmost major ice shelf on the Antarctic continent. The third region is a series of smaller ice shelves along the West Antarctic coastline bordering the Amundsen and Bellingshausen Seas (ABS Region). These ice shelves are warmer and experience more surface melting than Ross Ice Shelf, but cooler than and experience less surface melt in general than Larsen Ice Shelf. The ABS region includes the Wilkins Ice Shelf, notable for its partial collapse in 2008 and 2009; the Wordie Ice Shelf, which receded over several decades in the late 20th century and has since disappeared; and the Abbot and Getz ice shelves, which are substantially larger than either Wilkins or Wordie but remain stable at this time.

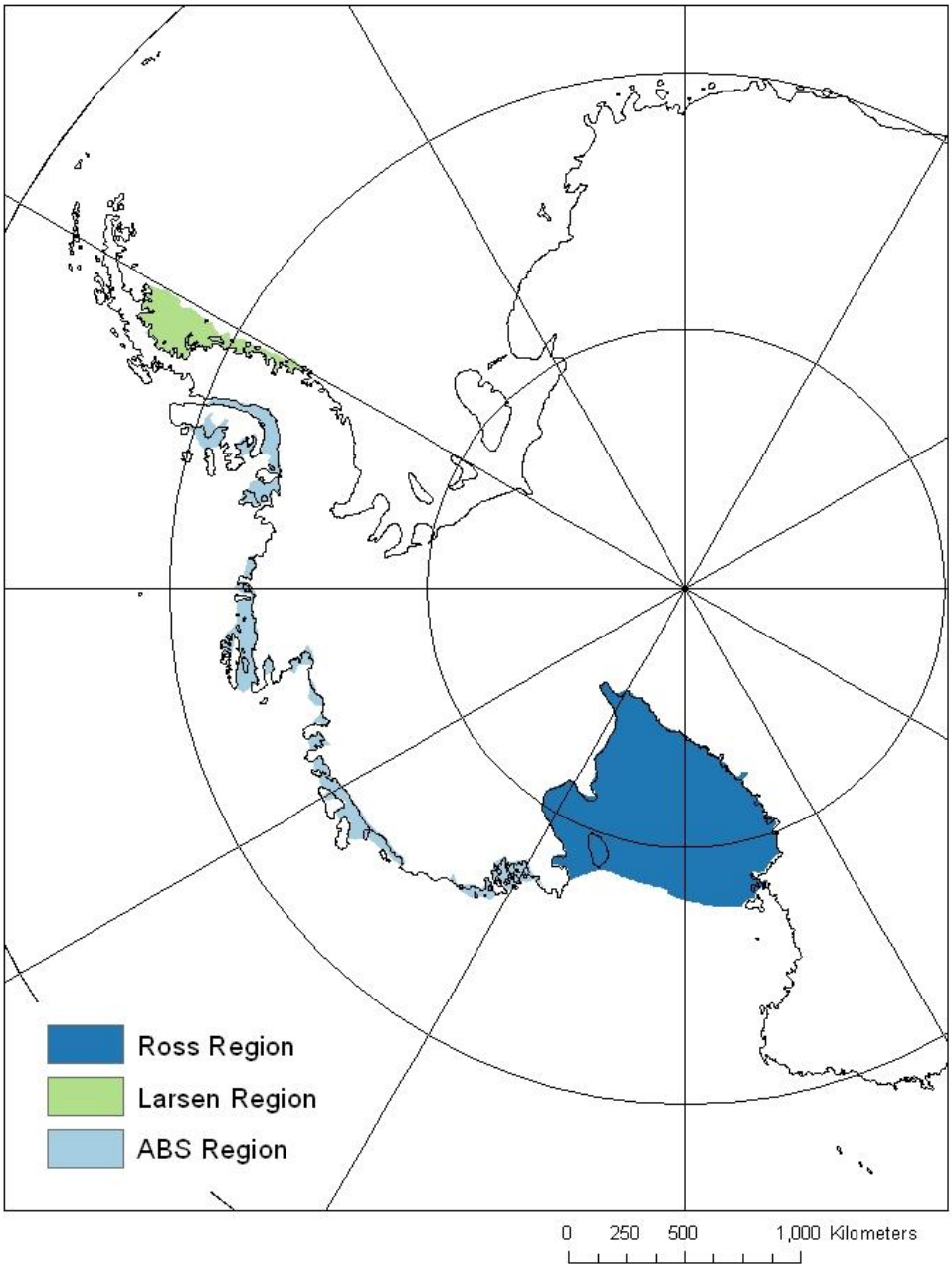

Figure 3-1: Study Area Regions

Data and Methods

The data and methods used in this study consist of three parts: 1) an analysis of passive microwave-derived surface melt extent for three regions of West Antarctica; 2) an analysis of weather patterns and energy balance variables in West Antarctica; and 3) the comparison of surface melt occurrence to the weather variables. This comparison will determine which weather variables and energy balance components are most closely associated with either increased or decreased surface melt extent in West Antarctica.

Cross Polarized Gradient Ratio (XPGR)

Passive microwave satellite data from the Special Sensor Microwave Imager (SSM/I, Armstrong and Brodzik, 1995, updates through 2011) have been used to detect the presence of surface melt conditions for the ablation seasons between 1987-88 and 2001-02 for all of West Antarctica (Areas shown in Figure 3-1). Melt occurrence was determined through the use of the Cross-Polarized Gradient Ratio (XPGR), developed by Abdalati and Steffen (1995 and 1997) to detect the presence of surface melting at concentrations greater than 1% volumetric liquid water fraction. Melt detection is dependent on changes in the dielectric constant of the ice surface as the firn begins to melt. An increase in the XPGR value above an empirically-derived threshold indicates the presence of liquid water in the snowpack. Therefore, this method produces a binary melt/no melt assessment of surface conditions as often as satellite orbit geometry permits—typically this is a once-daily assessment because of the convergence of orbits over higher latitudes. XPGR melt assessment was accomplished using Special Sensor Microwave Imager (SSMI) imagery at a resolution of 25km using the average values of the ascending and descending nodes.

In this study, the XPGR was calculated for the months of December and January—the two warmest months of the Antarctic summer. As higher latitude clouds are essentially transparent in the microwave frequencies due to the absence of intense convection, the XPGR does not suffer from the same cloud constraints as the MODIS infrared methodology presented in Chapter two of this dissertation. This allows for a daily, spatially continuous dataset that is particularly well-suited to a study of synoptic-scale weather patterns. A substantial portion of the satellite record is missing in 1987 and 1988, but only sporadic days are missing in subsequent years. The final XPGR product is a daily, 15-year dataset with melt occurrence for all of West Antarctica at a 25km resolution.

Self-Organizing Maps (SOMs)

Self-Organizing Maps (SOMs) are an artificial neural networking based approach to classifying spatial data. This approach is different than an empirical orthogonal function analysis in that it can identify non-linear variations in data. In this study, SOMs are used to categorize seven weather variables: Sea-Level Corrected Atmospheric Pressure (Pressure), Latent Heat Flux (LH Flux), Sensible Heat Flux (SH Flux), Incoming Shortwave Radiation (SW Down), Reflected Shortwave Radiation (SW Out), Incoming Longwave Radiation (LW Down), and Outgoing Longwave Radiation (LW Out). Atmospheric pressure was chosen to provide a characterization of the synoptic weather patterns that were occurring, whereas the other variables were chosen to ascertain controls on the physical energy balance at the surface. These physical variables are important in generating and forcing physical models to understand surface melting processes. Output from the Polar MM5 forced by ERA40 reanalysis was used to generate the SOM product for the 1987-88 through 2001-02 ablation seasons. This time period corresponds to the overlap period between the SSM/I record and the ERA40 reanalysis. The domain for the SOM analysis

was the entire Southern Hemisphere south of 40^{o}S. This large area was chosen to minimize any error associated with choosing an artificial boundary for the SOM domain and provides an indication of the macro-scale forcing of Antarctic climate. SOM output was generated using the vfind function of the SOMPAK software, which automatically repeats different random initialization and training procedures to optimize output (Kohonen et al., 1995). Rectangular topology and a bubble neighborhood type were chosen for the SOM procedure.

Only the warmest months of the year, December and January, were considered in this study because they contain the largest number of surface melt events. For each month, each day was associated with one of 15 weather types for each variable, and each variable was considered separately. Fifteen weather types were used to minimize internal variability—too few types will cause within-type heterogeneity, while maximizing variability between types—too many types will result in similar patterns classified as two different types. The number associated with each type is arbitrary. That is, a day that was classified as "Type 1" for LH Flux might not necessarily be classified as "Type 1" for SH Flux. The final product of the SOM analysis was a calendar for each of the 436 December days and each of the 453 January days with one weather type associated with each day for each variable.

XPGR and SOM comparison

Following the completion of the 15-year daily XPGR surface melt extent archive, a daily surface melt archive was created for each of three regions of interest (Ross, Larsen and ABS) by extracting the melt extent from each region from the original XPGR archive. The melt extent for each region was then compared with the SOM classification to determine the mean melt extent and melt extent variability (standard deviation) for each region for each synoptic weather pattern. Days for which greater than 10% of the melt extent was missing for a particular region were

excluded from the analysis. A modified Bonferroni procedure (Holm, 1978; Simes, 1986) was used to determine which of the 618 SOM patterns was associated with statistically significantly surface melt anomalies from the 15-year average. This procedure uses the p-value from each cased ranked sequentially from lowest to highest, then iteratively examines each case in order to determine if one case with that p-value would be statistically significant. This process continues until a statistically insignificant case is found, after which all other cases are treated as insignificant. While 618 individual t-tests would produce 52 types with a p-value of less than 0.05, the type-I error—the potential for a falsely positive "significant" value—from conducting multiple t-tests is non-trivial. The Bonferroni correction ensures that the mathematical likelihood of any case resulting in a false positive is less than α, typically 0.05, although in this situation the next most significant value has nearly a 95% chance of being significant. This method is highly conservative in that there is a high chance of discarding a significant case. Therefore, a modified version of the Bonferroni method (Simes, 1986) has been derived such that a less conservative method produced a type-I error probability upper bound at 0.05 over 10,000 trials. It is this modified method that is used in this analysis.

The modified Bonferroni method uses a series of t-tests to determine the likelihood that each sample is significantly different from the long-term mean, but a correction is applied to account for the type-I error. The p-values are then sorted by descending p-order, and an iterative process is used to test each case (in this situation the correlation between synoptic weather type and surface melt extent in a particular region) sequentially. The most statistically significant case (lowest p-value) is assigned a p-order of "1"; the second most significant case is assigned a value of "2", and so on for all cases. If the p-value of the i^{th} test is greater than $i\alpha /n$, where α is the error probability threshold (0.05) and n is the number of samples (in this case, 618), the null hypothesis is not rejected. All subsequent tests will produce the same result, so all further cases can be rejected. If p is less than $i\alpha /n$, then that case is considered to be significantly different from the

mean melt extent value. This method isolated seven synoptic weather types that were associated with above-average melt, and four weather types that were associated with below-average melt. These are each described in the following section.

Results

Synoptic Weather Pattern Type Frequency

This section examines each of the weather types associated with either significantly more or significantly less surface melt extent than the average for each region. The frequency of each of the synoptic weather types (whether statistically significant or not significant) is presented below for December (Table 3-1) and January (Table 3-2). Several weather types have a frequency value of '0', meaning that the only instances of this weather type occurred during days when the SSM/I satellite record was missing. Each of these patterns are excluded from the study. Because the SOM algorithm is inherently non-linear, the frequency of the weather types is not uniform, and because each of the variables is classified using a different SOM, the same weather type number cannot be assumed across variables.

Table 3-1: December Synoptic Weather Type Frequency

	Pressure	SH Flux	LH Flux	SW Down	LW Down	LW Out	SW Out
1	80	62	125	49	45	33	5
2	11	7	5	24	37	9	7
3	5	4	14	5	15	17	4
4	22	4	3	12	10	19	2
5	57	148	60	75	83	95	127
6	23	11	16	15	8	11	27
7	5	1	0	13	11	3	8
8	6	1	1	3	7	6	4
9	4	3	4	5	8	19	13
10	16	8	39	27	29	48	15
11	91	118	46	113	58	113	181
12	13	22	7	8	46	15	10
13	1	19	7	24	25	12	5
14	20	11	19	4	1	10	7
15	82	17	90	59	53	26	21
Total	436	436	436	436	436	436	436

Table 3-2: January Synoptic Weather Type Frequency

	Pressure	SH Flux	LH Flux	SW Down	LW Down	LW Out	SW Out
1	169	60	172	137	80	103	12
2	11	13	2	10	23	3	6
3	2	21	1	12	6	15	5
4	20	12	12	8	10	11	14
5	58	131	4	37	105	78	161
6	32	8	37	40	21	15	17
7	3	2	1	14	9	2	12
8	0	1	3	7	5	3	3
9	0	1	2	12	1	1	5
10	16	14	4	16	16	25	17
11	50	114	32	28	62	36	152
12	5	10	3	11	33	12	15
13	9	4	2	13	22	19	6
14	3	0	15	34	9	14	13
15	75	62	163	74	51	116	15
Total	453	453	453	453	453	453	453

Eleven synoptic weather types showed a statistically significant relationship with surface melt extent (Table 3-3). Statistical significance as determined by the modified Bonferroni method requires that [(iα/n)-p], be positive, where "i" is the p-order, α is the statistical significance level (0.05), n is the number of t-tests performed (618), and p is the t-test p-value. While only 12 types (11 significant and one insignificant) are shown below in Table 3-3, the remaining 606 types were statistically insignificant.

Table 3-3: Modified Bonferroni method for Statistical Significance (Magenta indicates not statistically significant, 607 out of 618 types not statistically significant)

Region	Month	Variable	Type Number	Sample Mean	Overall Mean	P-value	P-order	(iα/n)-p
Larsen	Dec	SW Out	5	0.1543	0.3626	5.02E-11	1	0.00008
Larsen	Dec	SW Out	11	0.5200	0.3626	8.24E-10	2	0.00016
Larsen	Jan	LW Down	1	0.5046	0.6681	3.56E-08	3	0.00024
ABS	Dec	SW Out	5	0.0894	0.1686	1.82E-06	4	0.00032
Ross	Dec	Pressure	14	0.0438	0.0025	0.00003	5	0.00038
ABS	Dec	LW Out	1	0.3201	0.1686	0.00003	6	0.00046
Ross	Dec	SH Flux	12	0.0388	0.0025	0.00005	7	0.00051
Larsen	Jan	LW Down	15	0.8034	0.6681	0.00018	8	0.00046
ABS	Dec	LW Down	11	0.0760	0.1686	0.00021	9	0.00052
Ross	Dec	LH Flux	14	0.0373	0.0025	0.00027	10	0.00054
Ross	Jan	SH Flux	13	0.2466	0.0073	0.00038	11	0.00051
ABS	Dec	SW Out	11	0.2120	0.1686	0.00127	12	-0.00030

Descriptions of each of the statistically significant types are presented below, grouped by ice shelf geographic region. Four patterns were associated with surface melt in the Ross region, four with melt in the Larsen region, and three with melt in the ABS region.

Ross Ice Shelf Region

Anomalous surface melt in the Ross Ice Shelf region was associated with changes in either surface Sensible and/or Latent Heat Flux, or the presence of anomalously high pressure in the ABS coupled with a low-pressure center in the Ross Sea. None of the radiation flux variables showed a statistically significant relationship with surface melting for the Ross region. Average surface melt extent for all days in the Ross region was 0.25% in December and 0.73% in January. Each of the statistically significant patterns has a surface melt extent of at least 3.7% for the Ross region.

December Pressure Type 14 was associated with an increase in surface melting over the Ross region. The average sea-level pressure anomaly for all December Pressure Type 14 days is presented in Figure 4-2. This pattern of lower pressure north of the Ross Sea results in onshore flow in the eastern half of the Ross Ice Shelf (Roosevelt island), and offshore flow on the western half (McMurdo). This pattern occurred on 20 out of 436 December days, with surface melt extending over 4.38% of the Ross region on average.

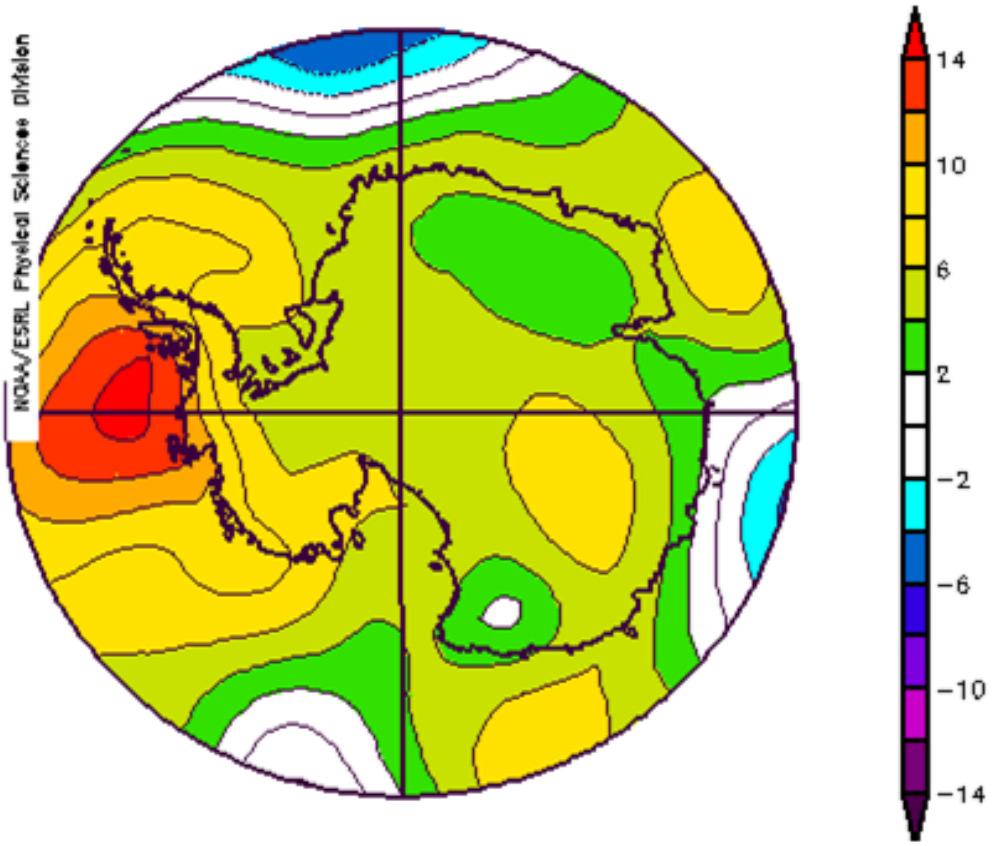

Figure 3-2: NCEP/NCAR Reanalysis (Kalnay et al., 1996) Composite Pressure (mb) Anomalies (December Pressure Type 14), Significantly Higher Melt in Ross Region

In addition to the one pressure type, three heat flux weather types were associated with increased surface melting in the Ross region. December SH Flux Type 12 (Figure 3-3) has a near-normal SH Flux over most of the center portion of Ross, but above normal SH flux at the ice shelf front and along the Transantarctic mountains near the grounding line. SH Flux anomalies from atmosphere to the surface are greater than 4 W/m^2 in the central portion of the ice shelf front, and range from 2-4 W/m^2 at the base of the Transantarctic range. This pattern occurred on 22 out of 436 December days, and average surface melt extent was 3.88% over the Ross region.

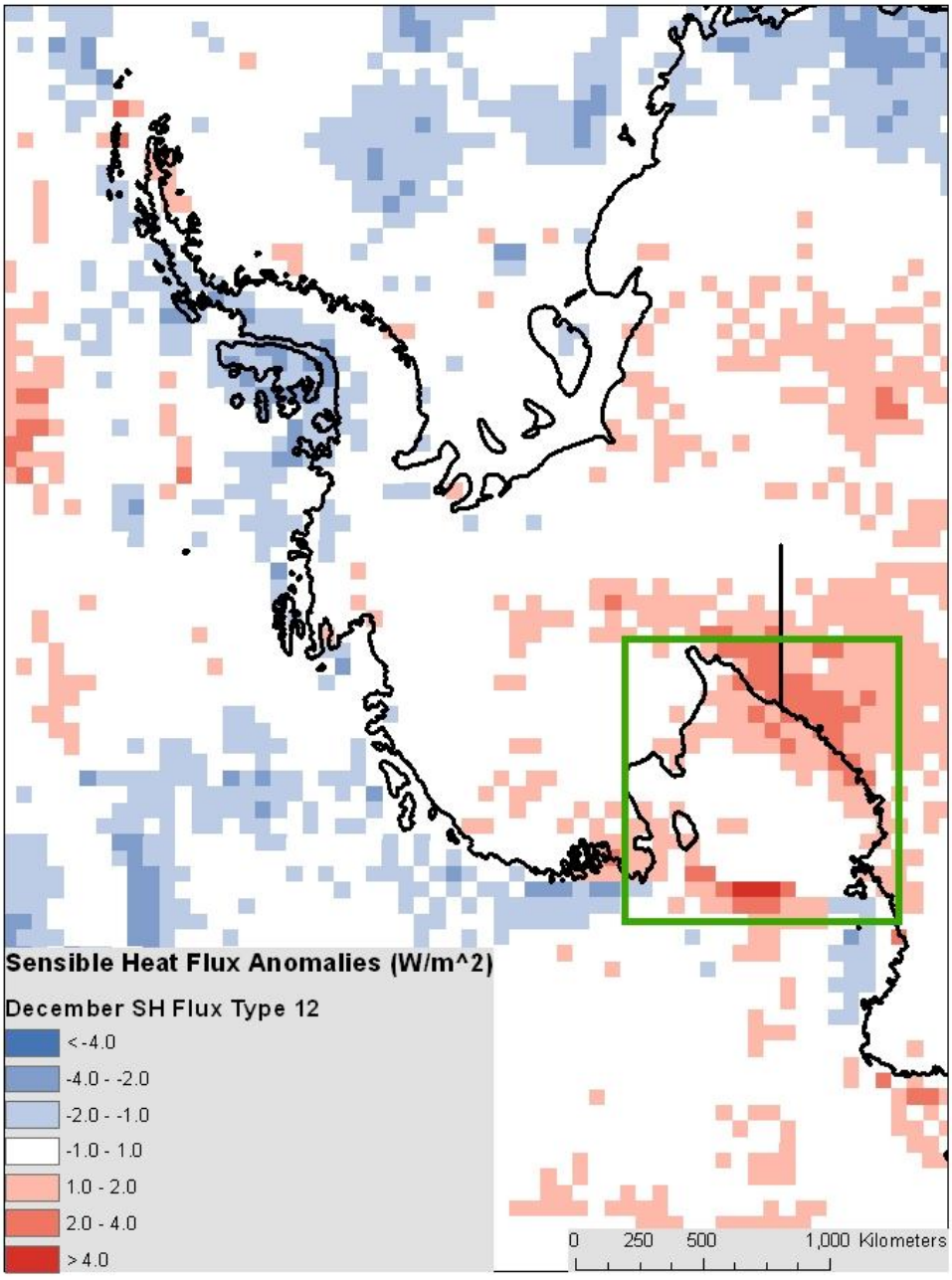

Figure 3-3: Sensible Heat Flux Anomalies (December SH Flux Type 12), Significantly Higher Melt in Ross Region

December LH Flux Type 14 (Figure 3-4) is also associated with increased surface melting in the Ross region. This pattern showed generally positive LH Flux anomalies (that is, a flux from the atmosphere to the surface) over most of Ross Ice Shelf of 1-2 W/m^2, and higher positive anomalies of over 2 W/m^2 in the area of the Ross Sea adjacent to the Ross Ice Shelf front. This pattern occurred on 19 out of 436 December days, and surface melt extent averaged 3.73% of the area of the Ross region on LH Flux Type 14 days.

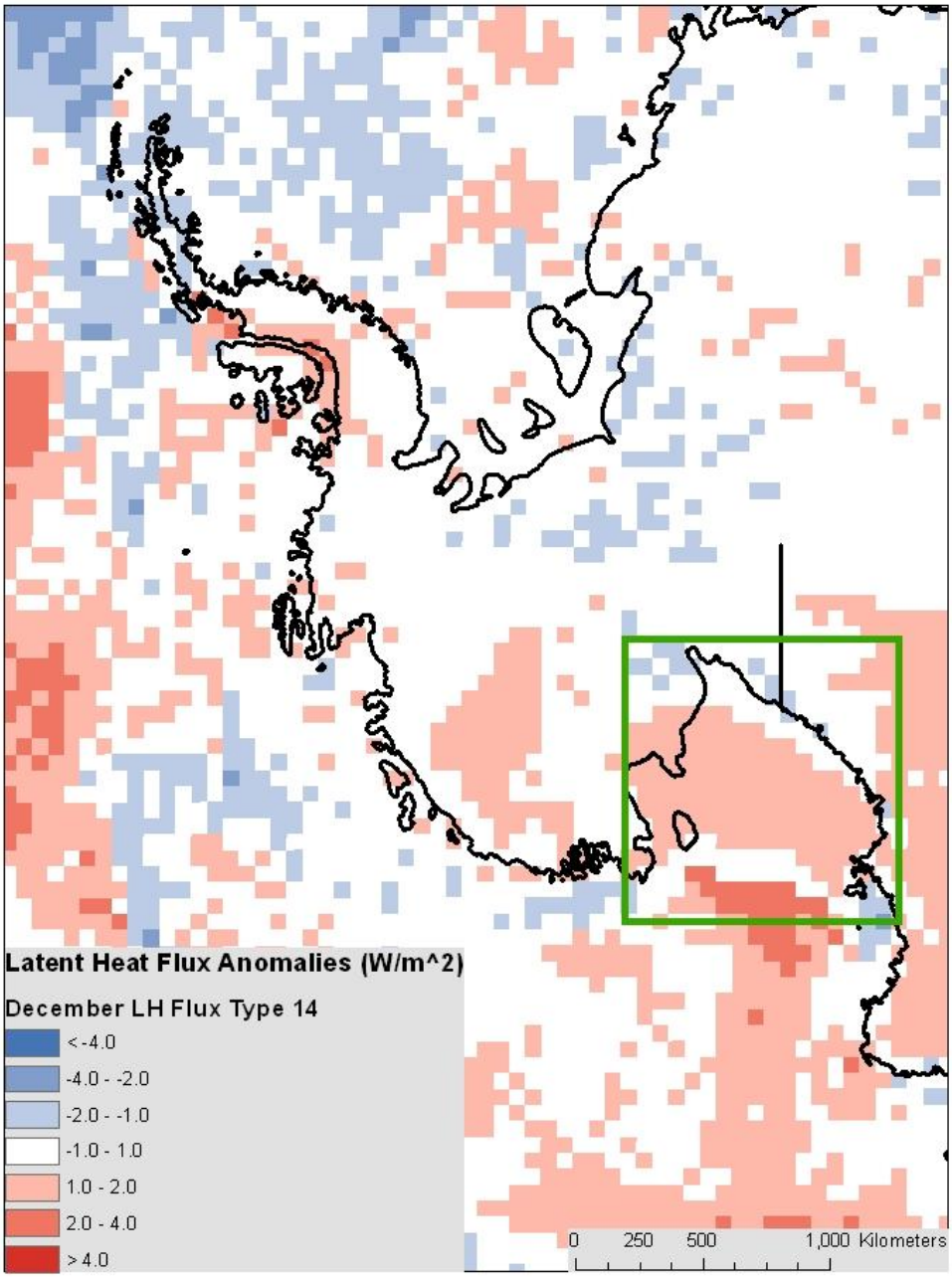

Figure 3-4: Latent Heat Flux Anomalies (December LH Flux Type 14), Significantly Higher Melt in Ross Region

The fourth significant pattern associated with increased surface melt extent in the Ross region is January SH Flux Type 13 (Figure 3-5). This pattern has an increased SH Flux from the atmosphere to the surface over the Transantarctic mountains, as well as on the Eastern Coastal portion of Ross Ice shelf, near Roosevelt Island. This pattern occurred on only 4 of 453 January days, but average surface melt extent was 24.66%, substantially higher than the 0.73% average for all January days. This pattern was associated with onshore flow in the eastern portion of the Ross Ice Shelf as shown in the Reanalysis Composite sea level pressure map (Figure 3-6).

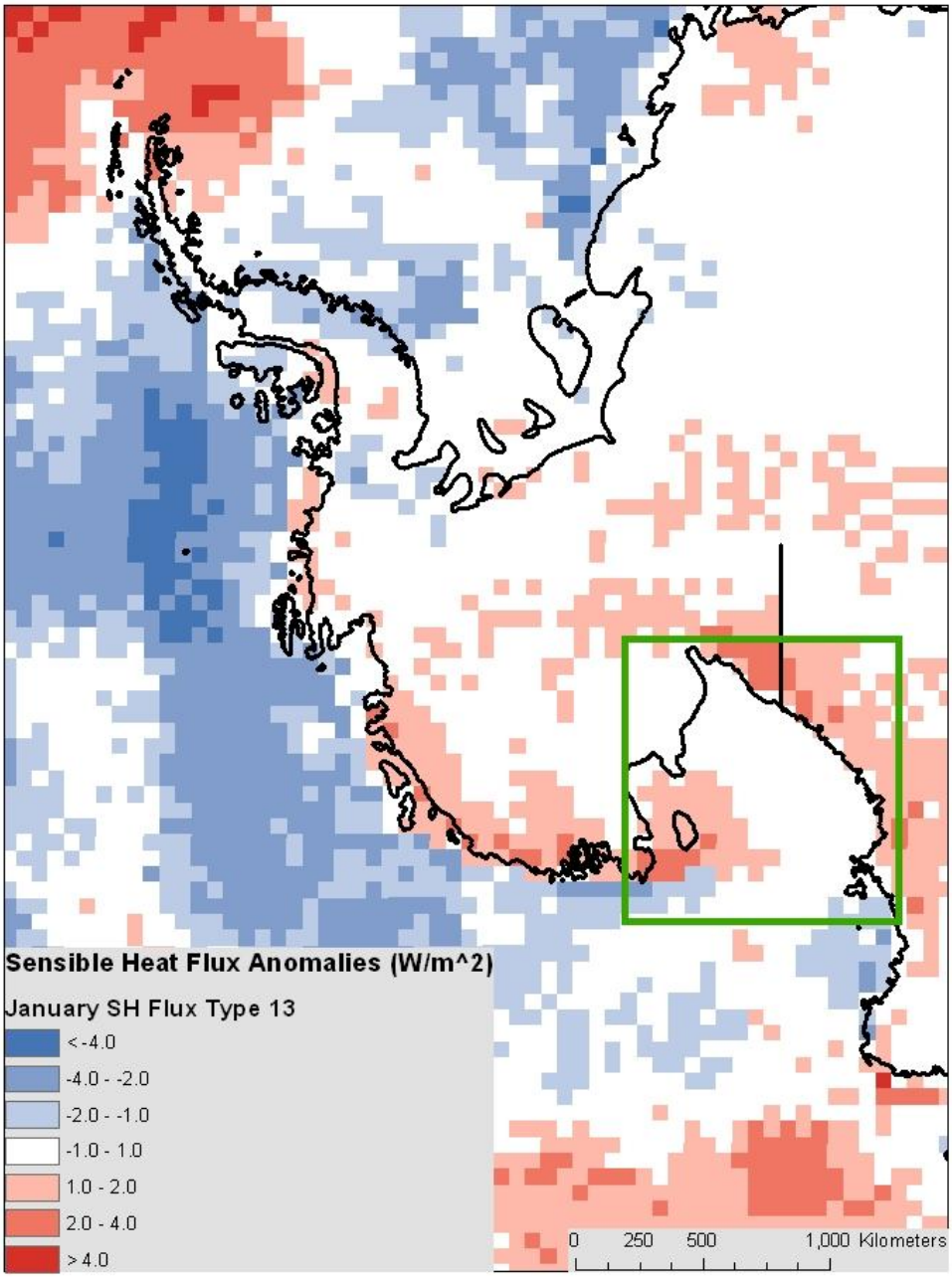

Figure 3-5: Sensible Heat Flux Anomalies (January SH Flux Type 13), Significantly Higher Melt in Ross Region

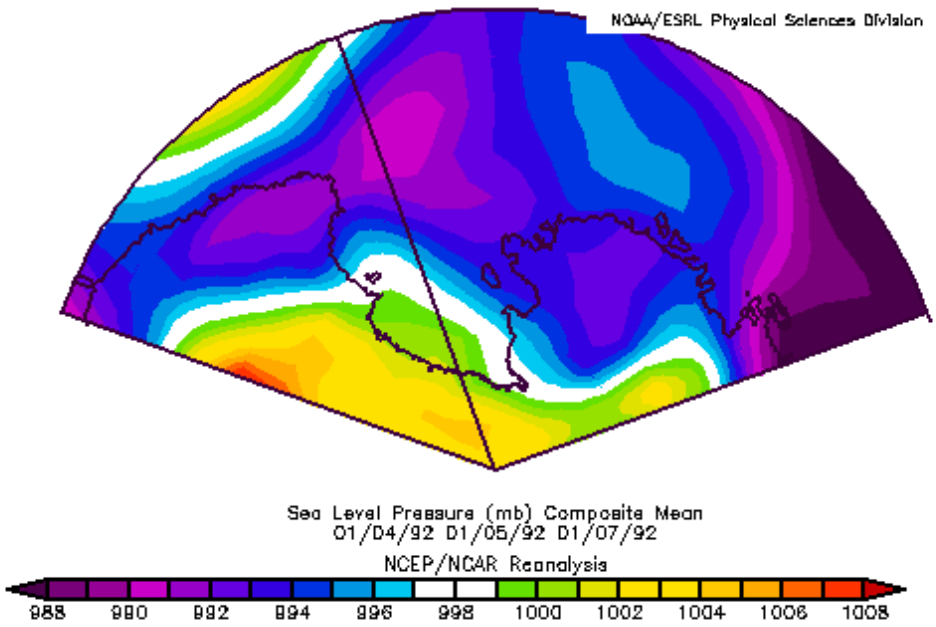

Figure 3-6: Sea Level Pressure Composite for January SH Flux Type 13 Days

Larsen Ice Shelf Region

In contrast to the Ross region, none of the patterns associated with increased or decreased surface melt in the Larsen region were associated with changes in surface heat fluxes or surface pressure. However, two statistically significant patterns were found among the reflected shortwave radiation types, and two in the incoming longwave radiation types.

The first of these patterns, December SW Out Type 5 (Figure 3-7) is associated with a **DECREASE** in surface melting in the Larsen region as well as a decrease in surface melting in the ABS region. This pattern exhibits positive reflected shortwave radiation anomalies through many areas to the east of the Antarctic Peninsula; however, near-average conditions are seen in the area surrounding Larsen C Ice Shelf. This pattern occurred on 127 out of 436 December days, and surface melt extended over 15.43% of the Larsen region on average on these days. This is compared to an average of 36.26% surface melt extent on all December days.

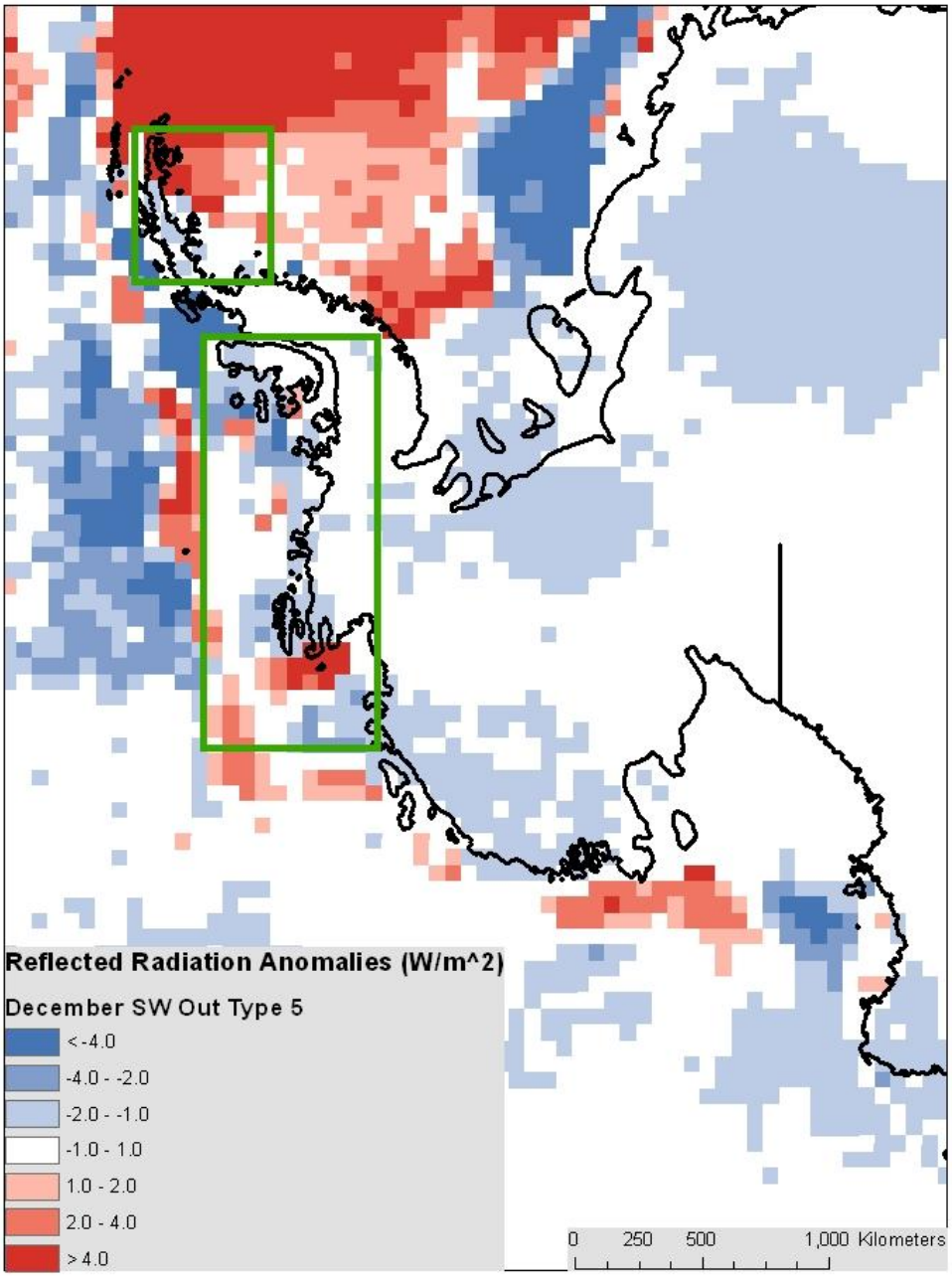

Figure 3-7: Reflected Shortwave Radiation Anomalies (December SW Out Type 5), Significantly Lower Melt in Larsen and ABS Regions

December SW Out Type 11 (Figure 3-8) is associated with increased surface melt extent in the Larsen region. This pattern is also associated with an increase in reflected shortwave radiation throughout the areas to the east of the Antarctic Peninsula, but near average fluxes for areas immediately adjacent to the Peninsula. This pattern occurred on 181 out of 436 December days, with average melt extent of 52.00% over the Larsen region as compared to 36.26% on all December days.

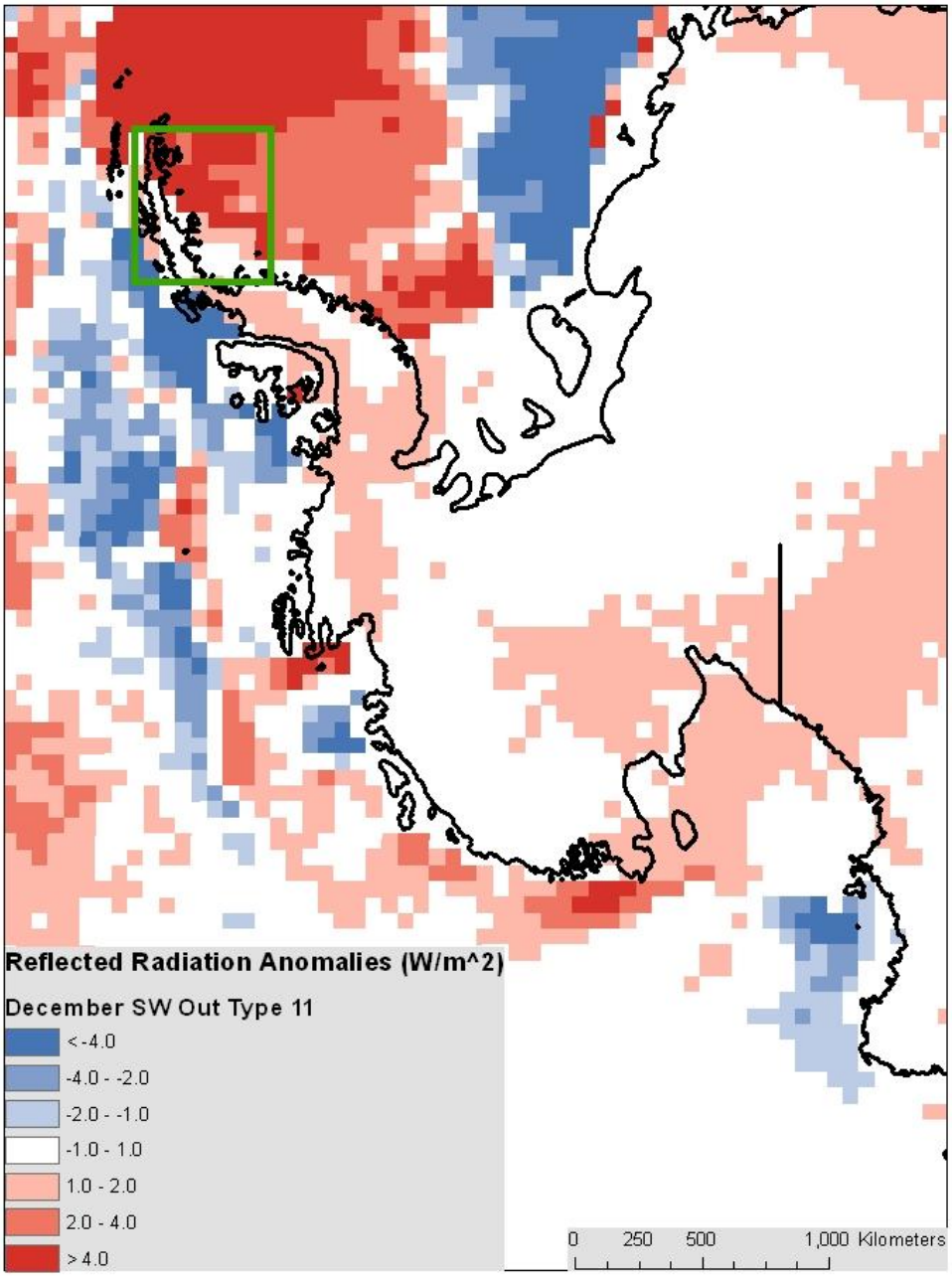

Figure 3-8: Reflected Shortwave Radiation Anomalies (December SW Out Type 11), Significantly Higher Melt in Larsen Region

Two downward longwave radiation patterns were associated with anomalous surface melt in the Larsen region. The first of these is January LW Down Type 1 (Figure 3-9), which is associated with significantly lower surface melt in the Larsen region. This pattern has generally negative incoming longwave radiation anomalies in the Antarctic Peninsula region, but close to average incoming longwave radiation over the Larsen ice Shelf proper. This pattern occurred on 80 out of all 453 January days, and surface melt extended over 50.46% of the Larsen region during LE Down Type 1 days on average as compared to 66.81% on all January days.

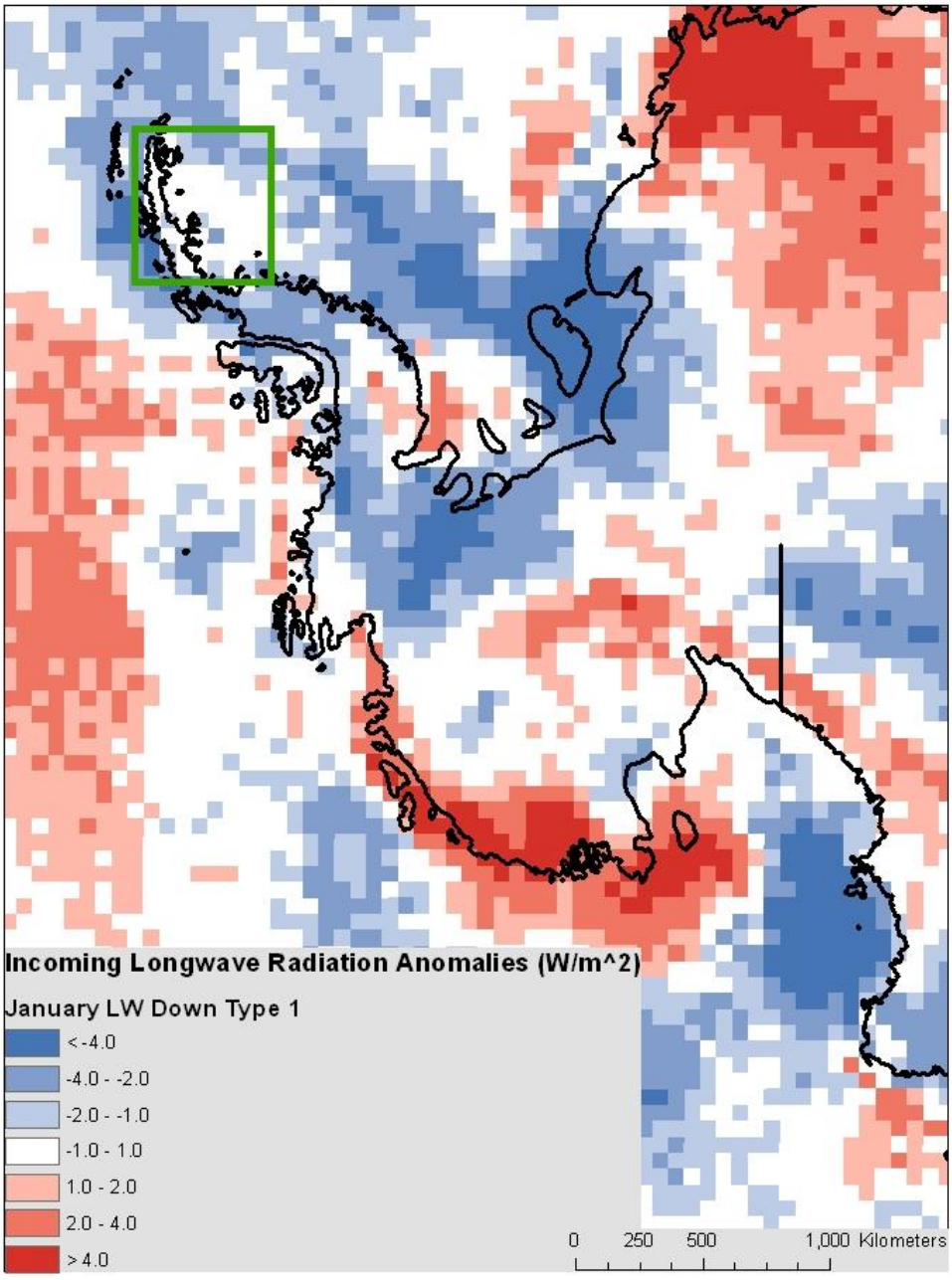

Figure 3-9: Incoming Longwave Radiation Anomalies (January LW Down Type 1), Significantly Lower Melt in Larsen Region

The fourth statistically significant pattern relating surface radiation fluxes to surface melt extent in the Larsen region is January LW Down Type 15 (Figure 3-10). This pattern is associated with increased surface melting on the Larsen Ice Shelves, with melt extending over 80.34% of the region on average. While many areas surrounding the Antarctic Peninsula experience negative radiation anomalies during January LW Down Type 15 days, there is a small (in magnitude and extent) positive radiation anomaly over the northern portion of the Peninsula. This would be associated with increased cloud cover over the Larsen ice shelf. This pattern occurred on 51 out of 453 January days.

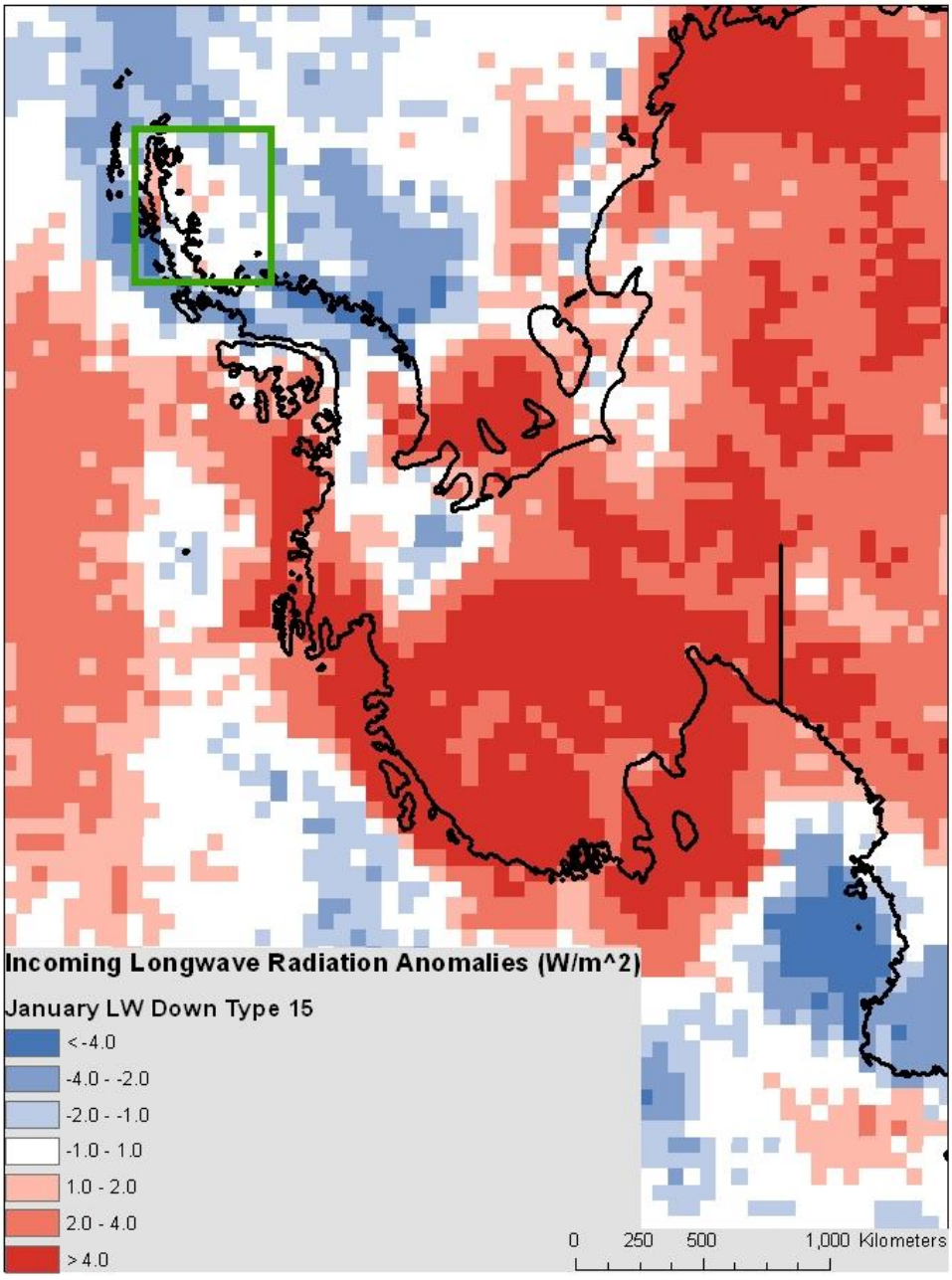

Figure 3-10: Incoming Longwave Radiation Anomalies (January LW Down Type 15), Significantly Higher Melt in Larsen Region

ABS Region

Three patterns showed a statistically significant relationship with surface melt extent for the Amundsen-Bellingshausen Seas region. The first of these patterns is a reflected shortwave radiation pattern, December SW Out Type 5 (Figure 3-7). This type exhibits a mixture of positive and negative shortwave radiation anomalies in the ABS region, making the relationship between surface melt extent and this weather type unclear. This pattern is associated with lower surface melt extents in the ABS region and is also statistically significant in the Larsen region. Average surface melt extent in the ABS region is 8.94% during this weather pattern as compared to 16.86% on average for all December days.

Another pattern associated with lower surface melt extent in the ABS region is December LW Down Type 11 (Figure 3-11). This pattern has areas of higher incoming longwave radiation interspersed with areas of lower incoming longwave radiation in the ABS region, making unclear the relationship between increased downwelling longwave radiation fluxes and surface melting. December LW Down Type 11 was associated with average surface melt extent of 7.60% of the ABS region as compared to an average of 16.86% on all December days, and this pattern occurred on 58 of 436 December days.

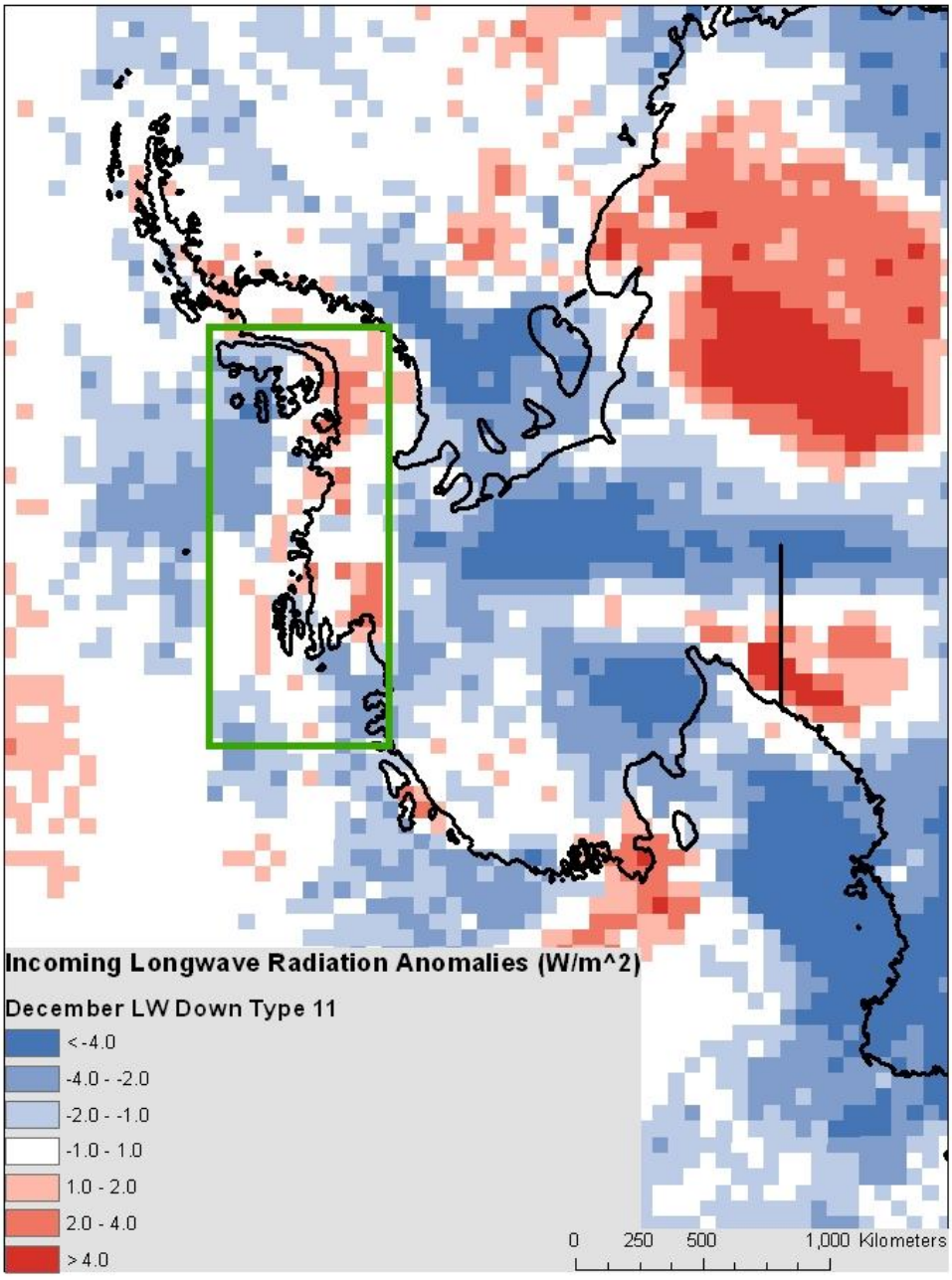

Figure 3-11: Incoming Longwave Radiation Anomalies (December LW Down Type 11), Significantly Lower Melt in ABS Region

The third and final pattern exhibiting a statistically significant relationship to surface melt extent in the ABS region is December LW Out Type 1 (Figure 3-12). This pattern exhibits positive outgoing longwave radiation fluxes throughout the entire ABS region with anomalies of up to 4 W/m^2 seen offshore in the Amundsen Sea. December LW Out Type 1 days averaged 32.01% surface melt extent as compared to 16.86% for all December days, and this pattern occurred on 33 out of 436 December days.

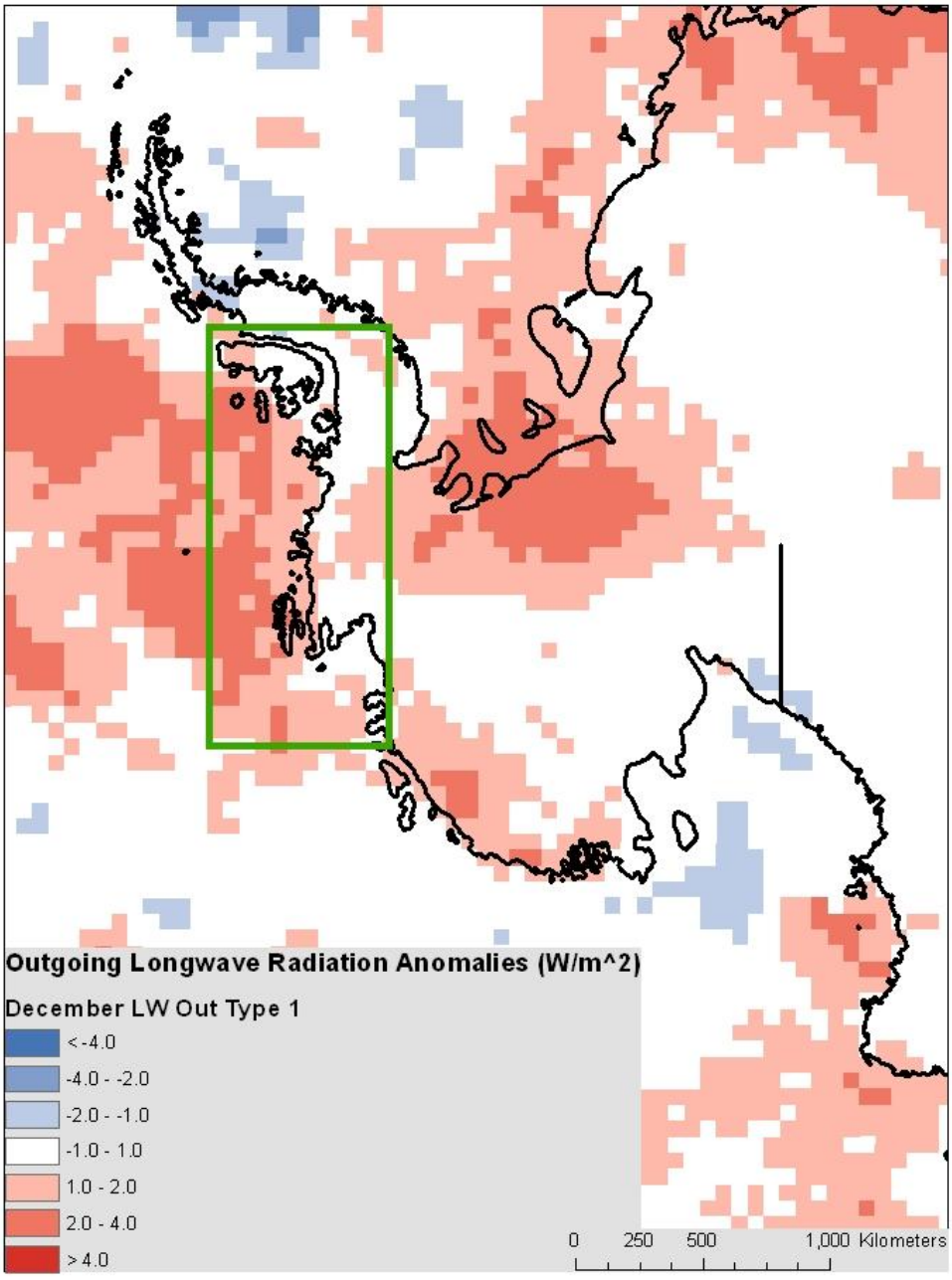

Figure 3-12: Outgoing Longwave Radiation Anomalies (December LW Out Type 1), Significantly Higher Melt in ABS Region

Summary of Results

Each of the three regions—Ross, Larsen, and ABS—exhibit different relationships between surface melt extent and weather variables (Table 3-4). In the Ross Ice Shelf region, surface melt is associated with higher downward heat fluxes (both sensible and latent) and the presence of a low pressure system in the Ross Sea that generates northerly (onshore) flow. In the Larsen Ice Shelf region, downwelling longwave radiation fluxes has a positive relationship with surface melt extent (in one case a positive melt anomaly associated with an increased downward flux, in another case a negative melt anomaly associated with less of a downward radiation flux), whereas reflected shortwave radiation showed in one case a positive relationship with surface melting, and in another case the relationship was unclear. In the ABS region, the only clear relationship between any weather type and surface melt was a positive relationship between emitted longwave radiation and increased surface melt extent.

Table 3-4: Summary of statistically significant relationships between surface melt extent and weather type (a positive flux is a flux toward the surface)

Region	Variable	Variable Anomaly	Melt Anomaly
Ross	Dec. Pressure 14	-	+
Ross	Dec. SH Flux 12	+	+
Ross	Dec. LH Flux 14	+	+
Ross	Jan. SH Flux 13	+	+
Larsen	Dec. SW Out 5	+/-	-
Larsen	Dec. SW Out 11	+	+
Larsen	Jan. LW Down 1	-	-
Larsen	Jan. LW Down 15	+	+
ABS	Dec. SW Out 5	+/-	-
ABS	Dec. LW Down 11	+/-	-
ABS	Dec. LW Out 1	+	+

Discussion

Relationship of Synoptic Weather Patterns to Surface Melt Extent by Region

There appears to be a clear distinction between the weather patterns associated with surface melting in the Ross region as compared to either the Larsen or ABS region. Because Ross Ice Shelf is further south than Larsen or any of the ice shelves in the ABS region, there is generally less surface melting there. Consequently, the surface melting that does occur tends to be under anomalous weather conditions, meaning larger heat flux anomalies are required to induce surface melting in the Ross region on the order of 2-5W/m^2. This is in contrast to the Larsen region, where almost every portion of the Larsen Ice Shelf exhibits melt at some time in each of the 15 years of this study. For this region, incoming longwave radiation showed the strongest relationship to surface melt extent, with cloudier conditions associated with higher surface melt extents. Surface melting in the Larsen region was also associated with increases in offshore reflected shortwave radiation, though the link between this reflectivity increase and surface melt extent was less clear.

One atmospheric pressure type was associated with increased surface melting for the Ross region—December Pressure Type 14 (Figure 3-2). This pattern represented an offshore low pressure system in the Ross Sea, and a corresponding high pressure center in the Amundsen Sea. Such a pattern creates two scenarios to produce melting on the Ross Ice Shelf. The first is the advection of relatively warm, moist air over the eastern half of the ice shelf, near Roosevelt Island. The second is the initiation of the Ross Ice Shelf Air stream. This feature is associated with cyclonic circulation in the Ross Sea, and descending air from the interior of Antarctica that flows along the western boundary of the ice shelf (Seefeldt and Cassano, 2012). Although the Ross Air Stream is typically a winter feature, its presence during the summer season can cause

the descent and adiabatic warming of air from the plateau such that surface melting occurs when ambient air temperatures are sufficiently high. While the Ross Air Stream is structurally similar in appearance to a katabatic wind, this feature is not thermally-driven, but rather is driven by a strong pressure gradient. This feature is explained further in Chapter 4.

The association between synoptic weather type and surface melt extent is more complicated in the ABS region than either Ross or Larsen. The large spatial extent of the region means that weather in the region at any time may be heterogeneous, even though the SOM records only one particular synoptic type for each variable per day. The variations are not only in magnitude, but often in sign as well. In the case of December LW Down Type 11 (Figure 4-11), incoming longwave radiation fluxes varied between less than -4 W/m^2 in the area surrounding Wilkins Ice Shelf to nearly +4 W/m^2 at Pine Island Glacier. Even though this synoptic weather type was associated with decreased surface melt extent, it is difficult to make the physical association between the weather pattern and surface melt extent because of this variation in sign with nearly equal variation on either side of zero.

Analysis of Synoptic-Scale Melt Mechanisms in West Antarctica

I propose three mechanisms for generating surface melting in Antarctica: Advective, Adiabatic, and Radiative. Advective melting is caused by the movement of an air mass that transports either sensible or latent heat which then induces surface melting. Adiabatic melting is the result of descending air warming as it traverses the ice sheet to ice shelf boundary. This type of melting would not occur in a strictly katabatic setting as katabatic winds are driven by the negative buoyancy of cold air typically found during polar night conditions. Rather, synoptic conditions are similar to that of the Ross Air Stream (Seefeldt and Cassano, 2012) where the presence of a polar low induces cyclonic circulation and descending air from the Antarctic

plateau which warms adiabatically as it approaches the ice shelf surface. Finally, radiative melting is the result of heat generated by incoming shortwave electromagnetic radiation. This type of surface melting happens in-situ and does not necessitate the movement of air masses.

Advective melting is likely the primary mechanism for surface melting on the Ross Ice Shelf. Each of the four synoptic weather types identified to have a statistically significant relationship with surface melt extent are evidence of weather patterns consistent with advective melting. In each of these cases, warm, moist air is advected from the Ross Sea onto the Ross Ice Shelf coincident temporally and spatially with a surface melt event.

Adiabatic melting is not identified by any of the synoptic weather types identified in this study. It is likely that any smaller mesoscale to microscale processes that would contribute to surface melt events are diluted because of the large spatial extent of the SOM study. However, this does not discount the presence of adiabatic melting entirely. In 2005, a surface melt event on the Ross Ice Shelf (Figure 3-13) extended along the western portion of the shelf as far south as Ice Stream A at 80^{o}S. There was also a substantial area of surface melting near Ice Stream C, but in this event there was no surface melt observed in the coastal areas of the Ross Ice Shelf. This surface melt event occurred while cyclonic circulation was present in the Ross Sea (Figure 3-14). This feature generated moderate to strong surface winds of up to 8 m/s along the grounding line (Figure 3-15), however this was associated with warm air temperatures of up to 274K. With surface air temperatures above freezing, it is not surprising that surface melting was occurring along the grounding line in this case. If the southerly winds were density-driven (katabatic), surface temperatures would have cooled and remained below freezing.

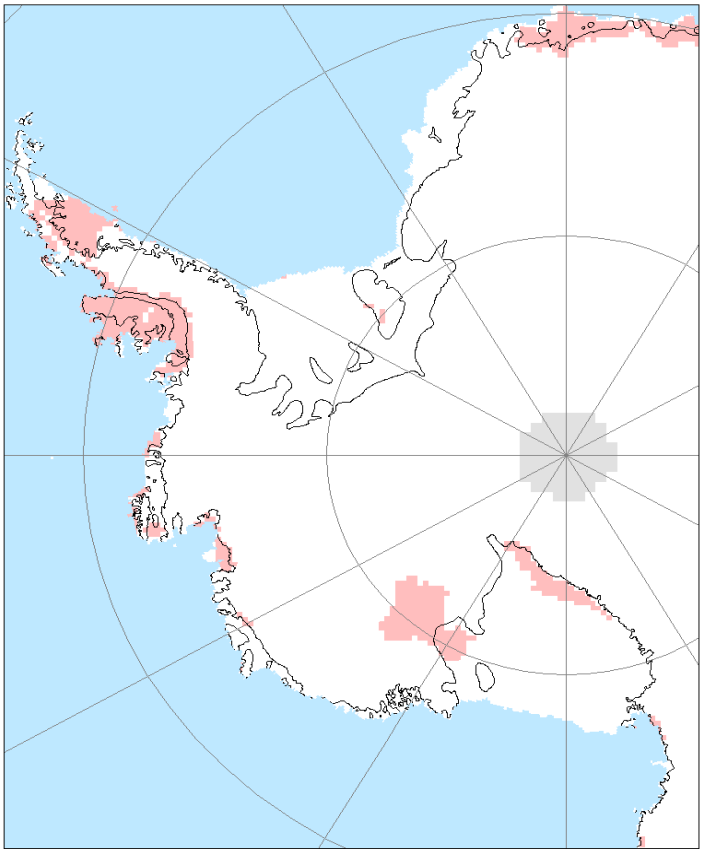

Figure 3-13: Surface Melt Extent on January 8, 2005

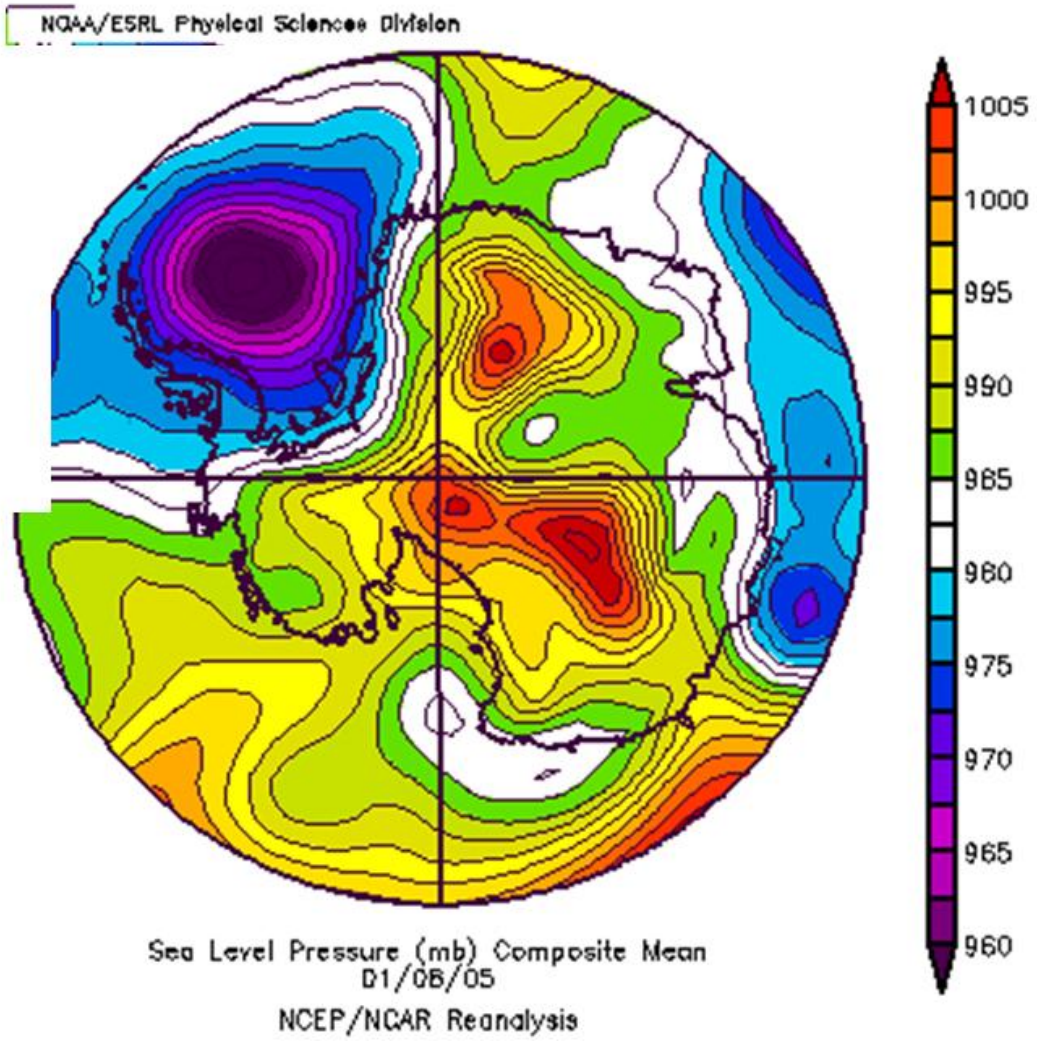

Figure 3-14: Surface Air Pressure (mb) January 8, 2005

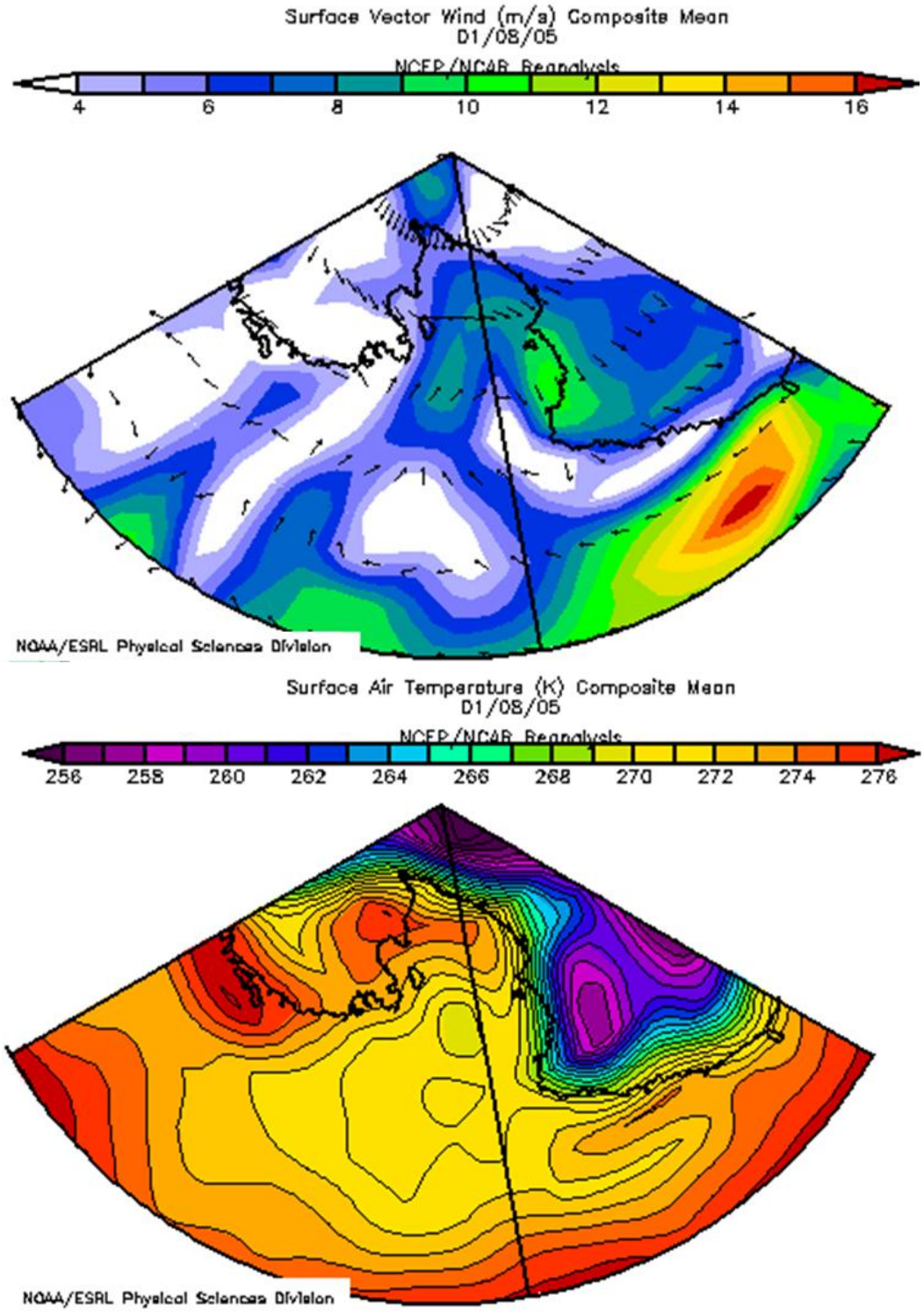

Figure 3-15: Daily Surface Vector Winds (Top) and Average Surface Air Temperature (Bottom), Ross Ice Shelf, January 8, 2005

In this study, radiative melting is related to both longwave and shortwave radiation fluxes. This appears to be the primary melt generation mechanism on the Larsen Ice Shelf as well as in the Amundsen-Bellingshausen Region. Radiative forcing can be further classified into two varieties. Changes in the outgoing shortwave radiation are associated with lower albedo, which increases absorption. Increases in the downward longwave radiation flux is associated with increased cloudiness, which can prevent nighttime radiational cooling in the more northerly Larsen region, which (unlike the Ross Ice Shelf) does experience a sunset even in the summer months.

Project Limitations

One limitation of this study is the conservative nature of the Bonferroni correction. Because the Bonferroni method is used solely to control for false positive significance (Type I error), this procedure will invariably cause several significant relationships to be rejected as insignificant (Type II error). The modified Bonferroni/Simes method used in this study is less conservative than the Bonferroni method, and is considered to be more appropriate than the traditional method for highly correlated test statistics (Simes, 1986). However the type II error as a result of the modified Bonferroni method remains uncorrected in any direct manner. This would indicate that there may be, and in fact, likely are, more relationships that are significant.

Another limitation is pertinent to the Ross region in particular, and that is the problem of missing data on surface melt extent during a large melt event in 1991-92. During the longest and most spatially-extensive surface melt event of the study, there was a substantial amount of missing passive microwave data such that the XPGR could not be calculated for 12 days. Because surface melt is infrequent in the Ross region, this amount of missing data would change the calculated average surface melt extent for the synoptic types that occurred during the event but

were not recorded in the XPGR record. The missing data may correspond to as much as 15% of the overall surface melt occurrence in the Ross region from 1987-2002.

The domain for the SOM portion of the study poses several important implications. For a holistic study to be comparable across regions, it is important that the SOM domain contain the entire study area; all three regions of West Antarctica. The domain must also be sufficiently large to account for large-scale (planetary and synoptic scale) weather patterns that extend beyond the study area, but have implications for the weather and climate in the study area. For instance, it has been suggested (Trusel et al., 2012) that there is a correlation between surface melt in Antarctica with larger scale teleconnections, specifically El-Niño Southern Oscillation (ENSO), Southern Annular Mode (SAM) and the Southern Oscillation Index (SOI). However, it might be useful to look at a smaller subset of the data than hemispheric. With a larger SOM domain, weather patterns that affect East Antarctica are also captured by the SOM, diluting the number of SOM patterns that are specific to the area of interest.

It is also important to note that this work does not firmly establish causation for the surface melt events. While it is unlikely that surface melting could cause the particular atmospheric pressure pattern seen to be associated with surface melting on Ross Ice Shelf, an increase in surface melting would likely change the sensible and latent heat fluxes in the Ross region, and may affect reflected shortwave radiation in the ABS region and Larsen through the ice-albedo effect. Surface melt can lower the albedo of the ice, which can cause further melting through the absorption of shortwave radiation. Further work will be necessary, specifically using physically-based mesoscale atmospheric modeling to determine the exact role of each weather variable in generating surface melt conditions. Mesoscale modeling using a coupled atmospheric-ocean-sea ice model can help elucidate the regional climate controls that drive ice shelf surface melt dynamics. Rather than relying solely on historical melt events, mesoscale models can

"predict" melt conditions given any number of hypothetical forcing conditions, thus making the determination of causality possible.

Conclusions

This study used SOM analysis to isolate eleven weather patterns associated with anomalies in surface melt extent for three regions of West Antarctica in the period from 1987-2002. In the area surrounding the Ross Ice Shelf, the weather variables most closely associated with surface melting were 1) the presence of a surface low in the Ross Sea and a surface high in the Amundsen Sea that, combined, drive mild northerly flow and increased cloud cover onshore 2) anomalous positive sensible heat flux, and 3) anomalous positive latent heat flux. In the Larsen region, incoming longwave radiation (related to cloud cover) and reflected shortwave radiation (related to surface albedo) are most closely associated with surface melt. For the spatially vast ABS region, the relationship between surface melt and synoptic scale weather patterns is less clear, but each of the significant relationships found in this study were related to a radiation flux rather than directly to an atmospheric pressure pattern or heat flux pattern.

In order to assess the potential for ice sheet collapse, it is vital to understand the processes (glacier acceleration, basal melt, and surface melt) that can contribute to ice sheet instability. As sea level rise from rapid dynamic changes in ice sheet acceleration remains one of the most prominent unknown factors in IPCC assessment reports (Solomon et al., 2007). This work is a small piece in a larger effort to understand these processes that can cause ice sheet collapse and subsequent acceleration in glacier forward speed.

References

Abdalati, W. and Steffen, K.: Passive Microwave-Derived Snow Melt Regions on the Greenland Ice Sheet. Geophysical Research Letters, 22, 787-790, 1995.

Abdalati, W. and Steffen, K.: Snowmelt on the Greenland Ice Sheet as Derived from Passive Microwave Satellite Data. Journal of Climate, 10, 165-175, 1997.

Armstrong, R.L. and Brodzik, M.J.: An Earth-Gridded SSM/I Data Set for Cryospheric Studies and Global Change Monitoring. Advances in Space Research, 16, 155-163. 1995. Data available online: http://nsidc.org/data/docs/daac/nsidc0032_ssmi_ease_tbs.gd.html

Brewer, C. A., 2012.Color Brewer v 2.0. Available online: http://www.ColorBrewer.org, accessed 1 June, 2012.

Curry, J.A.; Schramm, J.L.; and Ebert, E.E. (1995). Sea Ice-Albedo Climate Feedback Mechanism. *Journal of Climate*. **8**, pp. 240-247.

Hewitson, B.C. and Crane, R. G.: Self-organizing maps: Applications to Synoptic Climatology. Climate Research, 22, 13-26. 2002.

Holm, S. A Simple Sequentially Rejective Multiple Test Procedure. Scandinavian Journal of Statistics, 6, 65-70, 1979.

Kalnay, E., Kanamitsu, M., Kistler, R., Collins, W., Deaven, D., Gandin, L., Iredell, M., Saha, S., White, G., Woollen, J., Zhu, Y., Leetmaa, A., and Reynolds, B.: The NCEP/NCAR Reanalysis 40-year Project. Bulletin of the American Meteorological Society, 77, 437-471, 1996.

Kohonen, T.; Hynninen, J; Kangas, J.; and Laaksonen, J. (1995). SOM_PAK, The Self-Organizing Map Program Package, Version 3.1 user manual. Available Online: http://www.cis.hut.fi/research/som_pak/som_doc.txt

Kottmeier, C. and Engelbart, D. (1992). Generation and Atmospheric Heat Exchange of Coastal Polynyas in the Weddell Sea. *Boundary-Layer Meteorology*. **60**, pp. 207-234.

Ledley, T.S. (1988). A Coupled Energy Balance Climate-Sea ice Model: Impact of Sea Ice and Leads on Climate. *Journal of Geophysical Research*. **93**: D12, pp. 15,919-15,932.

Liu, H.; Wang, L.; and Jezek, K. C. (2006). Spatiotemporal Variations of Snowmelt in Antarctica Derived from Satellite Scanning Multichannel Microwave Radiometer and Special Sensor Microwave Imager Data (1978-2004). Journal of Geophysical Research, 111, F01003.

Oppenheimer, M. (1998). Global Warming and the Stability of the West Antarctic Ice Sheet. *Nature*. **393**, pp. 325-332.

Rignot, E. and Jacobs, S. S. (2002). Rapid Bottom Melting Widespread near Antarctic Ice Sheet Grounding Lines. *Science.* **296**: 5575, pp. 2020-2023.

Rind, D.; Healy, R.; Parkinson, C.; and Martinson, D. (1995). The Role of Sea Ice in 2 X CO_2 Climate Model Sensitivity. Part I: The Total influence of Sea Ice Thickness and Extent. *Journal of Climate.* **8**, pp. 449-463.

Scambos, T.A, Bohlander, J.A., Shuman, C.A., and Skvarca, P.: Glacier Acceleration and Thinning after Ice Shelf Collapse in the Larsen B Embayment, Antarctica. Geophysical Research Letters, 31, L18402, 2004.

Seefeldt, M.W. and Cassano, J. J. (2012). A Description of the Ross Ice Shelf air stream (RAS) through the use of Self-Organizing Maps (SOMs). Journal of Geophysical Research, **117**.

Simes, R.J. (1986). An Improved Bonferroni Procedure for Multiple Tests of Significance. Biometrika, 73, 751-754.

Solomon, S.; D. Qin; M. Manning; Z. Chen; M. Marquis; K.B. Averyt; M. Tignor; and H.L. Miller (eds.). (2007). Contribution of Working Group I to the Fourth Assessment Report

of the Intergovernmental Panel on Climate Change, 2007. Cambridge University Press, Cambridge, United Kingdom and New York, NY, USA.

Steig, E.J.; Schneider, D.P.; Rutherford, S.D.; Mann, M.E.; Comiso, J.C.; and Shindell, D.T. (2009). Warming of the Antarctic Ice Sheet Surface since the 1957 International Geophysical Year. *Nature*. **457**, pp. 459-462.

Trusel, L. D.; Frey, K. E.; and Das, S. B. (2012). Antarctic Surface Melting Dynamics: Enhanced Perspectives from Radar Scatterometer Data. *Journal of Geophysical Research*, **117**. doi:10.1029/2011JF002126

Turner, J.; Colwell, S.R.; Marshall, G.J.; Lachlan-Cope, T.A.; Carleton, A.M.; Jones, P.D.; Lagun, V.; Reid, P.A.; and Iagovkina, S. (2005). Antarctic Climate Change During the Last 50 Years. *International Journal of Climatology*. **25**: pp. 279-294.

Sergienko, O.; and MacAyeal, D. R. (2005). Surface Melting on the Larsen Ice Shelf, Antarctica. *Annals of Glaciology*. **40,** pp. 215-218.

van den Broeke, M.: Strong Surface Melting Preceded the Collapse of Antarctic Peninsula Ice Shelf. Geophysical Research Letters, 32, L12815, 2005.

Yarnal, B.; Comrie, A.C.; Frakes, B.; and Brown, D.P. (2001). Developments and Prospects in Synoptic Climatology. *International Journal of Climatology*. 21: 1923-1950.

Chapter 4

Synoptic-Scale Weather Forcing of a Prolonged Surface Melt Event on Ross Ice Shelf, Antarctica as Classified by Self-Organizing Maps

Introduction

The Ross Ice Shelf is located across the 180^{o} meridian at the boundary between West Antarctica and East Antarctica. As mentioned in the previous chapter, surface melt events on this ice shelf are infrequent, owing to generally sub-freezing temperatures year-round. During the 1991-92 austral summer, a prolonged surface melt event occurred on the eastern half of the ice shelf from December 27 through January 21. This event was the most extensive and longest duration of any melt event on the Ross Ice Shelf in the period 1987-2008 (Liu et al, 2006). This chapter examines in detail this anomalous melt event and the weather conditions that were present both during and immediately preceding it using Self-Organizing Maps (SOMs) and identifying anomalously-frequent weather patterns.

Background

The ice shelf-ocean-atmosphere system is a complex interface where there are a number of different heat and radiation fluxes that can affect the mass balance of the ice shelf (Figure 4-1). These include subsurface melting and freezing, advected heat flux off of the ocean or sea ice, in-situ warming from solar radiation, as well as advected air from the ice sheet proper, which may exert a warming or cooling influence depending on the temperature field. These forcings are in addition to dynamic glacial ice advance and other mechanical constraints on ice shelf mass balance that are not considered in this work.

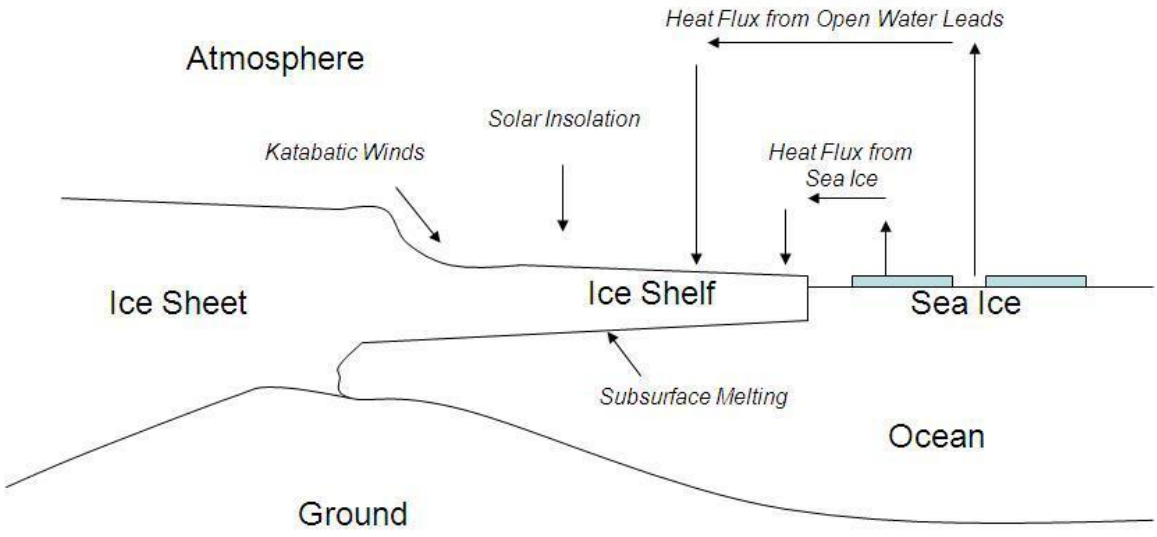

Figure 4-1: Generalized energy balance model for the ice shelf-ocean-atmosphere system

During the 1991-92 austral summer, a long-duration melt event took place over the eastern half of Ross Ice Shelf (Figure 4-2). Although events such as this are infrequent (occurring once every five or six years), understanding them may prove useful in determining what types of synoptic-scale weather patterns may cause surface melting on other ice shelves. Additionally, this information may prove helpful in determining the potential long-term forcing of surface melt on Ross Ice Shelf as temperatures increase due to climate changes noted by many over the West Antarctic region (Steig et al., 2009; King et al., 2002; and others). The surface melt event began abruptly on Dec. 27, and continued with a large extent through Jan. 6. During the middle part of January, the melt event abated somewhat, with the melt persisting longest to the east of Roosevelt Island, remaining there until Jan. 21 for a total of 26 consecutive days.

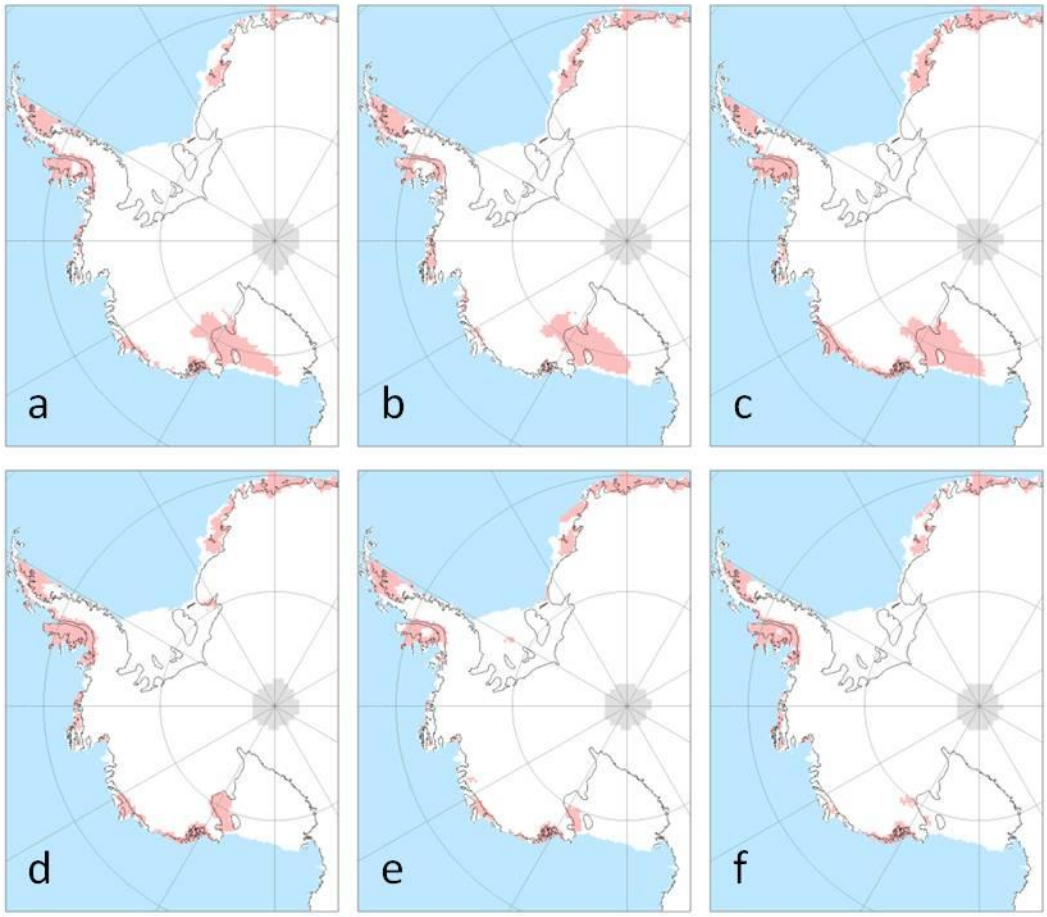

Figure 4-2: XPGR melt occurrence for the Dec. 1991 – Jan 1992 melt event on Ross Ice Shelf. a) Dec. 27, 1991; b) Jan 1, 1992; c) Jan 6, 1992; d) Jan. 11, 1992; e) Jan 16, 1992; and f) Jan. 21, 1992

Data and Methods

Cross-Polarized Gradient Ratio (XPGR)

Passive microwave satellite imagery from the Special Sensor Microwave Imager (SSM/I, Armstrong and Brodzik, 1995, updates through 2011) has been used (Liu et al., 2006) to detect the presence of surface melt conditions during a large-extent, long-duration surface melt event on the Ross Ice Shelf. In this study, melt occurrence was determined through the use of the Cross-

Polarized Gradient Ratio (XPGR), developed by Abdalati and Steffen (1995 and 1997) to detect the presence of surface melting at concentrations greater than 1% volumetric liquid water fraction. Detection of melt is dependent on changes in the dielectric constant of the substrate as the firn changes from a mixture of solid ice and air to a mixture of solid ice, liquid water, and air. When the XPGR value crossed an empirically-derived threshold, it indicates the presence of liquid water in the snowpack. Therefore, this method produces a binary melt/no melt assessment of surface conditions as often as satellite orbit geometry permits—typically once-daily. XPGR melt assessment was accomplished using Special Sensor Microwave Imager (SSMI) imagery at a resolution of 25km using the average values of the ascending and descending nodes. This provides a once-daily product with surface melt occurrence at a 25km resolution.

In this study, the XPGR was calculated for the Ross Ice Shelf and surrounding area for December 27, 1991 through January 21, 1992. This provides the spatial pattern of melt occurrence for the long-duration melt event in question. There is a substantial portion of data that is missing from the satellite record in this area from December 28 through December 30, but the presence of melt both before and after the missing period, as well as the presence of surface melt in areas surrounding the missing data, indicates that the melt event was continuous throughout the study period.

Self-Organizing Maps (SOMs)

Self-Organizing Maps are an artificial neural network-based approach to classifying spatial data. SOMs are used to generalize weather conditions to a user-defined fixed number of states, and can be used to determine the frequency of particular synoptic-scale weather patterns (Hewitson and Crane, 2002). SOMs provide a more robust tool than classification schemes based on principal components analysis alone (Reusch et al., 2005). In this study, SOMs are used to

categorize seven different weather variables: Sea-Level Corrected Atmospheric Pressure (Pressure), Latent Heat Flux (LH Flux), Sensible Heat Flux (SH Flux), Incoming Shortwave Radiation (SW Down), Reflected Shortwave Radiation (SW Out), Incoming Longwave Radiation (LW Down), and Outgoing Longwave Radiation (LW Out). These variables capture critical energy balance components, as well as synoptic-scale weather patterns in the sea level pressure variable.

It has been noted (Bromwich and Fogt, 2004) that many reanalysis products perform poorly in the high latitudes of the Southern Hemisphere, especially the NCEP/NCAR reanalysis. To remedy this problem, the weather variables used in this study are the gridded output of Polar MM5 forced by ERA40 reanalysis, which is considered a superior product. The use of Polar MM5 output rather than strictly reanalysis will more precisely capture smaller-scale variability in weather patterns that may be misrepresented in the reanalyses.

The domain for the SOM analysis was the entire Southern Hemisphere south of 40^{o}S. This large area was chosen to minimize any error associated with choosing an artificial boundary for the SOM domain and to capture the macro-scale forcing of the atmospheric circulation in the Antarctic region. SOM output was generated using the vfind function of the SOMPAK software, which automatically repeats different random initialization and training procedures to optimize output (Kohonen et al., 1995).

The SOM study period was summer 1987-88 through 2001-02, that being the overlap period between the SSM/I record and the ERA40 reanalysis. Only the warmest months of the year, December and January, were considered in this study as these months have the highest insolation and average temperatures. For each month, each day was then associated with one of 15 SOM-determined weather types for each variable, and each variable was considered separately. Therefore, a day that was classified as “Type 1” for LH Flux might not necessarily be classified as “Type 1” for SH Flux. The final product of the SOM analysis was a calendar for

each of the December days and each of the January days with one weather type associated with each day for each variable. This larger-scale SOM analysis (Chapter 3) provides a climatological context for the 1991-92 surface melt event, whereby the patterns that occurred frequently during the melt event can be analyzed with respect to their frequency over a longer time period.

Results

The 1991-92 "melt event" can be considered to comprise the time period of Dec. 20, 1991 through Jan. 21, 1992—the period during and one week immediately preceding the large-scale surface melt event on the Ross Ice Shelf. Four of the SOM classifications are presented here—those that occurred at least 3.5x more frequently during the melt event than would be expected based on climatological norm (Table 3-1 and Table 3-2) and occurred at least three times during the melt event and the seven days leading up to it. These patterns were an LW Down pattern, two SH Flux patterns, and a LH Flux pattern. Three of these patterns occurred in December, as the melt event was beginning, and one occurred in January.

The first of the anomalously-frequent patterns is a December LW Down pattern (Figure 4-3). This pattern showed a marked (~ 5-6 W/m^2) positive anomaly over the eastern Ross Ice Shelf and Siple Coast, which would typically be associated with an increase in cloudy conditions in this area. Negative anomalies are present over the western Ross Ice Shelf where there was no surface melting during this event. During the 1987-2002 SOM period, this pattern occurred on 22 out of 453 December days, or approximately 5.1% of all December days. However, during and prior to the 1991-92 melt event, this pattern occurred on 7 of 12 days, or 58.3% of the December melt days. Consequently, this pattern occurred 10x more frequently during the melt event than would be expected based on climatological norms.

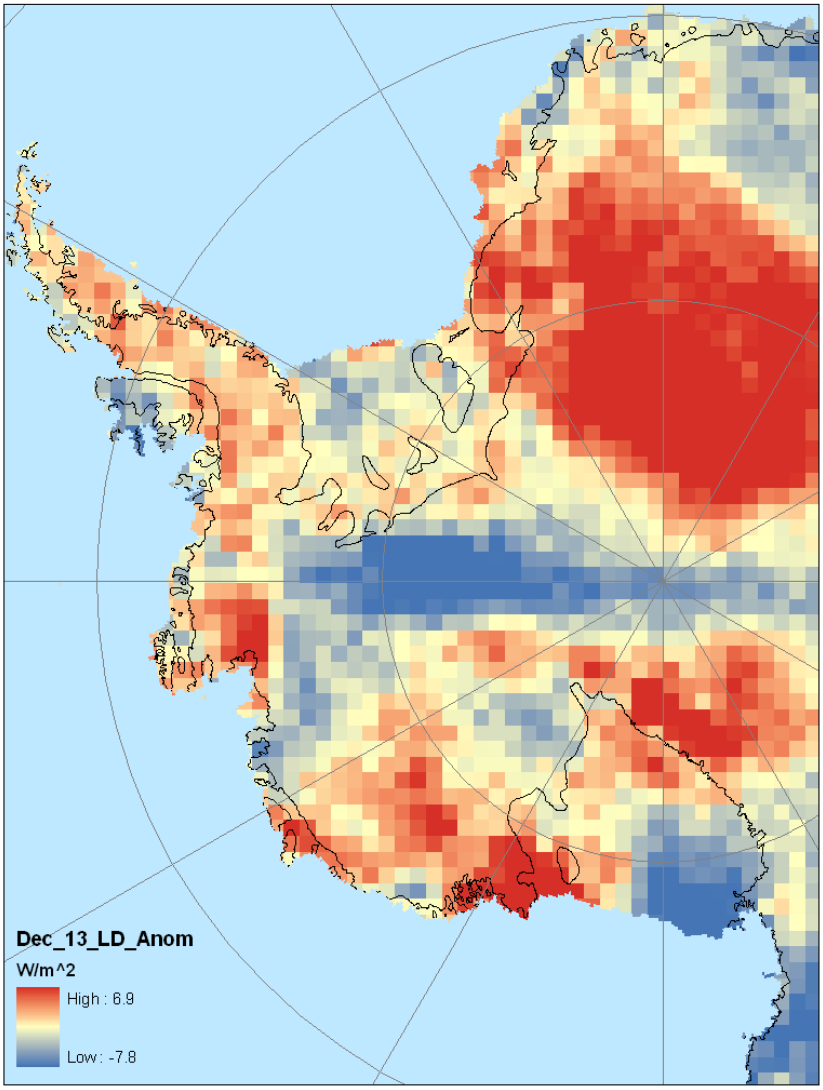

Figure 4-3: December LW Down Type 13 Anomaly from Climatological Norm

The second anomalously frequent pattern (Figure 4-4) is a December SH Flux pattern. This pattern exhibits generally average SH fluxes toward the surface throughout the Ross Ice Shelf region, with values ranging from -2 W/m^2 to +2 W/m^2 over Ross Ice Shelf and the Siple Coast. During the 1987-2002 SOM study period, this pattern occurred on 22 out of 436 December days, or approximately 5.1% of all December days. However, during and prior to the 1991-92 melt event, this pattern occurred on 4 out of 12 days, or 33.3% of the December melt days. This

pattern was 6.6x more frequent during the melt event than would be expected based on climatological norms.

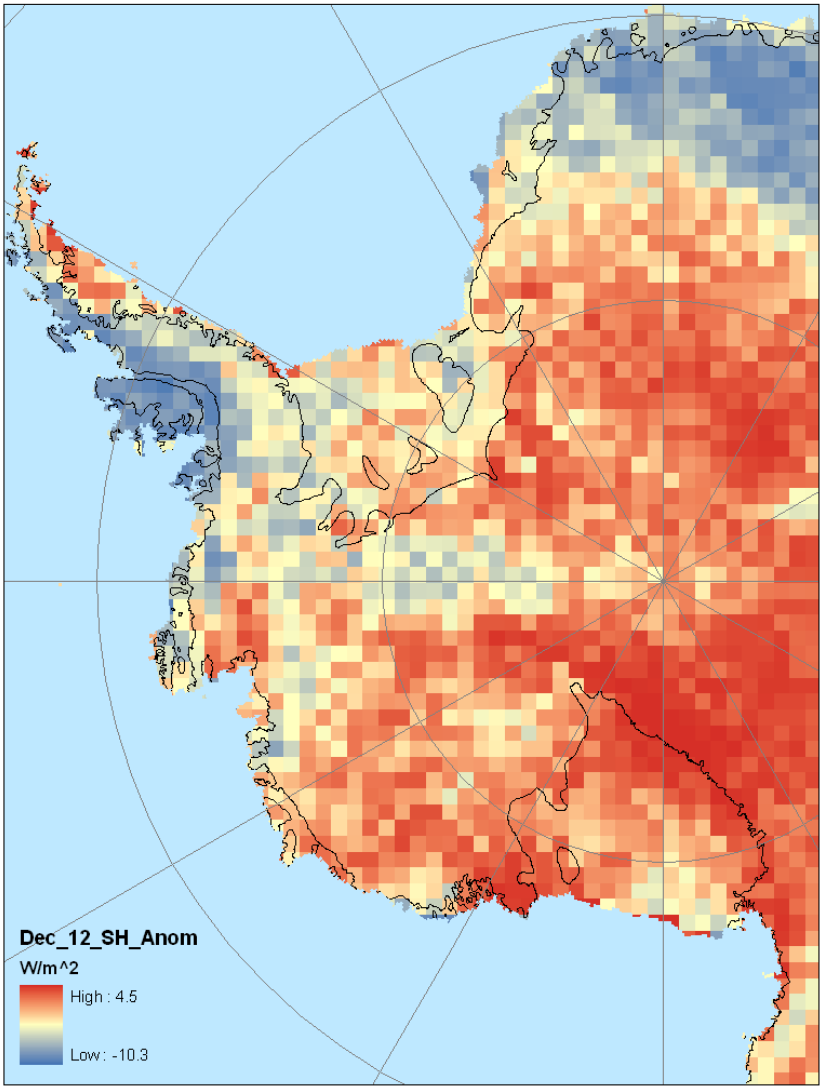

Figure 4-4: December SH Flux Type 12 Anomaly from Climatological Norm

The third anomalously frequent pattern (Figure 4-5) is a December LH Flux anomaly pattern. This pattern is one of generally positive LH Flux anomalies toward the surface over the entire Ross Ice Shelf, with anomalies approaching 8 W/m^2 over the central portions of the shelf. Positive LH Flux anomalies are associated with higher than average amounts of moisture being

advected into the region, depositing moisture and heat onto the ice shelf. This pattern occurred on 39 out of 436 December days, or approximately 8.9% of all December days. However, during and prior to the 1991-92 melt event, this pattern occurred on 4 out of 12 days, or 33.3% of the December melt days. This pattern was 3.7x more frequent during the melt event than would be expected based on climatological norms.

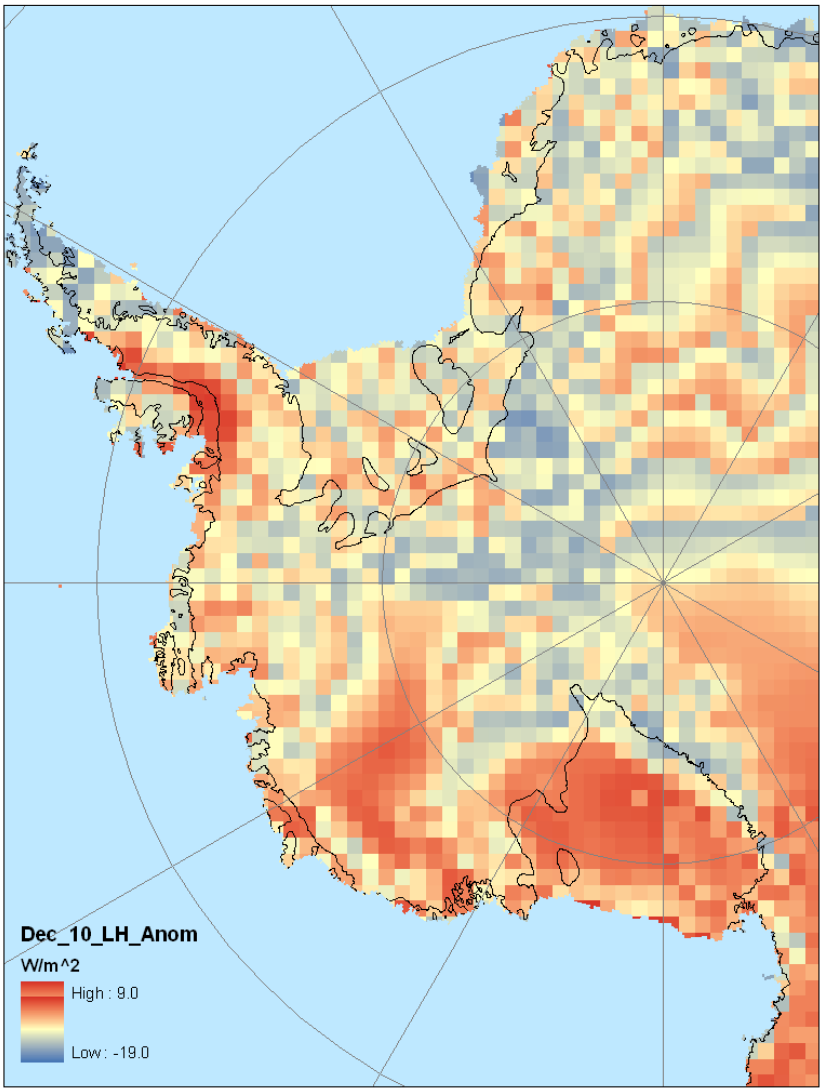

Figure 4-5: December LH Flux Type 10 Anomaly from Climatological Norm

The fourth and final anomalously frequent pattern (Figure 4-6) was the only January pattern for any variable that occurred significantly more frequently than would be expected. This was a SH Flux pattern that had positive anomalies toward the surface of around 4 W/m^2 over the eastern portion of the Ross Ice Shelf, and negative anomalies over the Western Ross Ice Shelf. This pattern occurred on only 4 of the 453 January days, or approximately 0.9% of all January days. However, three of these four days occurred during the melt event, comprising 14.3% of the January melt days. This pattern was 15.9x more frequent during the melt event than would be expected based on climatological norms.

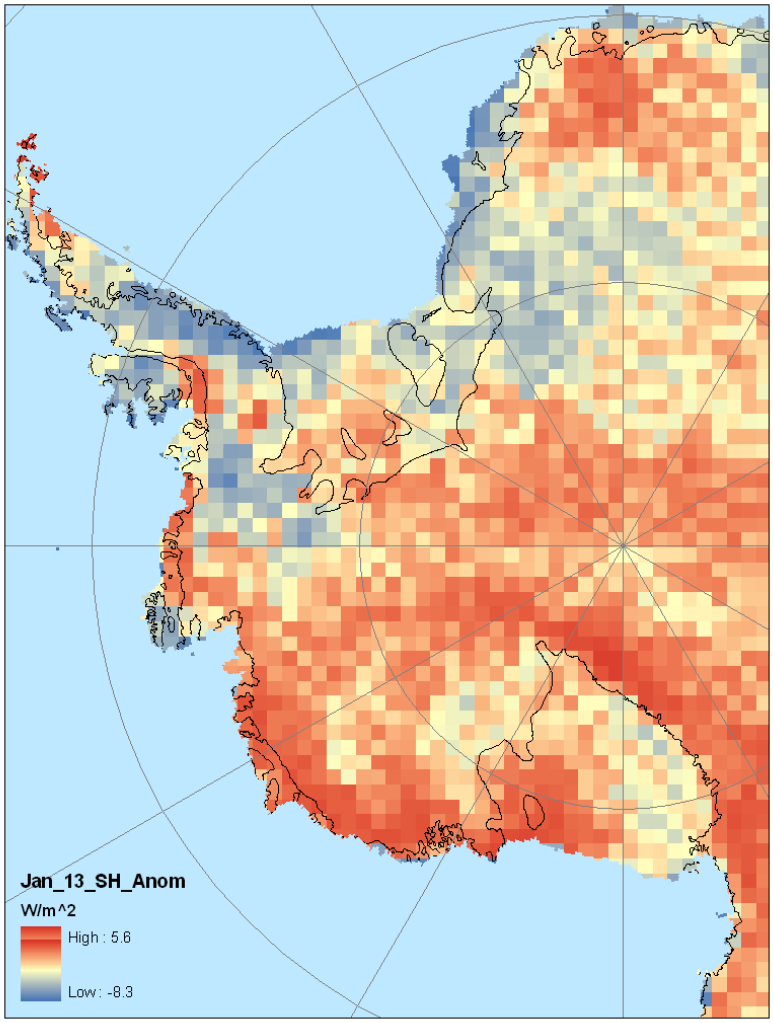

Figure 4-6: January SH Flux Type 13 Anomaly from Climatological Norm

Discussion

Three of the four anomalously frequent weather types exhibit spatial patterns that would be particularly conducive to the production of surface melt on the eastern Ross Ice Shelf. December LW Down Type 13 (Figure 4-3), with an increased longwave radiation flux toward the surface, indicates that cloudy conditions were prevalent during the melt event. December LH Flux Type 10 (Figure 4-5) indicates an increased amount of moisture in the atmosphere, transporting latent heat towards the surface of the ice shelf. Finally January SH Flux Type 13 (Figure 4-6) indicates that there was an increase in sensible heat flux to the surface as well, which may be caused by the advection of maritime air onto the ice shelf. The combination of increased cloudiness, increased moisture, and increased sensible heat would indicate that stormy conditions, coupled with advection of warm and moist air contributed significantly to the generation of surface melt during this event. The fourth anomalously frequent pattern (December SH Flux Type 12, Figure 4-4) showed near-average sensible heat flux conditions for December, which would neither contribute to nor inhibit surface melting, but which preceded the anomalously positive SH flux conditions of January.

These analyses show that larger downward latent and sensible heat fluxes are associated with this surface melt event. However, it is difficult to discern just from the spatial patterns whether the increases in heat fluxes are causing the surface melting, or the presence of liquid water in the snowpack is forcing an increase in latent and sensible heat fluxes. One way to determine whether this association is correlative or causative is to examine the synoptic-scale circulation that was present during the melt event. The NCEP/NCAR Reanalysis daily climate composites (Figure 4-7, Image provided by the NOAA/ESRL Physical Sciences Division, Boulder Colorado from their Web site at http://www.esrl.noaa.gov/psd/, Kalnay et al., 1996) confirm the presence of a persistent cyclonic circulation over the Ross Sea, directing

northeasterly flow over the ice shelf at the beginning and peak of the surface melt event. This flow would advect relatively warm and moist air over the eastern Ross Ice Shelf, and would result in offshore flow on the western half of the ice shelf. This pattern is consistent with both the observed synoptic weather types that occurred during the melt event as well as the spatial patterns of the surface melt (large extent on the eastern portion of Ross, but absent on the western half). The cyclonic flow that was prevalent at the beginning and peak stage of the melt event is a potential driver for the increase in sensible and latent heat fluxes in the melt region, and is consistent with the increased heat fluxes being a causative factor for the surface melt event.

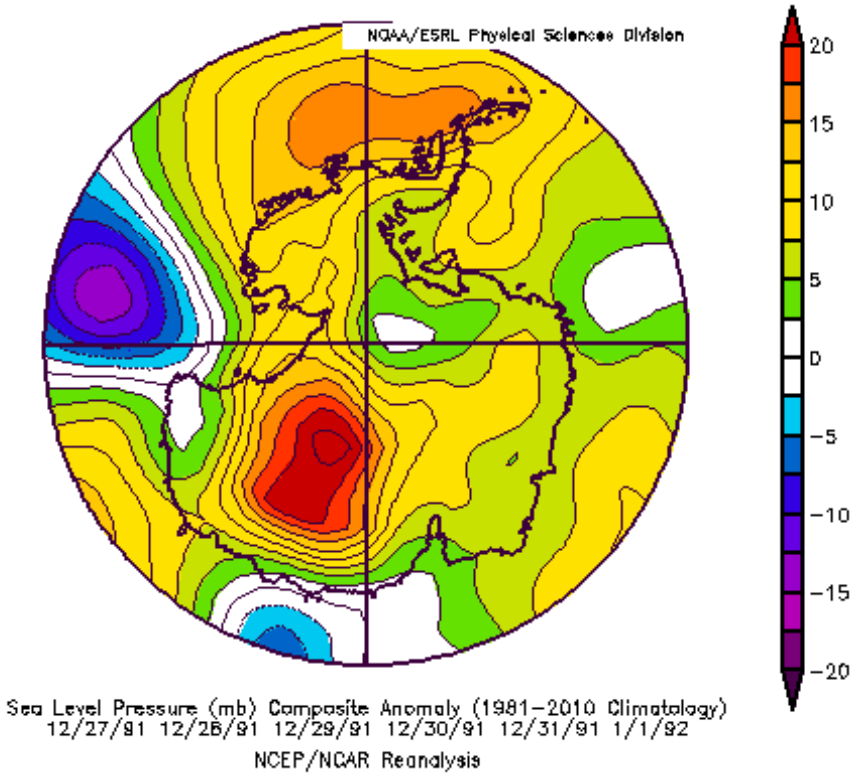

Figure 4-7: Sea-Level Pressure Composite Anomalies for Dec 27, 1991 through Jan 1, 1992.

Conclusion

The major surface melt event of 1991-92 on Ross Ice Shelf, the largest in the passive microwave satellite record, is shown to be associated with a set of internally consistent anomalies in climate fields. These are positive anomalies in downwelling longwave radiation, and positive anomalies in both latent and sensible heat flux (i.e. atmosphere to surface forcing). The warm, moist, cloudy conditions isolated by the SOM analysis during the melt event indicate cyclonic conditions in the Ross region, which was confirmed by NCEP/NCAR reanalysis multi-day average output.

References

Abdalati, W. and Steffen, K.: Passive Microwave-Derived Snow Melt Regions on the Greenland Ice Sheet. Geophysical Research Letters, 22, 787-790, 1995.

Abdalati, W. and Steffen, K.: Snowmelt on the Greenland Ice Sheet as Derived from Passive Microwave Satellite Data. Journal of Climate, 10, 165-175, 1997.

Armstrong, R.L. and Brodzik, M.J.: An Earth-Gridded SSM/I Data Set for Cryospheric Studies and Global Change Monitoring. Advances in Space Research, 16, 155-163. 1995. Data available online: http://nsidc.org/data/docs/daac/nsidc0032_ssmi_ease_tbs.gd.html

Bromwich, D.H. and Fogt, R.L.: Strong Trends in the Skill of the ERA-40 and NCEP-NCAR Reanalyses in the High and Midlatitudes of the Southern Hemisphere, 1958-2001. Journal of Climate, 17, 4603-4619, 2004.

Hewitson, B.C. and Crane, R. G.: Self-organizing maps: Applications to Synoptic Climatology. Climate Research, 22, 13-26. 2002.

King, J.C., Turner, J., Marshall, G.J., Connolley, W.M., and Lachlan-Cope, T.A. Antarctic Peninsula Climate Variability and its Causes as Revealed by Analysis of Instrumental Records. British Antarctic Survey, Natural Environment Research Council. 2002.

Kohonen, T.; Hynninen, J; Kangas, J.; and Laaksonen, J. (1995). SOM_PAK, The Self-Organizing Map Program Package, Version 3.1 user manual. Available Online: http://www.cis.hut.fi/research/som_pak/som_doc.txt

Liu, H.; Wang, L.; and Jezek, K. C.: Spatiotemporal Variations of Snowmelt in Antarctica Derived from Satellite Scanning Multichannel Microwave Radiometer and Special Sensor Microwave Imager Data (1978-2004). Journal of Geophysical Research, 111, F01003, 2006.

Reusch, D.B.; Alley, R.B.; and Hewitson, B.C.: Relative Performance of Self-Organizing Maps and Principal Component Analysis in Pattern Extraction from Synthetic Climatological Data. Polar Geography, 29, 188-212. 2005.

Steig, E.J., Schneider, D.P., Rutherford, S.D., Mann, M.E., Comiso, J.C., and Shindell, D.T.: Warming of the Antarctic Ice Sheet Surface since the 1957 International Geophysical Year. Nature, 457, 459-462, 2009.

Chapter 5

Conclusions

This dissertation has examined surface melt on Antarctic ice shelves, adopting both climatological and case studies in an empirical framework and offers important insights to surface melt detection in the case of Chapter 2, and surface melt dynamics at the synoptic scale in the case of Chapters 3 and 4.

Regarding surface melt detection, it is shown in Chapter 2 that:

1. Surface melt can be detected and quantified using coupled MODIS near-infrared and Ice Surface Temperature retrievals.
2. This coupled Near-IR and IST technique permits ice surface melt to be detected at a higher spatial resolution than many conventional melt detection algorithms that rely on passive microwave retrievals.
3. Because clouds are opaque in the IR portion of the electromagnetic spectrum, it is not possible to obtain complete coverage of large areas at the daily scale. Consequently, the effective temporal resolution of the coupled Near-IR and IST technique is lower than that of passive microwave melt detection methods.
4. The coupled Near-IR and IST technique is intended to complement and not replace traditional melt detection techniques using the microwave portion of the EM spectrum.

Regarding surface melt dynamics (Chapters 3 and 4), it is shown that:

1. Surface melt during the most substantial melt event on Ross Ice Shelf was driven by increased Sensible Heat Flux and increased Latent Heat Flux.
2. Surface melt in general on Ross Ice Shelf appears to be driven by increases in Sensible and Latent Heat Fluxes and appears unaffected by changes in radiation fluxes.
3. Surface melt on Ross Ice Shelf can be enhanced when there is a weakening in the typically-present ABS surface low pressure, with relatively high pressures in the ABS region and relatively low pressures in the Ross Sea. This allows for the advection of maritime air from the Ross Sea over the Eastern portion of Ross Ice Shelf, and induces a phenomenon similar to the mesoscale Ross Air Stream over the western portion of Ross Ice Shelf.
4. Surface melt on Larsen Ice Shelf and on the smaller ice shelves of the ABS region appears to be associated with changes in radiation fluxes at the surface,

but the impact of either sensible or latent heat fluxes in these locations appears minimal.

5. Because of the number of synoptic weather patterns derived by the SOM analysis, there may be other weather patterns that affect surface melting that did not register as statistically significant. Further work is necessary to determine the extent to which other weather patterns may be related to surface melt extent.

Given that the polar regions, especially West Antarctica, have experienced one of the largest temperature increases on Earth over the last few decades, an understanding of Antarctic climate has become more urgent. In a warming world, surface melt on Antarctic ice shelves is becoming a more urgent problem, and an increased understanding of how climate change is affecting Antarctic ice shelves is an invaluable approach for assessing vulnerable regions of the Antarctic that may be prone to further ice shelf instability.

VITA

Christopher Karmosky

Ph.D. Geography, Pennsylvania State University (2013)
Adviser: Dr. Derrick Lampkin
Dissertation Title: Synoptic and Mesoscale Climate Forcing on Antarctic Ice Shelf Surface Melt Dynamics
M.S. Geography, University of Delaware (2007)
Adviser: Dr. Daniel Leathers
Master's Thesis: Synoptic Climatology of Snowfall in the Northeastern United States: An Analysis of Snowfall Amounts from Diverse Synoptic Weather Types
B.A., Geography and Geology, Colgate University (2004)
Advisers: Dr. Adam Burnett (Geography) and Dr. Karen Harpp (Geology)
Graduated with Honors in Geography
Honors Thesis: The Role of Atmospheric Circulation in Recent Antarctic Peninsula Climate Change

Karmosky, C (2011). Climate Forcing on Antarctic Surface Melt. Pennsylvania State University Department of Geography Coffee Hour (Part of Physical Geography Grad Student "TED" Talks). February, 2011. University Park, Pennsylvania. Oral Presentation.

Lampkin, DJ and **Karmosky, C**. (2011). Estimation of Surface Melt Magnitude over Ross Ice Shelf, Antarctica using Satellite-Derived Estimates of Liquid Water Fraction. (Submitted January, 2011 to *Antarctic Science*.)

Lampkin, DJ and **Karmosky, C** (2009). Surface Melt Magnitude Retrieval over Ross Ice Shelf, Antarctica Using Coupled MODIS Optical and Thermal Satellite Measurements. (The Cryosphere Discuss., 3, 1069-1107, 2009)

Baum, SD; Haqq-Misra, JD; and **Karmosky, C** (2009). Climate Change: Evidence of Human Causes and Arguments for Emissions Reduction. (Science and Engineering Ethics, DOI 10.1007/s11948-011-9270-6.